Superheated Steam Scrubbing and Utilization for Power Generation

Vijay Chauhan

Doctor of Philosophy
May 2019

School of Science and Engineering

Reykjavík University

Ph.D. Dissertation

Superheated Steam Scrubbing and Utilization for Power Generation

Dissertation of 180 ECTS credits submitted to the School of Science and Engineering

at Reykjavík University in partial fulfillment of the requirements for the degree of

Doctor of Philosophy (Ph.D.)

May 2019

Thesis Committee:

Guðrún Arnbjörg Sævarsdóttir
Associate Professor, Reykjavík University

Maria Guðjónsdóttir
Assistant Professor, Reykjavík University

Halldór Pálsson
Professor, University of Iceland

Oleh Weres, Examiner
PowerChem, Reno, Nevada, USA

Bjarni Pálsson, Examiner
Landsvirkjun Power, Iceland

Superheated Steam Scrubbing and Utilization for Power Generation

Vijay Chauhan

May 2019

Abstract

Superheated steam from high enthalpy vapor dominated geothermal fields offers an opportunity to extract greater exergy per unit flow with higher thermodynamic output efficiency compared to conventional geothermal wells. The first full scale well drilled with the objective to deliver superheated steam, IDDP-1, produced steam with an enthalpy of $>$ 3070 kJ/kg and pressure up to 15 MPa. Flow rate up to 48 kg s^{-1} of steam was achieved which might result in power output up to 48 MW. Utilizing the superheated steam, however, faces challenges because of dissolved silica and chloride carried with the superheated steam. The silica that is present in the superheated steam precipitates when lowering down the pressure which can cause scaling. Presence of chloride in steam causes problem related to corrosion if the steam temperature drops below the acid dew point temperature. In order to avoid the corrosion due to the temperature drop, it is, therefore, necessary to do mitigate the impurities before utilization. However, applying traditional methods for mitigation, like wet scrubbing, causes loss in the steam superheat and hence output exergy.

This work aims to develop a method to utilize the superheated steam consisting of high chloride and silica content as experienced in high enthalpy vapor dominated geothermal fields in a more efficient way than is currently available. To achieve this, a step by step approach is followed in this work. The first step aims to study silica particle transport and deposition in superheated steam flow using Computational Fluid Dynamic (CFD). For this, advection-diffusion model based on Euler-Euler approach is implemented using OpenFOAM. The implemented model was validated by experimental measurements for silica particle deposition in superheated steam flow. Experiments were performed to understand the effect of different parameters on particle deposition velocity. The results from the measurements show agreement with the simulated results. An increase in deposition velocity in the diffusion-impaction regime is observed, signifying silica particle agglomeration as an important factor controlling deposition. The second step aims to propose a method for scrubbing acid gas and silica impurities from the steam without loss in its superheat. To achieve scrubbing without loss in superheat, boiling point elevation property of aqueous potassium carbonate solution is exploited. A power cycle utilizing the scrubbing method is proposed while considering the parameters affecting deposition as concluded from the computational study. A comparison study of the thermodynamic performance of the proposed cycle for the case of IDDP-1 well is done where it is compared to that of the cycle

utilizing traditional wet scrubbing. Simulation results for the production curve of IDDP-1 well show an increase in utilization efficiency up

to 7% and an increase in net work output up to 12% using aqueous potassium carbonate for scrubbing compared to basic wet scrubbing. The third step aims at computational modeling and experimental study on aqueous potassium carbonate droplets in superheated steam to obtain a better understanding of the proposed scrubbing method. For this, a computational model using the Eulerian-Lagrangian approach is developed in OpenFOAM. Effect of injected solution salt concentration on droplet temperature and concentration were studied using model simulation and experiments. Results from the simulations were in accordance with experimental results, where an increase in boiling point elevation with the increase in injected salt solution concentration was observed. The final step aims at performance analysis of the proposed method using experiments for silica scrubbing from superheated steam using aqueous potassium carbonate solution. Measurements for the effect of injected salt solution concentration on scrubbing efficiency and degree of superheat retained while scrubbing are done. Results from the experiments show an increase in the degree of superheat retained and an increase in scrubbing efficiency with increased aqueous salt concentration.

The overall study demonstrates a technique for scrubbing superheated steam using aqueous potassium carbonate. The proposed technique helps in retaining the steam superheat while scrubbing. To study the behavior of the scrubbing medium in the superheated steam, a computational model for simulating salt solution droplets in superheated steam is developed and validated experimentally. In addition, advection-diffusion model is implemented for simulating silica particle deposition in superheated steam flow. The results from the model simulation were validated experimentally.

Superheated Geothermal Steam Scrubbing and Utilization for Power Generation

Vijay Chauhan

May 2019

Útdráttur

Með því að nýta yfirhitaða gufu úr þurrgufusvæðum með háu vermisinnihaldi fæst vökvi með hærra orkuinnihald á massaeiningu sem gefur kost á hærri varmafræðilegri nýtni samanborið við nýtingu á hefðbundnum jarðhitaholum. Fyrsta framleiðsluholan sem boruð var með það að markmiði að flytja yfirhitaða gufu, IDDP-1, skilaði gufu með vermi > 3070 kJ/kg og þrýsting að 15 MPa. Massaflæði úr borholunni var allt að 48 kg s^{-1} sem gæti skilað orkuframleiðslu upp á 48 MW.

Nýting yfirhitaðrar gufu felur í sér áskoranir vegan uppleysts kísíls og klórs sem gufan ber með sér. Kísillinn getur fallið út þegar þrýstingur gufunnar er lækkaður og valdið skeljun. Klóríð í gufunni getur valdið tæringarvandamálum þegar hitastig gufunnar fellur niður fyrir sýrudaggarmark.

Til að koma í veg fyrir tæringu vegna hitastigslækkunar er nauðsynlegt að hreinsa óhreinindin úr áður en til nýtingar kemur. Hefðbundnar aðferðir eins og vothreinsun valda tapi á yfirhitun og þar með orkutapi.

Markmiðið með þessu verkefni var að þróa nýja og skilvirkari aðferð til að nýta yfirhitaða gufu með háu klór- og kísilinnihaldi líkt og finna má í þurrgufusvæðum. Verkefninu var skift í þrjá fasa. Fyrsti fasinn var að rannsaka flutning og áfellingu kísils í yfirhitaðri gufu með því að nota aðferðir úr tölulegri straumfræði (CFD). Massaburðar-sveimis líkan (Advection-diffusion) byggt á Euler-Euler aðferð var notað í OpenFoam. Líkanið var sannreynt með mælingum fyrir áfellingu kísilagna úr yfirhitaðri gufu. Með tilraunum voru rannsökuð áhrif ýmissa stærða á áfellingarhraða agnanna. Niðurstöður úr mælingunum eru í samræmi við niðurstöður úr líkanagerðinni. Aukning varð á áfellingarhraða á sveimis-tregðufærslu (diffusion-impaction) svæðinu sem sýnir að kekkjun kísilagnanna er mikilvægur þáttur þegar kemur að áfellingu. Annar fasinn fólst í að þróa aðferð við að hreinsa sýru á gasformi og kísilagnir úr gufunni án þess að tapa yfirhitun hennar. Til að hreinsa gufunnar án þess að tapa yfirhitai, var nýttur sá eiginleiki kalíum karbónat lausnar að hafa hærra suðumark en hreint vatn. Orkuferli sem nýtir þessa hreinsunaraðferð var lagt til þar sem tekið var tillit til þátta sem stjórna áfellingarhraðanum skv. niðurstöðum úr

fyrsta fasanum. Varmafræðileg greining var gerð á því orkuferli og sem og orkuferli sem nýtir hefðbundna vothreinsun. Niðurstöður útreikninga

þar sem kennilína IDDP-1 holunnar var notuð, sýna aukningu í nýtni upp á 7% og aukningu á heildarvinnu um 12% með því að nýta kalíum karbónat lausnina í stað hefðbundinnar vothreinsunar.

Þriðji fasi verkefnisins fjallaði um hegðun dropa úr kalíum karbónat saltlausn í yfirhitaðri gufu, og fólst bæði í tilraunum og tölvulíkanagerð. Tölvulíkan byggt á Eulerian-Lagrangian aðferð var þróað í OpenFOAM. Áhrif styrks lausnarinnar á dropahitastig og styrk karbonat lausnarinnar voru rannsökuð með líkanagerð og tilraunum. Niðurstöður úr líkönum voru í samræmi við niðustöður tilraunanna þar sem aukning á suðumarkshækkun með hækkun á saltstyrk var staðfest.

Lokafasinn var að framkvæma afkastagreiningu á þessari aðferð með því að gera tilraunir á afköstum þess að hreinsa kísil úr yfirhitaðri gufu með kalíum karbónat lausn. Mælingar voru gerðar á áhrifum styrks saltlausnarinnar á hreinsunarnýtni og hversu vel yfirhitun var við haldið. Niðurstöðurnar sýna að meiri yfirhitun er viðhaldið og aukning verður í hreinsunarnýtni með auknum styrk á saltlausninni.

Þessi rannsókn kynnir og greinir aðferð við að hreinsa yfirhitaða gufu með því að nota kalíumkarbónatlausn. Með þessari aðferð má viðhalda yfirhitun gufunnar á sama tíma og hún er hreinsuð. Til að rannsaka hegðun hreinsimiðilsins í yfirhituðu gufunni var tölvulíkan búið til til að herma eftir hegðum dropum saltlausnarinnar í yfirhitaðri gufu og voru þessar niðurstöður sannreyndar með tilraunum. Að auki var massaburðar-sveimis líkan þróað til að herma áfellingu kísilagna í yfirhitaðri gufu. Það líkan var jafnframt sannreynt með tilraunum.

The undersigned hereby certify that they recommend to the School of Science and Engineering at Reykjavík University for acceptance this Dissertation entitled **Superheated Steam Scrubbing and Utilization for Power Generation** submitted by **Vijay Chauhan** in partial fulfillment of the requirements for the degree of **Doctor of Philosophy (Ph.D.) in Mechanical Engineering**

28.05.2019

date

Thesis committee:
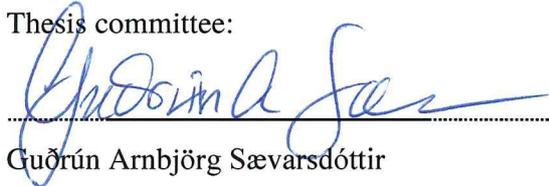
Guðrún Arnbjörg Sævarsdóttir
Associate Professor, Reykjavík University

Maria Guðjónsdóttir
Assistant Professor, Reykjavík University
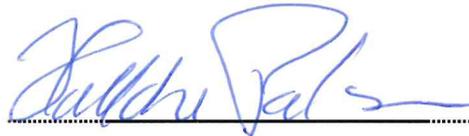
Halldór Pálsson
Professor, University of Iceland

Examiner:
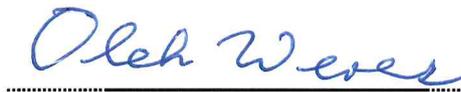
Oleh Weres
PowerChem, Reno, Nevada, USA
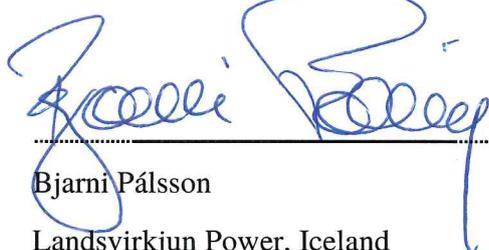
Bjarni Pálsson
Landsvirkjun Power, Iceland

The undersigned hereby grants permission to the Reykjavík University Library to reproduce single copies of this Dissertation entitled **Superheated Steam Scrubbing and Utilization for Power Generation** and to lend or sell such copies for private, scholarly or scientific research purposes only.

The author reserves all other publication and other rights in association with the copyright in the Dissertation, and except as herein before provided, neither the Dissertation nor any substantial portion thereof may be printed or otherwise reproduced in any material form whatsoever without the author's prior written permission.

28-05-2019

....

date

....

Vijay Chauhan

Doctor of Philosophy

Dedicated to my Grandmother

Nainu Devi Chauhan

Acknowledgements

First of all, I am grateful to the Almighty God for enabling me to complete my Ph.D Degree. I wish to express my sincere thanks to my supervisors Guðrun Arnbjorg Saevarsdottir and Maria Sigriður Gudjonsdottir for their guidance, patience, understanding and because of whom I am able to complete my research. I place on record, my sincere thanks to my teachers Arni Ragnarsson, Arni Gunnarsson and B.N. Banergee who continuously kept motivating me to complete my research.

I would like to thank my three friends who are also staff members at Reykjavik University, Olafur Þor Arason, Hannes Pall Þorðarson and Gisli Freyr Þorsteinsson for helping me building up the experimental facilty. Their technical support played a key role in completing my experimental work. I would also like to thank Finnbogi Oskarrson and other staff members of Iceland Geosurvey (ISOR) and Sigurdur Markusson, Bjarni Palsson and other staff members of Landsvirkjun for providing valuable support during my research.

I would like to thank Professor Halldor Palsson from University of Iceland and Professor Halldor Svavarsson and Professor Andrei Manolescu from Reykjavik University for their support.

I wish to thank Cari Covell, Samuel Perkin and Christopher Mathews for their help in proof reading the articles.

I would like to thank our administrative director Sigrun Þorgeirsdottir and other administrative and library staff and the I.T service for their instantaneous support whenever required.

I would like to thank my parents, my elder brother and my sister in law. They were always supporting and encouraging me with their best wishes.

I would like to thank Irma, Michal, Judy, Yu-Ren, Lahcen and Miguel, who as good friends, were always willing to help and give their best suggestions. I would like to thank my landlord Guðjon Guðbjornsson and his family for taking care of me like a family member.

The work was funded by GEORG, Landsvirkjun, Reykjavik Energy, HS Orka, Orkustofnun and the IDDP project. I would like to thank all the mentioned organizations for the financial support provided. I would also like to thank ISLOFT and Icelandic Geothermal Engineering for the additional infrastructure support provided for building up the experimental setup.

I also place on record, my sense of gratitude to one and all who, directly or indirectly, have lent their helping hand in this venture.

Preface

This thesis is submitted to the Reykjavik University for partial fulfillment of the requirements for the degree of philosophiae doctor.

This doctoral work has been performed at the School of Science and Engineering Reykjavik University, Iceland with Gudrun A. Sævarsdóttir as a main supervisor and with a co-supervisor Maria Guðjónsdóttir.

Contents

List of figures

List of Tables

List of publications

Papers from this work/study published and submitted to peer reviewed scientific Journals:

    i.   Chauhan, V., Gudjonsdottir, M., Saevarsdottir, G., Silica scrubbing from superheated steam using aqueous potassium carbonate solution: An experimental investigation. *Geothermics*, 80, 1-7, 2019.

    ii.   Chauhan, V., Gudjonsdottir, M., Saevarsdottir, G., Silica particle deposition in superheated steam in an annular flow: Computational modeling and experimental investigation, *Geothermics* (in review, 2nd).

    iii.   Chauhan, V., Gudjonsdottir, M., Saevarsdottir, G., Computational modeling and experimental investigation of aqueous potassium carbonate droplets in superheated steam flow, Journal of Heat and Mass Transfer (in review, 1st).

Conference papers from this work/study published:

    i.   Chauhan, V., Harvey, WS., G. Saevarsdottir, G., Chlorine mitigation for geothermal power plants using venturi scrubbers: *Proc. ECRES – 4th European Conference on Renewable Energy Systems*, Istanbul, TURKEY, 28-31 August 2016: 333-339.

    ii.   Chauhan, V., Gudjonsdottir, M., Saevarsdottir, G., Silica deposition in superheated geothermal systems: *Proceedings 43rd Workshop on Geothermal Reservoir Engineering*, Stanford University, California, SGP-TR-213, 2018.

    iii.   Chauhan, V., Gudjonsdottir, M., Saevarsdottir, G., Thermodynamic analysis of superheated geothermal steam scrubbing using aqueous potassium carbonate solution: *Geothermal Resources Council Transactions*, 42, 2018.

1 INTRODUCTION

Utilization of geothermal energy offers an environmentally friendly way of contributing to energy production. Geothermal energy can provide heat and base-load power generation by utilizing aquifer, dependent on temperature. Power generation utilizing geothermal energy involves energy conversion technologies such as flash steam cycles, dry steam cycles, binary cycles and enhanced geothermal systems (EGS). The stable power production utilizing geothermal resources is unaffected by climatic variations and results in high capacity factor up to 90%, making it suitable for base load production. The global installed capacity for electrical power generation using geothermal energy is 12.8 GW_e [1] as of today. This installed capacity is much lower compared to other conventional renewable energy sources in usage for electricity generation, such as solar, hydro and wind power. This is due to limited areas in the world that have hydrothermal resources with temperature and permeability feasible for power production. Additionally, the cost of generating electric power utilizing geothermal energy is high in comparison to other conventional renewable energy resources. A cost-effective way of harnessing geothermal energy can, therefore, help to propagate usage of this environmentally friendly energy potential. This can be achieved using high temperature sources which deliver superheated steam with a potential to extract greater energy per unit fluid, which could result in lower relative cost of drilling. Although most geothermal fields deliver saturated two-phase fluid consisting of a mixture of saturated steam and liquid water, a number of vapor dominated geothermal fields have been reported to deliver superheated steam [2]. Such vapor dominated geothermal fields with superheated steam offer the potential to extract more power with better thermodynamic efficiency and lower operational cost.

With the feasibility of adopting components for near supercritical steam conditions, studies have been done on geothermal energy systems achieving supercritical states of the fluid [3], [4]. Modeling results from Albertsson [5] shows that a well producing supercritical fluid could have an order of magnitude of higher power output than a conventional geothermal well due to higher enthalpy and mass per unit volume flow rate. To investigate the technical and economic feasibility of using unconventional, very high temperature geothermal systems, the Icelandic Deep Drilling Project (IDDP) was established in the year 2000 by a consortium of three Icelandic energy companies, HS Orka, Landsvirkjun and Orkuveita Reykjavikur, as well as Orkustofnun (National Energy Authority) [6]. In an attempt to achieve superheated steam, the first full scale well IDDP-1 was drilled in the year 2009 at the Krafla field in Iceland. The well was meant to be drilled down to 4.5 km depth but ended up in a magma intrusion at a depth of 2104 m. The well produced steam with an enthalpy of > 3070 kJ kg^{-1} and a pressures up to 15 MPa. Flow rate up to 48 kg s^{-1} of steam was achieved from the well. These observations correspond to a potential of 40 MW of electric power generation. Different tests with regard to well and fluid characteristics were

made for IDDP-1 before it was shut down. Though the primary goal of drilling and testing a hydrothermal system with supercritical conditions through IDDP-1 was not entirely achieved, and considering the scope of utilization of unconventional systems delivering high enthalpy superheated fluid, the project has moved further with a plan to drill similar wells. The next deep drilling well IDDP-2 in Reykjanes, South-West Iceland was completed in January 2017 and achieved the targeted depth of 4659 m. The well is still under observation. The discharge test is planned in the year 2019. Usage of the unconventional superheated geothermal system provides an opportunity to utilize geothermal resources with greater efficiency and cost effectiveness compared to conventional geothermal systems. However the utilization faces challenges with regards to thermophysical and chemical characteristics of the fluid extracted. As observed from the IDDP-1 well, the fluid may consist of acid gas and solid impurities carried with superheated steam. Presence of such impurities in the fluid makes it challenging for utilization. Measurable levels of chloride from several reservoirs are reported by Ellis and Anliker [2]. Presence of chloride in steam causes pitting corrosion in pipelines, and stress corrosion cracking, which reduces the turbine reliability, thus incurring significant cost increase and maintenance difficulties. Presence of a considerable amount of silica dissolved in superheated steam can lead to precipitation and the deposition when pressure is lowered. Deposition of silica on components such as the heat recovery system reduces their effectiveness and lowers power plant efficiency. Mitigation of silica and chloride is therefore necessary before utilizing steam for power generation.

Wet scrubbing is the conventional method for removing acid gases and solid impurities from superheated steam. Steam coming from the well is made saturated by adding water or brine. Impurities are then removed in the separator along with the liquid phase. The method works well for steam with saturated vapor or with two-phase conditions. However, the application of wet scrubbing for cleaning superheated steam has a major drawback. Since the turbine efficiency decreases with a decrease in the dryness fraction of steam, a considerable loss in exergy output occurs due to quenching of superheat as required for wet scrubbing. Increasing wetness also causes a decrease in component lifetime. A comparative study of the thermodynamic performance of cycles utilizing different scrubbing methods for chlorine mitigation in superheated steam was done by Hjartarson et al. [7] for the case of IDDP-1. The main result show nearly 14% loss in work output due to wet scrubbing. Additionally, a heat recovery system in combination with wet scrubbing is an efficient way of utilizing superheated steam like that from IDDP-1. The thermodynamic analysis, however, does not take presence of silica into consideration. Presence of silica dissolved in superheated steam increases the risk of scaling due to precipitation from lowering down of pressure. Scaling cause a reduction in heat recovery system effectiveness with time and hence reduces the overall efficiency of the cycle.

1.1 Motivation, objectives and goals

The issues discussed in the previous section must be addressed at the design stage before the utilization of an unconventional resource is made. New methods of utilizing geothermal fluid are important to develop in order to overcome problems related to silica and chloride without sacrificing efficiency. The following objectives are defined:

- Study of silica particle transport and deposition in superheated steam flow using computation modelling and experimental investigation.

- Developing new methods for scrubbing both silica and chloride from superheated steam and its thermodynamic performance analysis.
- Computation model development and experimental investigation of a proposed new method used for scrubbing.

The project tasks were performed with the following goals:

- Understanding the mechanism of silica particle deposition in superheated steam flow and the parameters affecting the deposition rate.
- Developing techniques for effective utilization of superheated steam with acid gas and silica impurities for electric power generation.

This thesis included the following publications, appended as supplements:

Supplement 1: Chauhan, V., Gudjonsdottir, M., Saevarsdottir, G., Silica scrubbing from superheated steam using aqueous potassium carbonate solution: An experimental investigation. Geothermics, 80, 1-7, 2019.

In this paper a study on scrubbing of superheated steam containing silica impurities using an aqueous potassium carbonate solution is presented. Experiments were performed to determine the effect of injected salt solution concentration on the scrubbing performance and the degree of superheat retained. Results indicate improved scrubbing performance obtained using aqueous potassium carbonate solution as compared to that obtained using traditional wet scrubbing, while allowing the superheat to be conserved.

Supplement 2: Chauhan, V., Gudjonsdottir, M., Saevarsdottir, G., Silica particle deposition in superheated steam in an annular flow: Computational modeling and experimental investigation, Geothermics (in review, 2nd).

The paper presents a study on silica particle deposition in superheated steam flow. Computer simulation were done to understand the effect of different parameters affecting deposition velocity. Simulation results for deposition of silica particles in superheated steam flow were validated experimentally. Deposition velocity was measured for silica fume particles ranging from 1- 20μm in diameter. The measured data shows agreement with the implemented model simulation results, showing an increase in deposition velocity with increase in particle relaxation time in diffusion impaction regime thus signifying the effect of agglomeration on deposition velocity.

Supplement 3: Chauhan, V., Gudjonsdottir, M., Saevarsdottir, G., Computational modeling and experimental investigation of aqueous potassium carbonate droplets in superheated steam flow, Journal of Heat and Mass Transfer, (in review, 1st).

The paper presents computation model development of aqueous potassium carbonate droplets in superheated steam flow. The developed computation model includes the effect of salt concentration on boiling point and other thermo physical properties of the salt solution. Experimental investigation was carried out to verify the computation model. Results from the simulation were in accordance with experimental measurements, showing an increase in boiling point elevation and collected droplet salt concentration with an increase in injection salt solution concentration.

Supplement 4: Chauhan, V., Gudjonsdottir, M., Saevarsdottir, G., Silica deposition in superheated geothermal systems: Proceedings 43rd Workshop on Geothermal Reservoir Engineering, Stanford University, California, SGP-TR-213, 2018.

The paper presents implementation of the advection-diffusion model in OpenFOAM for modelling silica particle transport and deposition in superheated steam flow. The model includes effect of Brownian diffusion, turbulent diffusion, turbophoresis, Saffman lift force, drag force and thermophoresis on silica particle motion. The OpenFoam solver developed was validated using results from the literature for the gas particle flows showing good agreement.

Supplement 5: Chauhan, V., Gudjonsdottir, M., Saevarsdottir, G., Thermodynamic analysis of superheated geothermal steam scrubbing using aqueous potassium carbonate solution: Geothermal Resources Council Transactions, 42, 2018.

The paper describes application of boiling point elevation property of aqueous salt solution for scrubbing acid gas and solid impurities from superheated geothermal steam. Using IDDP-1 fluid characteristics as an example, a comparison study in terms of the thermodynamic performance was done for the power cycle utilizing aqueous potassium carbonate with that of the power cycle utilizing traditional wet scrubbing. Results from the simulation shows increase in work net output of 12% and 7% increase in the utilization efficiency using aqueous potassium carbonate for scrubbing rather than basic wet scrubbing.

Supplement 6: Chauhan, V., Harvey, WS., G. Saevarsdottir, G., Chlorine mitigation for geothermal power plants using venturi scrubbers: Proc. ECRES – 4th European Conference on Renewable Energy Systems, Istanbul, TURKEY, 28-31 August 2016: 333-339.

The study proposes application of venturi scrubbers for mitigating chlorine from superheated geothermal steam. A comparative study in terms of the thermodynamic performance is done for the IDDP-1 well fluid conditions of the power cycle utilizing venturi scrubbing with that of the cycle utilizing traditional wet scrubbing. Result shows improved thermodynamic performance obtained using the venturi scrubber.

1.2 Literature review

Presence of volatile chloride and silica in the superheated steam of IDDP-1 well was reported by Armannsson et al. [8]. Volatile chloride present in the steam incurs significant costs and maintenance difficulties. Problems caused by corrosion have been reported by Allegrini and Benvenuti [9]. Presence of chloride causes pitting corrosion in pipelines, and stress corrosion cracking reduces the turbine reliability. Corrosion due to volatile chlorides in the geothermal application has been well explained by Hirtz et al. [10]. Presence of chloride in gaseous form as an HCl molecule does not cause corrosion. However, when the HCl molecule comes in contact with liquid water due to quenching of steam superheat or local condensation, the HCl molecule ionizes to form hydrogen and chloride ions, and causes the process of corrosion in the absence of oxygen as governed by the following reaction:

$$2HCl(aq) + Fe^0 \Rightarrow H_2 + FeCl_2(aq) \qquad (1.1)$$
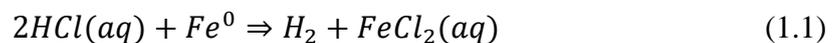
The reaction product is a highly soluble salt. The salt can exist with the solvent up to a higher degree of superheat before it gets precipitated. Such a solution, however, can dissolve some of the HCl present in the steam to form a more corrosive solution which causes the corrosion process to accelerate. It is therefore required to have some degree of steam superheat greater than the precipitation limit of the salt formed. Hirtz et al. [11] suggest a temperature range of 20°C superheat, above which corrosion is unlikely to continue.

Various techniques have been proposed for scrubbing geothermal steam with high chloride content. The techniques include 'steam washing', where clean water taken from the condenser is mixed with steam to dissolve unwanted substances and this water is subsequently removed in a separator (or 'demister') prior to the turbine. Another scrubbing technique is to utilize the mechanism of absorption or adsorption, popularly known as 'dry scrubbing' since the impurities are removed while keeping the steam in a dry state. The mechanism requires a reactor vessel or a fluidized bed, followed by a separation process. The technique has not yet been utilized on a commercial scale.

Wet scrubbing is the conventional way of cleaning steam in geothermal power plants by using brine or caustic injection into the steam. Injection of caustic into steam causes the following reaction to occur with hydrochloric acid formed by gaseous chloride below dew point:

$$NaOH(aq) + 2HCl(aq) \Rightarrow NaCl(aq) + H_2O \qquad (1.2)$$
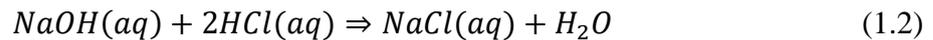
The sodium chloride salt formed as the product of the reaction is in the solution state which is removed in the separator placed after the wet scrubbing unit. Other solid impurities like silica stay with the liquid phase as slag and also get separated by collecting at the separator bottom. Analysis regarding optimization of scrubbing efficiency of a wet scrubbing process was done by Hirtz et al. [10]. An analytical model for predicting the performance of wet scrubbing for different flow conditions and geometry of the scrubbing unit is given by Paglianti et al. [12]. Results from the model show good agreement for the existing power plant scrubbing units.

Although a robust way of cleaning steam is achieved using wet scrubbing, the method causes a loss in power output when applied to superheated steam. Quenching superheat is important to make the fluid in two-phase as required for separation to occur. Loss in power output occurs due to exergy destruction while mixing and a decrease in turbine efficiency with a decrease in the dryness fraction of steam. Therefore, there is interest to develop new methods for scrubbing steam while steam superheat remains constant.

Performance analyses of cycles utilizing different chlorine mitigation methods for IDDP-1 was done by Hjartarson et al. [7]. Mitigation methods include the cycle utilizing wet scrubbing with and without an additional turbine, wet scrubbing using heat recovery, the binary power cycle, and the cycle utilizing dry scrubbing. Result show that the cycle with heat recovery system is an efficient and practical way to retain superheat of the geothermal fluid while mitigating the chloride using traditional wet scrubbing. The work done, however, does not take the presence of silica in superheated steam into consideration. Due to extremely high pressure in the reservoir, the fluid contains a considerable amount of dissolved silica in gaseous form. This occurs due to an increase in silica solubility with pressure near the supercritical region as discussed by Bahadori and Vuthaluru [13]. Lowering wellhead pressure causes silica to precipitate as observed during IDDP-1 well testing [14]. The precipitated silica were found as particles carried within the superheated steam flow and

were deposited on surfaces of different components causing scaling. Silica scaling in geothermal heat exchangers and the impact on pressure drop and performance for the Wairakei power plant was studied by Zarrouk el al. [15]. Studies show major long term negative effects on the power plant performance. For superheated steam similar to that of IDDP-1, a considerable amount of liquid injection is required for adding inhibitors, and would cause quenching of superheat hence reducing the exergy of the geothermal fluid.

The power cycle with a heat recovery system, as proposed by Hjartarson et al. [7] allows superheated steam to enter the heat recovery system directly from the wellhead. Keeping the steam in the superheated state while passing it though the heat recovery system helps to avoid the risk of corrosion due to acid chloride. However, the presence of precipitated silica in the steam can cause scaling along the heat exchanger surface, hence reducing its effectiveness with time. Therefore, to have an efficient utilization of superheated steam which consists of both chloride and silica impurities, it is necessary to model and understand the mechanism of silica particle transport and to develop a new method for scrubbing which makes simultaneous removal of acid chloride and silica present in steam without any loss in its superheat.

1.2.1 Silica particles deposition in superheated geothermal steam flow

The particle deposition in fluid flows is observed in many processes, such as chemical aerosol transportation and pollutants in the atmosphere. In the power generation and transport industry, deposition plays an important role in determining the performance and lifetime of many components. Figure 1.1 (a) shows the deposition of volcanic ash material in gas turbine vanes. Operation related problems due to deposition of particles in a gas turbine engine are discussed by Dunn et al. [16]. Deposition of mineral precipitates such as silica and carbonates from the fluid phase causes the formation of a hard coating on the boundary surfaces commonly known as scaling. Figure 1.1 (b) shows the scaling occurring due to silica deposition in a test chamber pipe for IDDP-1 [17].

(a)   *(b)*
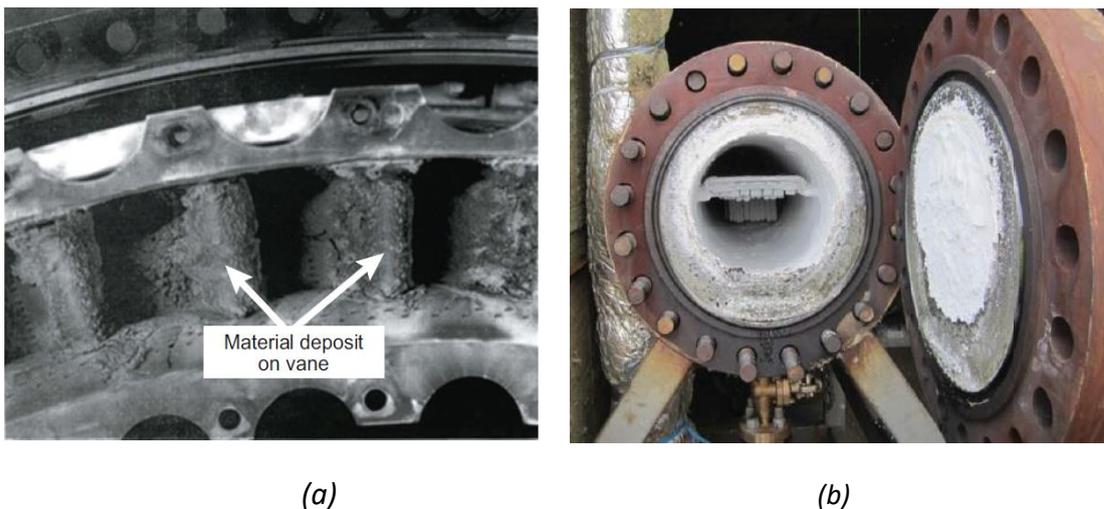
FIGURE 1.1 (a) Deposition of volcanic ash material on gas turbine vanes [16] (b) Silica scaling due to deposition in a test chamber pipe for IDDP-1 [17].

The mechanism of silica scaling occurring in two-phase geothermal fluid flow is well understood. The process of silica scaling involves precipitation, agglomeration and deposition on the component surface. The precipitation occurs as the solubility of silica

decreases with temperature and pressure. Fluids which are supersaturated with respect to amorphous silica; the mechanism responsible for the majority of silica precipitation is the formation of colloids. The colloids agglomerate through bridging to form bigger particles by flocculation. The formed particles flow as a dispersed phase in the fluid and may deposit along the component surface. To model scaling in two-phase flow that involves steam in the saturated state, researchers have followed different approaches for modelling. An equilibrium model based on minimizing free energy of the system with solute activities described by the semi-empirical equations of Pitzers model was proposed by Moler et al. [18]. The model is able to demonstrate the effect of temperature on silica scale formation. A mathematical model for silica scaling in geothermal wells with two-phase flow was proposed by Nizami and Sutopo [19]. The model was developed by integrating the solubility-temperature correlation and two-phase pressure drop in a wellbore.

Research and development on utilizing geothermal fluid with steam in superheated state is quite recent. The theory of silica carry over by superheated steam as observed in IDDP-1 is yet to be developed. For reservoir of IDDP-1 well with superheated steam, the dissolution is assumed to occur by hydrolysis of solid silica such as quartz in the rock by steam molecules forming silicic acid as shown by the following reaction:

$$SiO_2(s) + 2H_2O(g) \leftrightarrow Si(OH)_4(g) \qquad (1.3)$$
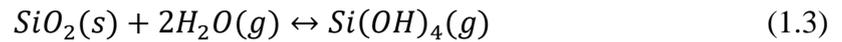
For complex environment involving components such as fluoride, other mechanism such as Silicontetrafluoride (SiF_4) in gaseous form can also be carried with the superheated steam. The occurrence of dissolved silica in the deep superheated steam in the Krafla field is also justified by the drawdown experienced with time in the well in the past as it was operated at low pressure. The silica from IDDP-1, formed after precipitation is in the amorphous form as observed from the scanning electron microscope images [20].

For the flow involving silica in superheated steam, modelling silica particle transport can help in understanding the process of silica deposition and the controlling factors occurring in the later stage after precipitation. A study on scaling under controlled hydrodynamic conditions was done by Brown and Dunstall [21] to understand the effects of different hydrodynamic parameters such as fluid velocity on particle transport. The study shows that the overall effect of scaling increases with an increase in flow velocity and particle diameter. The study, however, does not provide a definite theory or model to predict the silica scaling rate.

1.2.1.1 Modeling silica particle transport and deposition in steam flow

A better insight into the mechanism of silica particle transport and deposition can be obtained using Computational Fluid Dynamics (CFD). Computational Fluid Dynamics involves solving mass, energy and momentum conservation equations for different phases of a flow. The particle laden flow involves interaction between two phases of the flow; the particle phase and the gas phase. The order of coupling or the effect of the presence of one phase on the other depends on two factors: volume fraction (α_p) of the particles in the fluid and the ratio of particle relaxation time describing the inertia of a particle to the fluid Kolmogorov time scale. The particle relaxation time (τ_p) and the Kolmogorov time scale (τ_k) are given as:

$$\tau_p = \rho_p \frac{d_p^2}{18\rho v} \tag{1.4}$$

$$\tau_k = \left(\frac{v}{\varepsilon}\right)^2 \tag{1.5}$$

where ρ_p is the density of the particle, d_p is the particle diameter, ρ is the fluid density, v is the kinematic viscosity of the gas phase and ε is the turbulence dissipation rate. Figure 1.2 shows the classification proposed by Elghobashi [22]. For highly diluted flows with $\alpha_p \leq 10^{-6}$, the particles are in a dispersed phase and one-way coupling is used. In one-way coupling, the carrier phase fluid has an influence on particle trajectory but not vice-versa. For larger volume fraction ($10^{-6} \leq \alpha_p \leq 10^{-3}$) two-way coupling is used such that the particles have an effect on turbulence in fluid flow and vice versa. In two-way coupling, the particles enhance turbulence production, while in three-way coupling the particles enhance turbulence dissipation. The degree of influence depends on the ratio of particle relaxation time (τ_p) to the Kolmogorov time scale (τ_K) or the turnover time of large eddies ($\tau_e = l/u$), where l is the turbulent length scale and u is the velocity magnitude. Further increase in particle volume fraction results in increased particle-particle interaction which is referred to as four-way coupling.
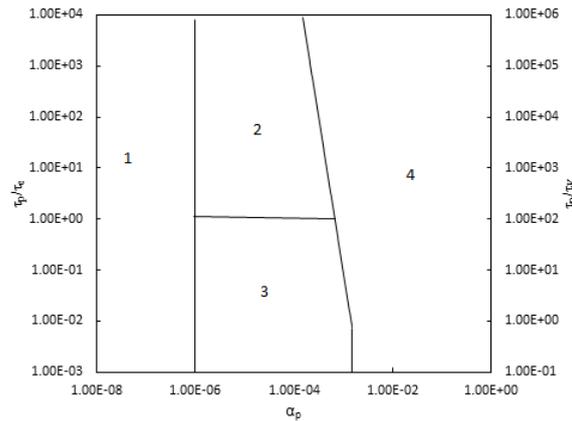
FIGURE 1.2: Classification of coupling schemes and interaction by Elghobashi [22]: (1) one-way coupling (2) two-way coupling with particles enhance turbulence production (3) two-way coupling with particles enhance turbulence dissipation (4) four-way coupling.

For silica in superheated steam flow observed in the geothermal system, the maximum concentration, or the volume fraction of silica in the superheated steam, can be approximated by solubility in superheated steam at a maximum pressure corresponding to the reservoir conditions. Figure 1.3 shows the solubility of amorphous and quartz silica as a function of temperature and pressure obtained using the thermodynamic model proposed by Karsek et al. [23] simulated in MATLAB R2014a. As shown by the magnified right hand view in the figure, the silica solubility increases with increase in pressure. An amount of 66 ppm of precipitated silica was measured in IDDP-1 [14]. This value of concentration corresponds to the region (1) in figure 1.2 with $\alpha_p \leq 10^{-6}$. The present study thus assumes silica in the dispersed phase with superheated steam such that one-way coupling exists between two phases.

(a) Isometric view   *(b) Right hand view*
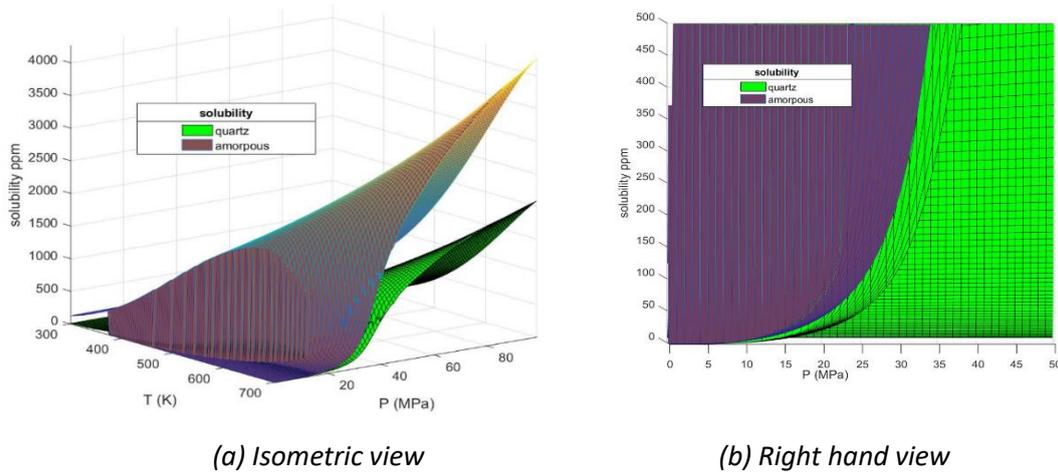
FIGURE 1.3: Amorphous and Quartz solubility at different temperature and pressure: (a) Isometric view; (b) Right-hand view

Researchers have tried various approaches using Computational Fluid Dynamics (CFD) to model two-phase flows. Two major approaches are used for modeling two-phase flow: the Lagrangian tracking approach, where equations are solved for tracking an individual particle in a flow field generated using different methods; and the Eulerian approach, where the particle phase is treated as a fluid-like carrier phase, resulting in a set of continuum equations for conservation of mass, momentum, and energy for the dispersed phase similar to the carrier phase. A detailed literature review regarding modeling transport and deposition of particles in gas flows is given by Guha [24]. Particle deposition in the simulated turbulent field was calculated by Kallio and Reeks [25] using the Lagrangian random-walk approach. The model, however, ignores deposition caused by Brownian diffusion. A similar approach with fluid flow determination using Direct Numerical Simulation (DNS) and Large Eddy Simulation (LES) of Navier-Strokes equations was followed by Ounis et al. [26]. Most commercial computational codes for dispersed particle laden flow are based on the mixed Eulerian-Lagrangian approach, where the fluid flow field is calculated by the Eulerian approach and particles are tracked using the Lagrangian method.

An assessment of particle tracking models for dispersed particle-laden flows was done by Greifzu et al. [27]. Results from the simulation for benchmark problem shows good comparison with the experiments by Fessler and Eaton [28] and by Boree et al. [29]. The Lagrangian tracking models offer a number of advantages in comparison to Eulerian models. Problems involving polydispersity in size, particle growth and particle interaction with the wall boundaries are easy to model using the Lagrangian approach. However, as the number of particles increases, the computation time proportionally increases. To avoid unreasonable computational time, a small number of particles called parcels are tracked to get an overall picture of the flow. However, when the particle concentration needs to be considered, the problem becomes serious. The intensiveness of Lagrangian models provides a good understanding of physics of the flows, but is computationally expensive for application to practical engineering problems.

Predicting particle transport using the Eulerian approach overcomes major disadvantages with the Lagrangian approach. It is more convenient to assume the particle phase as a continuous phase as treated in the Euler-Euler approach which makes the overall computation efficient. Problems involving particle deposition were first solved using Euler-

Euler approach. The Free Flight model based on Euler-Euler approach was given by Friedlander and Johnstone [30] for predicting deposition of small particles suspended in a gas flow through a pipeline. Deposition characteristics are obtained by solving the continuity equation for the particle phase. The Free Flight models assume diffusion of particles in a flow up to a certain distance called the stop distance after which they are assumed to have a free flight to the wall. The model has been frequently used in engineering applications. To predict the deposition characteristics more accurately, modifications were made in the further work done by Davies [31] and Beal [32] based upon the prescription of free flight velocity. Free Flight model, however, has limitations as the particle size increases. The model shows a monotonic increase in deposition velocity with increasing particle relaxation time, which contradicts the experimental values of deposition velocities shown in Section 1.2.1.2 showing the third regime where the particle velocity decreases as relaxation time increases. Later, developments in the Euler-Euler two fluid approach were made as discussed by Reeks [33], where conservation equations were obtained by averaging instantaneous equations of mass, momentum, and energy for the particle phase. The averaged equations obtained are coupled and require closure relations for particle Reynolds stress and carrier flow velocity field. Numerical aspects of the Eulerian two-fluid solver for gas-particle granular flows are discussed by Venier et al. [34]. The model, however, neglects lift force, which plays a major role in transport phenomena for particles in diffusion-impaction regime.

Despite high computation efficiency, application of Eulerian two-fluid approach relies on constitutive relations or closure equations to be obtained by heuristic or empirical approach. A simplified Eulerian model called diffusion-inertia model was developed for isothermal flows by Zaichik et al. [35] and for flows involving heat transfer by Zaichik et al. [36]. Both models are applicable only for low inertia particles. The models are based on the kinetic equation for probability density function of particle velocity distribution which is one way coupled to the fluid Reynolds Average Navier Stokes Equations. The models offer an advantage that solving the particle momentum equation is not necessary and the particle dispersion is solely obtained from the equation of the particle concentration. Later improvements were made by Zaichik et al. [37] in the model using two way-coupling to include the back effect of particles on fluid. The model, however, suffers from the disadvantage of limited application to low inertia particles.

Complexity in Euler two-fluid models can be reduced by using the simple advection-diffusion equation. Advection-diffusion approach for modelling particle deposition on a vertical wall was first applied by Johansen [38]. Major mechanisms contributing to deposition such as Brownian and turbulent diffusion, turbophoresis, Saffman lift, and electrostatic force were accounted for in the model. Further studies on the advection-diffusion model were done by Young and Leeming [39] and by Guha [40]. An important aspect of the model derived independently by Young and Leeming [39] and by Guha [40] is that the advection-diffusion equation is uncoupled from the equation for mean particle velocity which is used in the advection-diffusion equation itself. The deposition features such as wall normal flux and concentration can be successfully reproduced using the model for the case of turbulent flow through a pipe. An improvement in the model was made by Eskin et al. [41] by adding a factor for the probability of particles sticking to the wall applicable to low inertia particles. The study was done for a case of vertical turbulent pipe flow. The numerical model simulation work shows the effect of a change in concentration profile with a change in the probability of particles sticking to the wall. Since the calculation

of the convective velocity is not related to the concentration profile, the effect on deposition velocity is negligible in the inertial limit, as discussed by Guha [24].

Despite having simplicity in solving equations in the advection-diffusion model, difficulty arises in solving problems with particle discontinuities and correct treatment of boundary conditions. A time-marching method was proposed by Slater and Young [42] for calculating two-dimensional, dilute, non-turbulent, gas-particle flows using the Eulerian formulation. The technique is able to overcome problems related to the prediction of density field concentration in the vicinity of discontinuities and particle separations from solid surfaces. Computation using a similar approach including the effect of turbulence was done in the work of Slater et al. [43]. The work involves deriving the advection-diffusion model using the same theoretical approach as described by Young and Leeming [39] with particle continuum equations averaged using density weighted method. The work also shows the application of the derived model for more complicated geometry involving gas-particle flow through turbine.

The dissertation study implements the advection-diffusion model for simulating silica particle transport and its deposition in superheated steam flow using OpenFOAM [44], an open source CFD package. The existing turbulence models and solvers in OpenFOAM were used directly to solve continuum equations for fluid to obtain fluid flow variables, which are required to solve the particle flow equations. Continuum equations for particle flow were written in OpenFOAM notation and boundary conditions are applied directly on the variables as described in Section 2.1.

1.2.1.2 Experimental investigation on particle deposition in phase flow

The two-phase flow models discussed in section 1.2.1.1 are verified using benchmark experiments involving particles in a gas phase, mainly air. No reference to experiments on particle behavior in superheated steam flow was found in the literature. Therefore, it was deemed necessary to experimentally confirm the applicability of two-phase flow models to the particle-steam system. Extensive work regarding experimental studies on particle deposition in vertical tubes with air flow exists in the literature, which was used to inform the design of experiments within this study. Figure 1.4 shows the data from the literature for the variation of non-dimensional deposition velocity (v_+) with respect to non-dimensional relaxation time (τ_+). The deposition velocity is defined as the particle mass transfer rate normalized by the mean or bulk concentration. The equations for non-dimensional relaxation time and deposition velocity are given by Equation 2.17 and 2.18 defined later in Section 2.1.3. The deposition curve as shown by Figure 1.4 is mainly divided into three regimes: diffusion regime, diffusion-impaction regime and inertia regime. The division is based on the type of forces governing the deposition process.
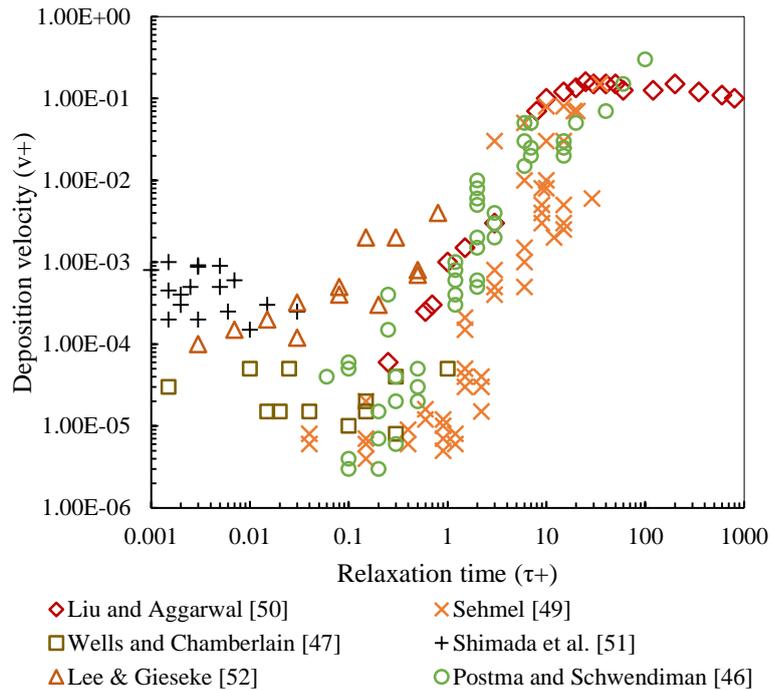
FIGURE 1.4: Results from previous experiments on the variation of non-dimensional deposition velocity with respect to the non-dimensional relaxation time

The first experimental study regarding particle deposition was done by Stavropoulos [45] using 24.5μm lycopodium spores, deposited on a vertical glass tube coated with petroleum jelly. The deposition rate was determined using microscopy, by measuring the flux of deposited particles. Measurements for deposition velocities for flows with varying Reynolds number were made by Postma and Schwendiman [46] for 2-4 μm diameter ZnS particles and 30μm glass spheres. Aluminum, steel and brass tubes of different diameters were used in the study. The experiments were performed in flows with several Reynolds number in the range of 3000 – 20000. Experiments on the effect of surface roughness on deposition were done by Wells and Chamberlain [47]. A hydraulically smooth brass surface and a surface with the fibrous roughness elements with an average length of about 100 μm were selected for deposition. Tricresyl phosphate and polystyrene particles with a relative density of 1.18 and 1.05, and respectively ranging from 0.17 to 5μm of diameter were used. The experimental study was done for a range of flow Reynolds number up to 50000. The result shows a substantial increase in deposition with an increase in surface roughness. Deposition on surfaces with different levels of micro scale roughness was also studied by El-Shobokshy [48] where a substantial effect of surface roughness on deposition was found in the studies. To study the effect of surface roughness on deposition, Sehmel [49] classified some pipes in his study as smooth or rough based on visual inspection. Sehmel [49] concluded an increase in a deposition in one of his experiment and no effect in the other experiment due to surface roughness. Deposition of olive oil aerosols in vertical turbulent flows over a wide range of flow conditions was studied by Liu and Agarwal [50]. The results show that the deposition velocity varies in direct proportion to the square of particle relaxation time. However, at high relaxation time, the deposition velocity decreases as particle size increases. Data for the deposition in diffusion regime by collecting particles on a 6 mm diameter tube is provided by Shimada el. [51]. Lee and Gieseke [52] conducted experiments on deposition onto pipe walls in turbulent flow. The measurement covers both turbulent-diffusion and diffusion-impaction regimes.

12

In order to study the effect of gravitational force on deposition, flow with horizontal configuration is required. Deposition in a horizontal pipe was first studied by Alexander et al. [53]. Water droplets with an average diameter of 25 μm were used. The study concluded that the main resistance to the particle deposition occurs at the viscous layer next to the wall. Namie and Ueda [54] and McCoy and Hanratty [55] carried similar experiments for larger size droplets. It was concluded that for larger size particles, inertial diffusion and gravitational settling are the dominating mechanisms of deposition. Experimental investigation on the deposition of non-spherical particles in turbulent flow was done by Kvasnak el al. [56]. Measurements were done for spherical beads and irregularly shaped dust particles and were compared with the results from empirical models.

Experimental validation of the deposition models, as reported in the literature above, was carried out with air as a flow medium, which is not surprising as most relevant systems refer to particles in the air. The experimental designs used for measuring deposition in the referred studies are not possible to use for a gaseous medium other than air. The current work focuses on the study of deposition occurring in geothermal systems with superheated steam as a transport medium, with precipitated silica particles in a dispersed phase. The particles occurring in geothermal steam flow consist of silica agglomerates of irregular shapes and varying sizes, dependent upon the degree of agglomeration. The flow medium, that is superheated steam, has different hydrodynamic properties from air. The computation model validation for geothermal system applications, therefore, requires an experimental investigation involving silica particles in the superheated steam flow. To achieve this, an experimental setup was designed and constructed and a study was performed to determine silica deposition in superheated steam flow.

1.2.2 Scrubbing superheated geothermal steam

The conventional way of removing impurities from gases is wet scrubbing. The technique is used in various applications such as air pollution control and geothermal industry. Application of wet scrubbers as an effective air pollution control device that can simultaneously remove both gas pollutants and dust particles have been reported by Frack and Nancy [57]. The process of wet scrubbing involves capturing of particles by droplets and gas removal by dissolving or absorption on the droplet surface as explained by Manyele [58]. An experimental study on SO_2 and NO removal from flue gas by wet scrubbing using an aqueous $NaClO_2$ solution was done by Chien and Chu [59]. Results show the possible removal of gas impurities of up to 100%. A study on removal characteristics of HCl gas contaminants by a wet scrubber with different packing materials of a packed bed scrubber at various liquid-gas volume ratio and pH values was done by Han et al. [60]. Results show an increase in gas removal efficiency with an increase in liquid to gas volume ratio. An experiment on HCl gas scrubbing using an alkaline solution in a multistage dual-flow sieve plate wet scrubber was done by Kurella et al. [61]. Results show an increase in gas removal with an increase in scrubbing liquid flow rate, as well as a decrease with an increase in gas flow rate at constant alkaline solution concentration.

In the geothermal industry, the conventional method of wet scrubbing is applied by injecting water or brine into steam to form a two-phase mixture. The impurities are then removed along with the liquid phase in the separator. For HCl abatement from steam, caustic alkali is also used as a scrubbing medium. Details of the method used for HCl abatement in the geothermal power plant are discussed by Paglianti et al. [12]. Conventional wet

scrubbing offers an effective way of removing acid gas or solid impurities from the steam. Application of scrubbing superheated steam using wet scrubbing process, however, has one major drawback, that requires complete quenching of the steam superheat in order to form a two-phase mixture as required for the separation process. The quenching of steam superheat causes loss in power output due to reduced turbine efficiency.

Researchers have proposed various techniques for scrubbing steam in a dry state without quenching the superheat to obtain increased power output. Alternatives to traditional wet scrubbing for removing impurities from superheated steam were proposed by Fisher et al. [62]. Three conceptual techniques were proposed for cleaning of superheated steam i.e. dry scrubbing using agent by adsorption or absorption, oil washing and hybrid washing using the liquid/solid mixture. Experiments for dry scrubbing using amines and calcite bed absorption were made by Hirtz et al. [63]. An effective way of removing HCl from the steam was achieved with minor loss in superheat. The methods proposed in the literature provide ways for HCl abatement from steam without any loss of superheat. The analysis, however, does not take the presence of solid impurities such as silica into consideration. As observed from IDDP-1 well fluid characteristics, silica particles were present in addition to HCl gas in superheated steam due to increased silica solubility at high pressure and temperature as shown in Figure 1.3. The silica present in the superheated steam precipitates as the solubility decreases with decreasing pressure. Utilization of superheated steam thus requires a method to remove silica in addition to HCl gas impurities from steam without any loss in superheat.

1.2.2.1 Treatment with aqueous potassium carbonate

An efficient way of scrubbing superheated steam without any loss in its superheat can be achieved by the application of aqueous salt solutions having boiling point elevation properties as proposed by Weres and Kendrick [64]. The researchers suggested injection of aqueous potassium carbonate solution into a borehole for neutralizing acid gas impurities present in the dry geothermal steam. As described by Ge and Wang [65], the salt decreases the vapour pressure of the water, causing boiling point elevation.

Numerical model development and analysis for the calculation of lifetime of small water droplets containing sodium chloride in a high pressure steam environment were done by Gardner [66]. The result shows a reduction in droplet evaporation due to boiling point elevation caused by salt concentration. For geothermal applications, Weres and Kendrick [64] suggested aqueous potassium carbonate as an optimal scrubbing fluid for mitigating acid gas impurities from the dry geothermal steam. The boiling point elevation property enables the salt solution to stay in steam with a high degree of superheat without precipitation. Figure 1.5 shows the data from the literature for the total pressure above aqueous solutions of potassium carbonate at different concentrations [67]. The total pressure above the solution shown by the logarithmic scale on the y-axis decreases with increase in salt solution concentration. Also, total pressure drop increases with an increase in saturation pressure.
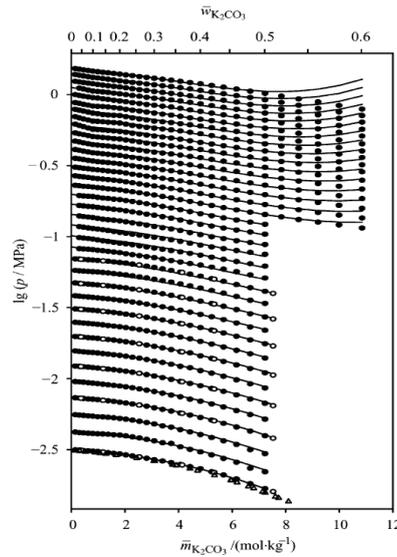
FIGURE 1.5: Total pressure above aqueous solutions of potassium carbonate at different concentration: ● experimental data by Aseyev [68]; o experimental data from Puchkov and Kurochkina [69]; ▲ isopiestic data by Sarbar el al. [70]

Weres and Kendrick [64] suggest injection of aqueous potassium carbonate solution into boreholes for neutralizing acid gas. During the process of borehole injection, the hydrogen chloride gas present in the superheated steam on coming in contact with the salt solution droplet surface causes the following reaction to occur:

$$K_2CO_3(aq) + 2HCl \Rightarrow 2KCl(aq) + H_2O + CO_2 \qquad (1.6)$$
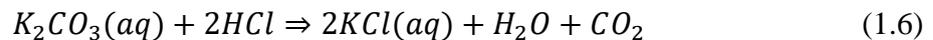
Treatment by injecting salt solution in boreholes as proposed by Weres and Kendrick [64] works well for neutralizing acid chloride impurities without losing superheat. Injection in boreholes, however, suffers from two major drawbacks. First, eliminating potassium chloride formed as the by-product of the reaction shown by Equation 1.6 is difficult. The potassium chloride by-product precipitates once saturation limit is achieved because of its low boiling point elevation. Second, the silica present in gaseous form is left untreated and precipitates whenever pressure drop occurs hence adding to the problem of deposition. To overcome these drawbacks, this dissertation proposes treatment of superheated steam using aqueous potassium carbonate above the surface. The proposed method aims to mitigate both chloride and silica impurities simultaneously as discussed later.

The proposed method follows similar processes and mechanisms for the neutralization of acid gas impurities as that of traditional wet scrubbing applied in geothermal industry. The only difference lies in the scrubbing medium used. In the geothermal industry, HCl removal is done by applying wet scrubbing using caustic alkali. Details of the methods used for HCl abatement in the geothermal power plant are well described by Paglianti et al. [12]. Assuming the proposed method to deliver similar performance as that of the traditional wet scrubbing, the detailed study of scrubbing HCl gas using the proposed method is therefore not detailed any further. The other challenge in the utilization of superheated geothermal steam is the presence of silica. The dissertation will discuss the performance analysis of the proposed method for scrubbing silica particle impurities from the superheated steam.

For solid impurities, scrubbing occurs by the mechanism of diffusion, interception and inertial impaction. The scrubbing efficiency for the process involving spraying liquid in a gaseous medium is governed by parameters and mechanisms such as droplet size, density,

breakup, diffusion, collision, and dispersion. A detailed study of the effect of different parameters affecting scrubbing performance is published by Pak and Chang [71]. For scrubbing solid impurities from the superheated steam using salt solution, an additional parameter effecting the scrubbing performance is the salt concentration. A change in droplet salt concentration causes thermal conductivity and density to change as reported by Liley et al. [72]. Changes in thermal conductivity and density effect the scrubbing efficiency and the degree of superheat retained by the steam.

To study the effect of injected salt solution concentration on steam superheat and scrubbing efficiency, an experimental investigation of the scrubbing process is done. A laboratory scale setup is designed and constructed for performing the experiment. Measurements were made for silica particle concentration, injected solute ion concentration at the endpoint and superheat retained for different solution injection concentrations.

1.2.2.2 Modeling salt solution droplets in superheated steam

Application of aqueous potassium carbonate proposed by Weres and Kendrick [64] for scrubbing acid gas impurities from superheated steam offers the advantage of scrubbing steam without significant loss in its superheat. The actual degree of superheat attained by the droplets without precipitation depends upon factors such as droplet concentration, droplet-steam volumetric ratio, temperature and residence time in the superheated steam flow. A detailed analysis of such a process is therefore required to know the actual performance of the system.

A better understanding of a two-phase flow system with liquid droplets in steam can be obtained using computational fluid dynamics (CFD). Numerical simulation to study the general behavior of a two-phase flow consisting of steam and water in a separator was done by Srikantiah and Wang [73]. The work uses the two-fluid model for simulating phase separation in a steam separator. However, the application is limited to the study of qualitative phenomena in the separator. For the case of wet scrubbing, liquid droplets exist as a dispersed phase in the steam. A detailed description of different phases and their interaction can be obtained using the Eulerian-Lagrangian approach. The approach consists of fluid flow equations as the continuous phase in the Eulerian field and the particles or the droplets are tracked independently in the Lagrangian field. Particle and gas phase equations are coupled to include the effect of one phase on another. A three-dimensional dispersed phase analysis code for studying droplet behavior of a fuel spray system built using Lagrangian-Eulerian approach was applied by Nakeo et al. [74] for studying the boiling water reactor dryer and the separator. The model estimates the amount of carryover at the outlet. However, the detailed behavior of the droplets in the flow passage was not clarified. An improvement for the two-dimensional case study was later made by Nakao et al. [75] for studying detailed behavior of the droplets along the flow taking into consideration the influence of droplet diameter. A numerical study of the droplet behavior in a wave-type flow channel of a separator using the Eulerian-Lagrangian approach was done by Jia et al. [76]. The model includes secondary droplet generation due to impingement of the droplets on the wall. The simulation result shows agreement with the experimental data for pressure drop and separator efficiency. For the process involving liquid injection into superheated steam, the effect of droplet heating and evaporation needs to be included. The first computational study on water droplet injection in superheated steam was carried by Frydman et al. [77]. The model includes the effect of droplet heating and evaporation and is able to predict important features such as steam flow velocity, temperature, droplet trajectories, and deposition on the

wall. The computational results were validated by a pilot-scale experiment. A computational study for a different drying process and its validation with experimental data is reported by Decept et al. [78]. The study uses the computational model proposed by Frydman et al. [77]. Simulation results from the model for the new drying process show agreement with the experimental data.

Water droplets in superheated steam are subject to heating and evaporation by boiling upon reaching boiling point temperature. Also, no evaporation by diffusion occurs in droplets, since the surrounding medium is the same of water. On the other hand salt solution droplets observe boiling point elevation because of dissolved salt ions. Therefore, computational modeling of salt solution droplets in superheated steam flow require calculation of boiling point elevation as a function of droplet salt concentration. The thermodynamic model proposed by Bialik et al. [79] will be used to obtain the value of boiling point elevation.

A computational study of salt solution droplets in superheated steam requires modeling droplets as discrete phase in order to track each droplet with given characteristics such as concentration and temperature independently. During recent years, OpenFOAM [44] as a free and open source software is becoming popular in use for studies involving spray. A solver named *sprayFoam* in OpenFOAM which is based on discrete particle modeling is commonly used in the study of processes involving spray. A study of gas motion generated by dispersion of nonevaporating ultrahigh-pressure diesel spray using *sprayFoam* and Large Eddy Simulation (LES) was done by Tsang et al. [80] and Yousefifard et al. [81]. Flash boiling in gasoline direct injection sprays was studied using OpenFOAM by Khan et al. [82]. Zhou et al. [83] used *sprayFoam* to study spray and thermal characteristics of R404A refrigerant flashing spray. The OpenFOAM includes libraries for thermophysical properties of various fluids including water. The available models and libraries can also be extended and modified as per the case study requirement. The present dissertation work uses OpenFOAM as a platform for modeling salt solution injection in superheated steam.

2 METHODOLOGY

2.1 Simulation of silica particle transport and deposition in superheated steam flow

The advection-diffusion model discussed in Section 1.2.1 needs to be implemented as a numerical model for simulating particles in superheated steam. OpenFOAM is used as a platform for implementing the model. Simulation of the advection-diffusion model requires solving conservation equations for the fluid and the particle phase. OpenFOAM provides built-in solvers for simulating the fluid phase to obtain the fluid flow variable fields which are used as input variables for solving particle phase equations. The particle phase equations, however, need to be implemented as a numerical sub-model.

2.1.1 Conservation equations

The conservation equations for the fluid and the particle phases are described as follows:

2.1.1.1 Fluid phase equations

Relations for velocity profile, eddy viscosity and velocity fluctuations of the fluid flow are required to solve conservation equations for the particle phase. For simple geometries, empirical relations are given by Kallio and Reeks [25]. For more complicated geometries, a more general method of solving conservation equations for the fluid phase is suggested. In the Eulerian frame, for incompressible turbulent flow of the carrier phase, assuming one-way coupling such that the fluid flow is not affected by the presence of particles, the well known Reynolds averaged Navier Stokes equations for mass and momentum conservation are given as:

$$\frac{\partial \bar{u}_i}{\partial x_i} = 0 \tag{2.1}$$

$$\frac{\partial \bar{u}_i}{\partial t} + \bar{u}_j \frac{\partial \bar{u}_i}{\partial x_j} = -\frac{1}{\rho_f}\frac{\partial p}{\partial x_i} + \nu_f \frac{\partial^2 \bar{u}_i}{\partial x_i \partial x_j} + \frac{\partial \overline{u_i' u_j'}}{\partial x_i} \tag{2.2}$$

where $\bar{u}_i$ is the Reynolds averaged velocity in direction i, p is the pressure, ρ_f and ν_f are the fluid density and kinematic viscosity respectively and the last term in equation 2.2 represent the gradient of velocity fluctuations. Velocity fluctuations and the scalar property eddy viscosity can be obtained using two equation turbulence models. A number of turbulence models are available in OpenFOAM [44]. Commonly used two equation models include k-ε model and k-ω model. Details of these models can be found in the literature [84].

2.1.1.2 Particle phase equations

For the particle phase, conservation equations are required for the particle concentration and the momentum balance. The equations are expressed in Cartesian tensor form as:

$$\frac{\partial c_p}{\partial t} + \frac{\partial(c_p v_i)}{\partial x_i} = 0 \tag{2.3}$$

$$\frac{\partial c_p v_i}{\partial t} + \frac{\partial(c_p v_i v_j)}{\partial x_j} = c_p\left(F_{drag,i} + F_{lift,i}\right) \tag{2.4}$$

where v_i is the particle velocity in the direction i, c_p is the particle concentration in mass per unit volume and F_i represents the force per unit mass acting on the particle in the direction i. Forces per unit mass acting on a particle, shown on the right-hand side of equation (2.4) are drag force and lift force and they are defined as follows:

2.1.1.2.1 Drag Force

This force acts as a mechanism by which a particle attempts to gain velocity equal to that of the surrounding fluid. The force acts opposite to the direction of relative velocity of the particle with respect to the fluid, and is given as:

$$F_{drag,i} = \left(\frac{u_i - v_i}{\tau_p}\right) \tag{2.5}$$

where u_i is the fluid velocity in direction i, τ_p is the particle relaxation time which for the Stokes regime is given as:

$$\tau_p = \frac{2\rho_p r_p^2}{9\mu_f} \tag{2.6}$$

where ρ_p and r_p are the density and radius of the particle, respectively, and μ_f is the dynamic viscosity of the fluid.
For particles with large inertia, slip velocity needs to be taken into consideration by incorporating the drag coefficient. The drag coefficient (C_d) is given as [85]:

$$C_d = \frac{24}{Re_p}\left(1 + 0.15 Re_p^{0.687}\right) \tag{2.7}$$

where Re_p is the slip Reynolds number given as:

$$Re_p = \frac{2r_p(u_i - v_i)}{\nu_f} \tag{2.8}$$

where ν_f is the kinematic viscosity of the fluid.
The resulting expression for particle relaxation time considering its inertia is given as:

$$\tau_{p,inertial} = \frac{24\tau_p}{Re_p C_d} \tag{2.9}$$

2.1.1.2.2 Lift Force

The lift force causes the particle to move perpendicular to the direction of flow. The expression for shear-induced lift force as derived by Saffman [86] is given as:

$$F_{lift,i} = 0.725 \sum_{\substack{j=1 \\ j \neq i}}^{3} \left[\left(\frac{\rho_g}{\rho_p} \tau_p \left| \frac{\partial u_j}{\partial x_i} \right| \right)^{1/2} \left(\frac{u_j - v_j}{\tau_p} \right) \right] \tag{2.10}$$

The lift force plays a major role to enhance deposition in the diffusion-impaction regime. After inserting the above expressions for the forces in equation (2.4), averaging needs to be done on equation (2.3) and (2.4) to obtain the final equations. Different approaches have been applied in the literature for averaging. Non-density weighted based Reynolds averaging is applied in Cartesian coordinates by Guha [40] and in cylindrical coordinates by Young and Leeming [39]. Density weighted averaging is used in the work of Slater et al. [43]. The density weighted averaging method offers the advantage of generating fewer turbulence terms. The averaged equations can be simplified further separating particle flux into its convective and diffusive components. However, the final equations obtained are similar to that obtained using the non-density weighted averaged method. The detailed derivation can be found in the work by Slater et al. [43]. The resulting equations are given as:

$$\frac{\partial \bar{c}_p}{\partial t} + \frac{\partial (c_p \bar{v}_i^c)}{\partial x_i} = \frac{\partial}{\partial x_i} \left[(D_B + D_T) \frac{\partial \bar{c}_p}{\partial x_i} \right] \tag{2.11}$$

$$\frac{\partial \bar{v}_i^c}{\partial t} + v_j^c \frac{\partial (\bar{v}_i^c)}{\partial x_j} = -\frac{\partial \left(\overline{\chi u_i' u_j'} \right)}{\partial x_j} + \left(\frac{\bar{u}_i - \bar{v}_i^c}{\tau_p} \right) + 0.725 \sum_{\substack{j=1 \\ j \neq i}}^{3} \left[\left(\frac{\rho_f}{\rho_p} \tau_p \left| \frac{\partial \bar{u}_j}{\partial x_i} \right| \right)^{\frac{1}{2}} \left(\frac{\bar{u}_j - \bar{v}_j^c}{\tau_p} \right) \right] \tag{2.12}$$

where $\bar{v}_i^c$ is the density averaged particle convective velocity, D_B is the coefficient of Brownian diffusion, D_T is the coefficient of turbulent diffusion and χ is the ratio of particle mean square velocity to the fluid mean square velocity. The left hand side of equation 2.12 represents the mean particle acceleration and the right hand side represents the forces per unit mass producing their acceleration. Closure of equations require values of these variables.

For a two dimensional boundary layer type flow with wall parallel to the direction of flow, assuming all forces in the direction *i*, normal to the wall to be neglected except the viscous drag and Reynolds stress, Equation 2.12 reduces to,

$$\rho_p v_i = -\tau_p \rho_p \frac{\partial \left(\overline{\chi u_i' u_i'} \right)}{\partial x_i} \tag{2.13}$$

The term on the right hand side of equation 2.13 represents the gradient of wall-normal component of the particle Reynolds stress which causes a drift flux of particles towards the wall. This phenomena is known as turbophoresis [87].
The value of Brownian diffusion is expressed by Einstein equation taking Cunningham correction for rarefied gas effects

$$D_B = \frac{K_B T_f (1 + 2.7 Kn)}{(6 \pi \mu_f r_p)} \tag{2.14}$$

where K_B is the Boltzmann constant, Kn is the Knudsen number and T_f is the fluid temperature.

Assuming isotropic turbulence, the value of the turbulent diffusion coefficient is estimated using Schmidt number which is assumed close to unity, therefore:

$$D_T = \nu_T \tag{2.15}$$

where ν_T is the turbulent viscosity of the gas.

In the case of a homogeneous isotropic turbulence, for a particle to be in local equilibrium with the turbulence, a relation for the mean square velocity ratio is available in the work by Reeks [88]. The relation is expressed as:

$$\chi = \frac{t_L}{\tau_p + t_L} \tag{2.16}$$

where t_L is the Lagrangian time scale for fluid turbulence given as:

$$t_L = \frac{\nu_T}{u_i' u_j'} \tag{2.17}$$

where u_i' and u_j' denotes the fluctuating part of the fluid velocity in i and j direction respectively

2.1.2 Implementation of advection-diffusion model in OpenFOAM

2.1.2.1 Fluid phase equations

The fluid flow variables; pressure and velocity fields are obtained using the solver *simpleFoam* [44]. The solver is based on SIMPLE algorithm [89] for accomplishing pressure-velocity coupling. A turbulence model is required in the solver to simulate turbulence. A number of models are available in OpenFOAM for simulating turbulence. The k-ω model was chosen and is available on OpenFOAM with *kqRWallFunction* and *omegaWallFunction* options, which are specified in wall boundary conditions for transport variables. Details of the chosen schemes for discretization, interpolation, and methods for solving equations are specified in Table 2.1. Note that good accuracy in the values of root mean square velocity and turbulent diffusivity are required near wall boundaries, in order to predict deposition accurately. Empirical relations from Kallio and Reeks [25] can be used as well. Application of the available turbulence models obliges to make some compromise in the accuracy of variables.

Table 2.1: Numerical methods and finite volume schemes for solving fluid flow equations required for the advection-diffusion model

Numerical method	P	U
solver	GAMG	smoothSolver
smoother	GaussSeidal	GaussSeidal
Under relaxation factor	0.3	0.7
Finite volume schemes		
divergence	Bounded Gauss linear	
Gradient	Gauss linear	
interpolation	linear	
Laplacian	Gauss linear corrected	

2.1.2.2 Particle phase equations

The solution for the velocity field of the fluid phase can be obtained directly using existing solvers and utility functions available in the OpenFOAM package. Since the problem assumes one-way coupling such that the fluid phase flow has an effect on particle phase flow but not vice-versa, the calculated fluid flow variables can be used directly in the equations for the particle phase. To solve the particle phase equations, the conservation equations need to be implemented to build up a new solver. The implemented model simulation starts with solving the momentum equation (2.12) to obtain a velocity field used in equation (2.11) to obtain the particle concentration. For solving the particle momentum equation, the field for different forces must be calculated. The calculation of the drag and the lift forces representing second and third term on the right-hand side of equation (2.12) requires calculation of particle relaxation time; which can be calculated using equation (2.9) using the initial particle velocity field, calculated fluid velocity field and particle radius and density. The turbophoretic force, represented by first term on right side of equation (2.12) acting due to turbulence gradient in flow field is calculated by summing up the gradient of the product of the mean square velocity ratio obtained using equation (2.16) and equation (2.17) and fluid mean square velocity obtained by solving fluid flow equations. Other forces such as gravitational and electrostatic forces can also be added on the right-hand side of equation (2.12) if required. Equation (2.12) can be solved directly using available solvers using time marching techniques. Obtaining the field for convective field velocity, the diffusion equation (2.11) is solved for particle concentration using any conservative solver available. For the present study *smoothSolver* was used. The values of concentration, velocity field and their flux are updated in the runtime loop until a steady state solution is achieved. A flowchart for the algorithm of the solver is shown in Figure 2.1. The initial conditions correspond to the inlet pressure and the outlet velocity field of fluid and particle inlet concentration. The final outcome from the solver is the concentration and the velocity field of the particle phase. Numerical methods and finite volume schemes chosen for solving the equations are given in Table 2.2.

Table 2.2: Numerical methods and finite volume schemes available in openfoam, selected for solving particle phase equations 2.11 and 2.12.

Numerical method	C	v^c
solver	smoothSolver	smoothSolver
smoother	symGaussSeidal	symGaussSeidal
Finite volume schemes		
divergence	Gauss linear upwind	
Gradient	Gauss linear	
interpolation	Linear	
Laplacian	Gauss linear upwind	
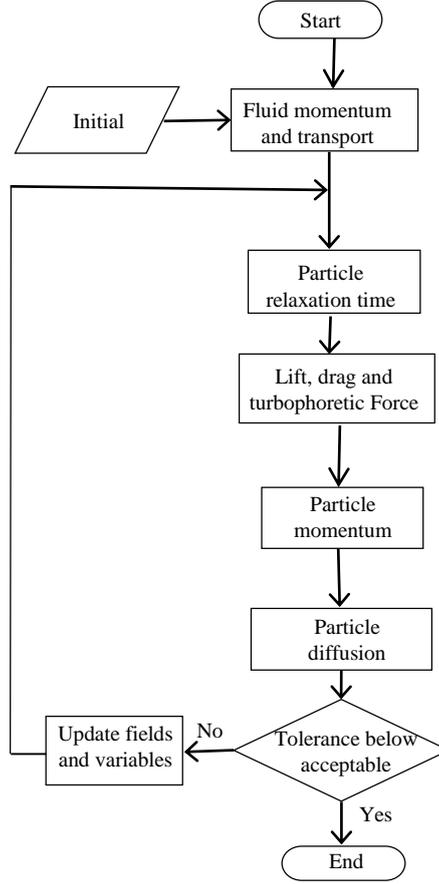
FIGURE 2.1: Flowchart for advection diffusion model as implemented in OpenFoam

2.1.3 Deposition modeling parameters and boundary conditions

The solver was used for studying silica particle transport in superheated steam flow. The input conditions for the simulation are kept consistent with that of the experiment. To compare the results from the simulation to that available in the literature for particle and air flow, the deposition velocity (v_{dep+}) and particle relaxation time (τ_+) are non-dimensionalized. The particle relaxation time and deposition velocity in non-dimensional form are given as:

$$\tau_+ = \frac{\tau_p u_*^2}{\nu_f} \tag{2.18}$$

$$V_{dep+} = \frac{J_w}{u_* \bar{c}_p} \tag{2.19}$$

where J_w is the particle flux per unit area towards the wall, $\bar{c}_p$ is the mean flow concentration and u_* is the friction velocity given as:

$$u_* = V_{av} \sqrt{\frac{f}{2}} \tag{2.20}$$

where V_{av} is the average fluid velocity and f is the Fanning friction factor calculated using Blasius law for turbulent flows and smooth walls given as:

$$f = 0.0791 Re^{-0.25} \tag{2.21}$$

Figure 2.2 shows the mesh description of the pipe. Block mesh structure is used such that the number of mesh per unit length increases towards the wall. This is done in order to capture concentration gradient, which increases sharply near the wall due to high turbulence gradient nearby the wall. The smallest size of the mesh is kept equal to the radius of the particles in the flow. The boundary conditions applied near the wall are perfect absorbing which assumes that the particles stick to the wall once they hit. To obtain perfect absorption, zero gradient particle concentration and velocity are applied.
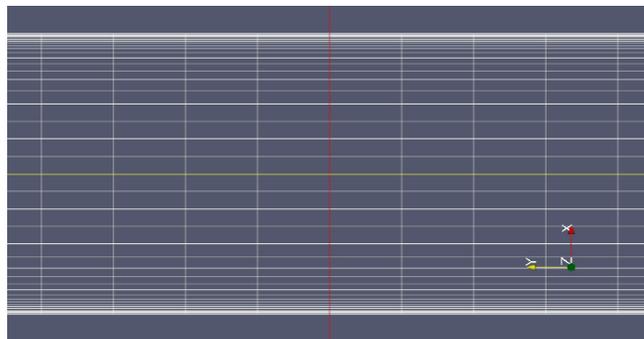
FIGURE 2.2: Mesh description for the pipe

2.2 Silica particle deposition in superheated steam flow: Experimental investigation

For validation of the computational model for simulating silica particles in superheated steam flow similar to IDDP, experiments for measuring silica particle deposition on a laboratory scale were performed. The experimental study performed was limited by factors such as the pressure and temperature of the steam from the boiler. The steam was, however, superheated in order to achieve gaseous phase without any liquid. The particle characteristics are described by non-dimensional relaxation time which is a function of particle diameter, density, flow velocity, and viscosity. The deposition velocity is normalized with respect to the mean concentration.

2.2.1 Experimental Setup

Figure 2.3 shows a schematic diagram of the experimental setup. The picture of the experimental setup is shown by Figure A.1 given in Appendix A. The setup consists of three subsystems: the steam generating system, the particle injection system and the test section assembly. The steam generating system consists of an 18 kW electric boiler with a water storage tank for a continuous supply. An airflow line from the compressor with a control valve (Cv_2) is connected to the steam flow line after the gate valve (Cv_1). This is required to run the setup with air at the beginning and at the end of the experiment. The wetness in the steam coming out from the boiler is removed in the cyclone separator (S_1). The saturated steam is then passed through a 500 W superheater (SH) to attain the superheat. The particle injection system (Figure A.2) consists of a micro screw feeder with a variable speed motor drive to control the feed rate. The micro screw feeding mechanism provides an almost constant feed rate of 40 mg min^{-1}. The particles delivered by the screw feeder are injected into the mainline by suction through the ejector. The ejector system provides an easy way to inject particles into the steam by mixing a fraction of air with the steam. This overcomes the drawback of using aerosol generators with air as the only carrying medium, as used in

experimental studies from previously defined literature. The mixing of a small quantity of air into the superheated steam is justified by the fact that the geothermal steam from the well also consists of additional non-condensable gases. The particle and steam mixture flows into another cyclone separator (S_2). The separator works as a mixing chamber and gives time for larger agglomerated particles to break up in order to form a uniform mixture and reduce eddies in the flow, which keeps the particles in the required relaxation time range.

The particle deposition test section consist of two 1.5 m long concentric steel pipes with outer diameter of inner pipe of 17.5 mm and inner diameter of outer pipe of 22.5 mm. The particles are deposited on the outer surface of the inner pipe. To facilitate access to the inner pipe, the ends of the pipe were fitted with a thread and screw attachments for closure, making pipe removal easy as required for sampling. The outer pipe consists of a conical section such that the annulus area decreases by a ratio of 1:10 at the entrance. The conical surface of the outer pipe contains an inlet to which a stainless-steel probe is attached, which is used for collecting particles and for measurement of the mean concentration of the mixture. The probe, which has a length of 10 cm and a diameter of 3.65 mm was sharpened at the front, while the other end was connected to a cone-shaped flask made of cast iron (Figure A.3). The material selection allows the flask to be heated in order to avoid condensation on the filter paper. The flask contains a wired mesh serving as a seat for the filter paper to collect particles. A membrane filter paper with 0.45μm pore size and 47 mm diameter is used for collection. The filter is stable in steam up to a temperature of 180℃. The flowing steam is passed through a control valve (Cv_5) to control the flow rate through the probe. The steam is then passed through a condenser (C_1) and then collected to measure the flow rate through the probe. The steam from the test section is also collected after condensation in the condenser (C_2) to measure the total flow rate. The system is well insulated and heated using heating tape to avoid heat loss from the flow.
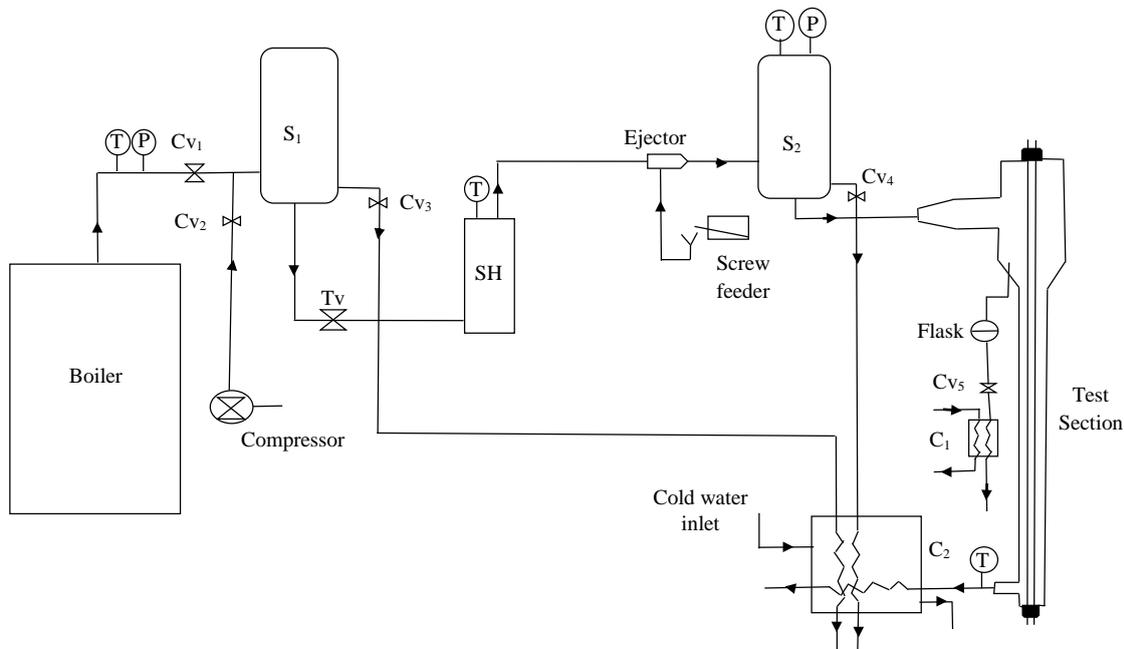

FIGURE 2.3: Schematic diagram of the experimental setup

2.2.2 Measurement procedure

The system was run with air in the beginning by keeping the control valve (Cv_1) closed and valve (Cv_2) open. The superheater (SH) was switched on to heat the setup using air. To ensure that there was no condensation in the test section at the start when the system was run using steam. Once the surface temperature of the equipment approaches the desired temperature for the experiment, control valve (Cv_2) was shut down and control valve Cv_1 opened. The steam was initially run through the system with air suction in the ejector and without particle feeding until steady mass flow, temperature, and pressure were obtained. The boiler capacity limits the steam flow rate, therefore the system was always run constantly at a mass flow rate of 150 l min^{-1} and a saturated pressure of 4.5 bar to achieve a steady state in the experiment. A large pressure drop occurs in the ejector due to an expansion of steam from the ejector nozzle. The inlet mixture to the test section was at 160°C and 1.4 bar. The temperature and pressure conditions during the experiment were low in comparision to the state of fluid from IDDP-1 well. However, the degree of superheat kept during the experiment is considerable in order to justify the model applications for simulating high temperature and pressure environment. Superheat of the steam flow up to 48 degree, kept during the experiment is enough to assure two-phase conditions consisting of dry steam with silica in dispersed phase. The flow had a Reynolds number of 3800 corresponding to a hydraulic diameter of 5 mm, a flow velocity of 16 ms^{-1}, and a dynamic viscosity of 14.6 μPa-s. The particles used in the experiment were silica fume of density 2200 kgm^{-3} with 97% purity. Silica fume is an amorphous polymorph of silica dioxide and thus possesses similar characteristics in terms of density, size and shape to the silica found in geothermal systems precipitated from solution in superheated geothermal steam. Silica fume has a grey color due to a minute percentage of carbon impurities, which increase its visibility on filter paper. The maximum particle concentration was kept less than 0.5% by weight, similar to the concentration observed in IDDP-1; which corresponds to a volume fraction of less than 10^{-6} to ensure one way coupling between the particle and flow turbulence as per the classification suggested by Elgobashi [22]. One experimental run consisted of steam and particles flow for an average duration of an hour, then shutting down the steam flow and particle injection. Finally, air was run again for a few seconds to remove all steam from the test section in order to avoid condensation upon cooling. The deposited particles were collected during the experimental run on a polished pipe surface in the test section, coated with polytetrafluoroethylene (PTFE) lubricant. The lubricant is thermally stable and insoluble in water. Coating causes a decrease in the coefficient of restitution, which is defined as the ratio of particle velocity after the impact to the velocity before the impact. Decrease in coefficient of restitution causes an increase in the energy loss of particles striking the surface, hence reducing the likelihood of rebound or re-entrainment from the surface. The test pipe section was coated with the lubricant to collect the total flux of particles striking the wall. The actual deposition rate on the surface is however, governed by the net flux of particles sticking to the wall. For flow with wet surface boundaries or high roughness occurring due to erosion or pre-existing deposits, it is high likely that the total flux of particles towards the wall are deposited. For smooth surfaces with no wetness, the actual rate of deposition depends upon the interacting forces between the particle and the surface which mainly are electrostatic, lift and drag force. Simulation and experimental

study was done by Abd-Elhady et al [90] regarding particle fouling in the heat exchanges. Result shows a limiting flow speed for particle of each size above which fouling is unlikely to occur. The limited speed is calculated based on the minimum velocity required to cause rolling movement of the particle against the drag and electrostatic forces. However, for any flow with particles of varying size, it is important to note that as the flow velocity is increased to reduce fouling, relaxation time of smaller particles increases which causes increase in deposition velocity as shown later. In addition, the maximum flow velocity is also limited by the amount of pressure loss in the heat recovery system. The increase in fluid velocity up to a limit is therefore supposed to have negligible effect on the total deposition rate. Considering the above mentioned factors for different surface conditions, it is ideal to follow an approach of measuring the total particle flux towards the wall and characterizing the deposition based upon the relaxation time.

In order to quantify particle deposition, a particle sampling and counting technique using a digital microscope and image processing was used, as described by Kvasnak et al. [56]. The surface of the pipe was heated using an induction coil as shown by Figure A.6. Heating was done to remove the lubricant by vaporization in order to enhance visibility. The images are then captured using a digital microscope as shown by figure A.7. The particle flux J_w towards the wall is calculated using an equation given as:

$$J_w = \frac{N_w}{t \cdot A_{image}} \tag{2.22}$$

where N_w is the number of particles for a given size on the surface image, A_{image} is the area of image of the surface and t is the time duration of the sampling.

To determine the mean flow concentration, flow samples were taken using the probe over a time span of 15 minutes. For isokinetic sampling, flow velocity through the probe was kept consistent with that inside the pipe. The required flow rate through the probe was obtained by adjusting the control valve (Cv5). The filter paper images were taken carefully after removing the filter paper from the flask.
The mean particle concentration is then given by:

$$\bar{c}_p = \frac{N_{filter} A_{filter}}{A_{image} A_{probe}} \frac{1}{t \cdot V_{probe}} \tag{2.23}$$

where N_{filter} is the number of particles of specific size on filter paper image, A_{filter} is the filter area, A_{probe} is the inlet cross section area of the probe and V_{probe} is the flow velocity through the probe.

The non-dimensional deposition velocity, V_+, is then given by:

$$V_+ = \frac{J_w}{u^* \bar{c}_p} \tag{2.24}$$

where u^* is the friction velocity defined in Section 2.1.

For particle distribution measurement, digital images of the surface with a picture area of 384μm by 288μm were statistically analyzed using ImageJ [91]. Figure 2.4 shows the resulting images from various steps of image processing, which are: original image (fig. 2.4a), filtered image (fig. 2.4b), threshold reverse image (fig. 2.4c), and the analyzed image (fig.2.4d). The silica particles are agglomerated, making their shape irregular. The current

approach assumes the projected area diameter as the diameter of a particle with a spherical shape. The number of particles in a given size range is obtained by averaging the size distribution measured from different sample images. Considering the size of each pixel, each particle size is averaged with a bandwidth of $\pm 0.5\mu m$.

(a)   *(b)*

(c)   *(d)*
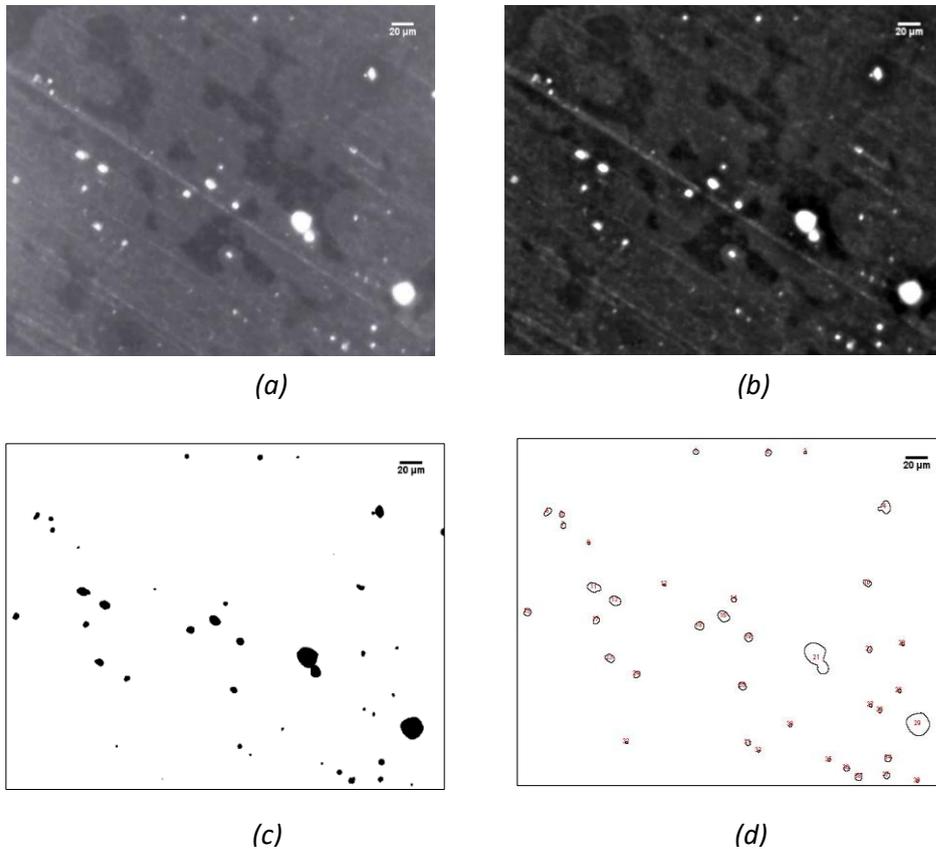
FIGURE 2.4: Images of the deposited particles on the surface (a) Original image (b) filtered image (c) threshold reversed image (d) analyzed image

2.3 Superheated steam scrubbing using aqueous potassium carbonate solution

Treatment of superheated steam by injecting aqueous potassium carbonate into the borehole as suggested by Weres and Kendrick [64] works well for neutralizing acid gas impurities. However, the method suffers from a drawback of the inability to get rid of the precipitates of the reaction by-product and other solid impurities from the borehole. To overcome this drawback, the dissertation proposes treatment of the superheated steam above the surface. As explained by Hirtz [11], the acid chloride gas does not cause corrosion with the steam flow when kept above a certain degree of superheat. Thus, steam come from the well without treatment is a better option, and hence not quenching the steam superheat. Thereafter, once the superheated steam reaches the surface, treatment with potassium carbonate is followed. Scrubbing superheated steam with characteristics of the fluid from IDDP-1 well requires simultaneous removal of chloride and silica impurities. Treatment for mitigating chloride using aqueous potassium carbonate solution can be applied using a similar mechanism as that of used for the traditional wet scrubbing. A study on characteristics and performance of a wet scrubbing process using aqueous sodium hydroxide was done by Culivicchi et al [92].

The scrubbing system investigated was installed in five locations for wells in Larderello geothermal field. The system consist of a spraying nozzle for scrubbing solution injection, a mixer line and a cyclone separator with a vane type demister. Data shows required performance achieved by the scrubbing units under observation. Wet scrubbing using aqueous sodium hydroxide occurs by reaction of chloride ions present in the two-phase flow which react with the sodium ions present in the liquid phase injected. The product of the reaction is sodium chloride which stays in the liquid phase of the two phase mixture due to its high solubility and is removed along with the liquid phase in the separator. Scrubbing superheated steam with high chloride impurities using aqueous potassium carbonate can be applied using same component assembly as that used for normal wet scrubbing. The process of scrubbing superheated steam, however, is governed by different principle of physics. The chloride in superheated steam is present in the form of HCl gas molecule. The gas molecule diffuses on the surface of liquid solution injected and then decomposes to hydrogen and chloride ions which then reacts with potassium ions present in the solution to form potassium chloride. The injected potassium carbonate also reacts with other impurities such as hydrogen fluoride and boric acid if present. The by-product formed precipitates due to its low solubility at high degree of superheat. The by-product, however, is suppose to stay as a separate undissolved solid phase with the liquid phase potassium carbonate solution forming a slurry. The solid-liquid phase separation is not supposed to occur in a normal cyclone separator designed for droplet-steam separation having high density ratio. The separation process, therefore, occurring while scrubbing superheated steam with aqueous potassium carbonate consist of removing salt solution droplets consisting of undissolved solid impurities from the superheated steam. The process of removal of solid impurities which do not dissolve in the liquid phase is also evident from the application of venturi scrubber for removing titanium oxide particles of mean diameter $1\mu m$. Experimental investigation done by Ali et al. [93] shows particle removal upto 99.5% achieved using water as a scrubbing agent. Separating liquid and solid phase require high rpm centrifugal separators for separation of the precipitated salt from the slurry [94]. A detailed investigation of the separation process is a scope for future study. The present work is limited to the study of scrubbing silica from superheated steam.

Scrubbing efficiency of a process is defined as the fraction of total concentration of the impurities removed from the flow medium. Achieving complete scrubbing efficiency using liquid droplet injection in a gas medium is difficult. The scrubbing process occurs by droplet breakup and attachment of the solid impurities by collision. The particle impurities with size below micro level have chances to get carried further with the steam without separation. To avoid deposition due to smaller size particles, application of heat recovery system after the separator is a viable option. Since the surface profile of a heat recovery system is straight, smaller particles with low relaxation time cause far less deposition. A feasible option to utilize superheated steam with silica and chloride impurities would be to use thermodynamic cycle with a heat recovery system as proposed by Hjartarsson et al. [7], with an additional scrubbing using aqueous potassium carbonate. For this, a thermodynamic cycle combining heat recovery and scrubbing using aqueous potassium carbonate is proposed. To demonstrate the improved performance obtained using the proposed cycle, a case study for well IDDP-1 is done. Figure 2.5 shows the fitted curve for the measured mass flow rates for well IDDP-1 as a function of wellhead pressure obtained during the flow test. The fluid enthalpy is set to 3100 kJ/kg [7]. Thermodynamic analysis of the proposed power cycle with a heat recovery system, along with utilizing the method of scrubbing with aqueous potassium carbonate, was done and compared to a power cycle utilizing traditional wet

scrubbing. Conservation laws for each component and a cycle as a whole are applied. For thermodynamic analysis, it is required to have boiling point elevation of the injected salt solution as a function of temperature and concentration. To obtain this, a thermodynamic model proposed by Bialik et al. [79] is used. Thermodynamic performance is calculated and compared in terms of exergy which represents the true performance of a thermodynamic system. Exergy destruction and loss of each component are calculated to know the overall contribution of each component to the cycle performance.
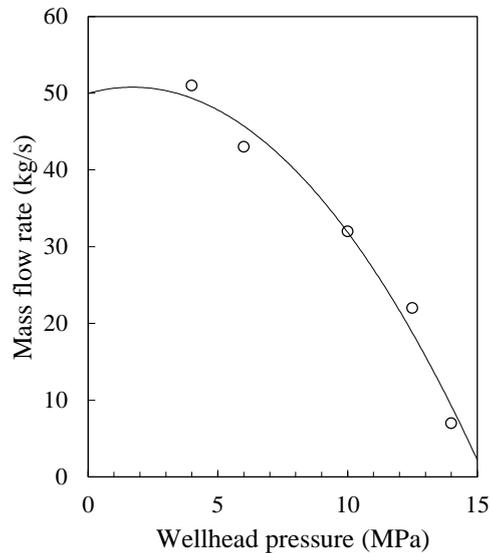

FIGURE 2.5: Fitted curve from the measured mass flow rate for IDDP-1

2.3.1 Proposed cycle

A schematic diagram of the baseline cycle utilizing aqueous potassium carbonate solution for scrubbing is shown in Figure 2.6. The superheated steam from the well at state point 1 is passed through a scrubbing unit before entering the heat recovery system at state point 5. The minimum amount of aqueous potassium carbonate to be added for scrubbing is governed by the amount required to neutralize the chloride impurity present in the steam. The amount of water in the solution is then governed by the level of superheat to be kept in the treated steam to prevent the by-product salt from precipitating. Injection of additional concentration of potassium carbonate into the scrubbing medium changes the limit of the degree of superheat that can be retained. As discussed in the previous section, the maximum degree of superheat, the steam can retain is governed by the solubility limit of potassium carbonate. For the superheated steam with chloride impurities, the precipitation of potassium chloride formed as the by-product of the reaction does not affect the superheat limit achieved as long as potassium carbonate is present in the solution. Presence of potassium carbonate in the solution having high degree of superheat causes formation of the slurry with the potassium chloride precipitate and therefore can be removed at the end point. Assuming thermal equilibrium between the liquid droplet and the superheated steam at the end point, the amount of water to be added into the solution is therefore decided by the heat to be removed from the superheated steam to achieve the final temperature of the flow system below the temperature of maximum degree of superheat, potassium carbonate solution can have at its maximum solubility limit for a given pressure. The amount of liquid injected would be therefore adjusted to provide the remaining superheat desired. In addition, the volumetric ratio of the salt solution to steam must be sufficient to enable effective scrubbing

30

of the steam. However, an increase in scrubbing efficiency can be obtained by increasing the residence time of the solution droplets in the scrubbing unit.

The saturated solution droplets mixed with the impurities and the by-product of the scrubbing are removed in the separator (S_1). Steam passing through the turbine at state point 10 requires a high degree of purity. To achieve this, a highly efficient removal is required in the separator S_1. The injected salt solution droplets and smaller size silica particles have chances to be carried away with the steam. An effective way of removing droplets from the steam can be achieved by controlling the injected droplet size distribution and by the application of additional components such as demisters. A way to control the droplet size distribution can be obtained by fixing spray nozzle injection parameters such as injection flow rate and pressure as discussed by Paglianti et al [12]. The detailed investigation is beyond the scope of this study and not discussed any further.

Presence of minute silica impurities escaping the removal and separation process can cause problem to the turbine effectiveness. The minute impurities can cause deposition occurring by impaction mechanism due to the curved profile of the blades. Therefore, the superheated steam is passed through the heat recovery system at state point 5 until saturation. Since particles with higher relaxation time are mostly removed by scrubbing in the separator, a lower rate of deposition is expected to occur as the leftover particles have a small size and thus have low relaxation time. In addition, plane surface profile of the heat recovery system also minimizes impaction that occurs on the surfaces with bends. The deposition occurs mainly due to turbulent and Brownian diffusion, contributing far less to deposition as compared to impaction. The saturated steam at the end of the heat recovery system (state point 6) is throttled to lower down the saturation temperature and gain pinch point difference temperature for the heat recovery system. To remove the remaining impurities present in the two-phase steam-liquid mixture, second separation is done causing leftover impurities to be removed in the liquid phase at state point 8. An improvement in removal efficiency can be obtained by an additional scrubbing using pure water if required. The additional scrubbing before separation, however, will not cause significant loss in work output efficiency since the steam is already in the two-phase state without any superheat. The steam then regains the superheat before entering the turbine. Figure 2.7 shows the pressure-enthalpy diagram for the proposed cycle.

FIGURE 2.6: Schematic of the proposed cycle

FIGURE 2.7: Pressure-enthalpy diagram for the proposed cycle, state numbers refer to Figure 2.6

2.3.2 Thermodynamic cycle analysis

Thermodynamic analysis of a power plant cycle requires applying three different laws for each component and the cycle as a whole. The first law relates to the conservation of mass entering and exiting a system in a steady flow. The second law refers to the conservation of energy for any system given by the first law of thermodynamics. The third law restricts the total conversion of heat into useful work by the second law of thermodynamics. The second law of thermodynamics describes the exergy term, which defines the maximum amount of useful work that can be obtained from a given heat source. The actual work obtained is always less than the maximum useful work because of the irreversibility due to entropy generation in any real process.

For a control volume with no chemical reaction, the equations for mass balance, energy balance, and exergy flow rate for steady flow are as follows [95]:

For any component of the cycle with no mass accumulation, the law of mass conservation is given as:

$$\sum \dot{m}_{in} = \sum \dot{m}_{out} \qquad (2.25)$$

where $\dot{m}$ is the mass flow rate of the working fluid in the cycle.

The first law of thermodynamics defining general steady-state energy balance for each component and the complete cycle is given as

$$\sum \dot{m}_{out} h_{out} - \sum \dot{m}_{in} h_{in} = \dot{Q} - \dot{W} \qquad (2.26)$$

where h is the enthalpy, $\dot{Q}$ is the heat, and $\dot{W}$ is the work exchange.

The flow exergy $(\dot{\epsilon})$ at each point of the system in a steady state is given as:

$$\dot{\epsilon}_i = \dot{m}_i [(h_i - h_o) - T_o(s_i - s_o)] \qquad (2.27)$$

where h_i and s_i are the enthalpy and entropy at point i, T_o, h_o and s_o are the reference state point temperature, enthalpy, and entropy. The reference state is assumed to be that of the surrounding.

For any real thermodynamic system, work loss occurs due to exergy destruction and exergy loss. Exergy destruction can occur due to friction or heat transfer across a temperature gradient, and the exergy that has been destroyed cannot be recovered. Exergy loss, on the other hand, defines the exergy lost to the outside environment which could have been used to extract work. In geothermal systems, exergy loss occurs when geothermal brine is reinjected into the ground.

For a system with no heat exchange with the surroundings, the actual work done $(\dot{W})$ is given as:

$$\dot{W} = \dot{\epsilon}_{in} - \dot{\epsilon}_{out} - \dot{\epsilon}_D - \dot{\epsilon}_L \qquad (2.28)$$

where subscript D and L denote destruction and loss of exergy, respectively.

Equations for thermodynamic analysis for each component of a geothermal power plant are described as follows:

2.3.2.1 Turbine

Work output is calculated assuming a value of isentropic efficiency for the turbine (η_T) given by

$$\eta_T = \frac{h_{in} - h_{out}}{h_{in} - h_{out,isen}} \qquad (2.29)$$

where the subscript on the enthalpy *in*, *out* and *out,isen* represents the inlet, out and the isentropic value at the outlet respectively.

The work output from a turbine is given as

$$\dot{W}_T = \dot{m}_{in}(h_{in} - h_{out}) \qquad (2.30)$$

For the efficiency of a turbine changing with the quality of steam, the isentropic efficiency of the turbine with a wet steam flow is estimated using the Baumann rule [96]:

$$\eta_{T,wet} = \frac{\eta_{turb,dry}(1+x_{out})}{2} \tag{2.31}$$

where $\eta_{t,dry}$ is the efficiency of turbine with dry steam, assumed to be 85% [97] and x_{out} is the dryness fraction at the exit of the turbine.

2.3.2.2 Injection and separation

For the case of traditional wet scrubbing, the amount of water added to superheated steam must surpass that required to make the steam saturated at a given pressure. In the case of aqueous potassium carbonate injection, the steam will still be in a superheated state at equilibrium while at a temperature below the boiling point of the salt solution for a given pressure. The degree of superheat available below the solution boiling point without salt precipitation as a function of pressure is calculated using the thermodynamic model discussed in Section 2.3.3. Therefore the amount of liquid injection required is smaller than in wet scrubbing. A concentration balance is required between the injected liquid at state point 2 and the droplets at the exit of the scrubber at state point 3 shown in Figure 2.6. The concentration balance equation is given as:

$$\dot{m}_2 c_2 = \dot{m}_{3,l} c_{3,l} \tag{2.32}$$

where c_2 and c_3 are the concentration of salt, and subscript l denote the liquid phase.

The mass of steam at the exit of the scrubbing unit is equal to the sum of mass entering and mass of liquid vaporized given by:

$$\dot{m}_{3,s} = \dot{m}_1 + \dot{m}_2 - \dot{m}_{3,l} \tag{2.33}$$

where subscript s denotes the steam phase. The enthalpy of the steam exiting corresponds to the superheated state at a temperature of precipitation limit of the salt solution injected.

The energy balance equation for separator 1 is given as:

$$\dot{m}_3 h_3 = \dot{m}_4 h_4 + \dot{m}_5 h_5 \tag{2.34}$$

2.3.2.3 Heat recovery and separation

The superheated steam entering the heat exchanger is made saturated and then throttled down at point 6 before separation. Throttling causes temperature drop required for heat exchange at constant enthalpy. A minimum pinch point difference is kept in the heat exchanger. The energy balance equations for the unit are given by:

$$\dot{m}_5(h_5 - h_6) = \dot{m}_9(h_{10} - h_9) \tag{2.35}$$

$$h_6 = h_7 \tag{2.36}$$

The energy balance equation for separator 2 is given as:

$$\dot{m}_7 h_7 = \dot{m}_8 h_8 + \dot{m}_9 h_9 \tag{2.37}$$

2.3.2.4 Condenser and reinjection

The working pressure of the condenser is set as 0.1 bar [7]. The heat transfer in the condenser section ($\dot{Q}_C$) is given as:

$$\dot{Q}_C = \dot{m}_{12}(h_{11} - h_{12}) \tag{2.38}$$

The total exergy destruction in the condenser is considered as the sum of exergy destruction due to heat transfer and exergy loss by transfer of exergy to the cold fluid. Since no useful work is done in the condenser, the total exergy destruction is represented by the equation given in Table 2.3. Reinjection causes loss of the remaining exergy in the geothermal fluid. The equation for calculation is given in Table 2.3.

Table 2.3: Relations for exergy destruction and loss in cycle components

Component	Exergy relations
Turbine	$\dot{\epsilon}_{D,HP} = \dot{\epsilon}_{10} - \dot{\epsilon}_{11} - \dot{W}_T$
Throttle	$\dot{\epsilon}_{D,T} = \dot{\epsilon}_6 - \dot{\epsilon}_7$
Heat exchanger	$\dot{\epsilon}_{D,HX} = (\dot{\epsilon}_5 - \dot{\epsilon}_6) + (\dot{\epsilon}_9 - \dot{\epsilon}_{10})$
Reinjection	$\dot{\epsilon}_{L,R,4} = \dot{m}_4[(h_4 - h_o) - T_o(s_4 - s_o)]$
	$\dot{\epsilon}_{L,R,8} = \dot{m}_4[(h_8 - h_o) - T_o(s_8 - s_o)]$
	$\dot{\epsilon}_{L,R,12} = \dot{m}_{12}[(h_{12} - h_o) - T_o(s_{12} - s_o)]$
Condenser	$\dot{\epsilon}_{D,C} = m_{11}[(h_{11} - h_{12}) - T_o(s_{11} - s_{12})]$

2.4.1.1 Cooling tower assembly

An induced draft type wet cooling tower is chosen for cooling flow through the condenser. Recirculating cooling water is used to transfer heat from the process (condenser) to the atmosphere. Referring to Figure 2.6, the mass and energy conservation equations are expressed as

$$\dot{m}_{17}h_{17} + \dot{m}_{air,x}h_{air,x} = \dot{m}_{14}h_{14} + \dot{m}_{air,y}h_{air,y} \tag{2.39}$$

$$\dot{m}_{14} - \dot{m}_{17} = \dot{m}_m = \dot{m}_{air}(\omega_y - \omega_x) \tag{2.40}$$

$$\dot{m}_{air,x} = \dot{m}_{air,y} \tag{2.41}$$

where ω_x and ω_y are the specific humidity of the air entering and exiting the cooling tower respectively.

The surrounding air is assumed to be at a constant relative humidity of 76% and 2.5 ℃, which are the average conditions in the surroundings of IDDP-1 for 4 years [7].

For pump analysis, isentropic efficiency (η_{Pump}) of 85% is assumed [97] which is related to flow enthalpies as:

$$\eta_{Pump} = \frac{h_{in} - h_{out,isen}}{h_{in} - h_{out}} \tag{2.42}$$

2.3.2.6 Performance evaluation

The performance of a geothermal power plant is measured in terms of utilization efficiency ($\eta_{utilization}$) which is defined as the ratio of net power output ($\dot{W}_{net}$) to the total exergy input from the geothermal steam flow at the wellhead conditions:

$$\eta_{utilization} = \frac{\dot{W}_{net}}{\dot{m}_{geo}[(h_{geo} - h_o) - T_o(s_{geo} - s_o)]} \tag{2.43}$$

Performance of each component of the cycle can be evaluated using exergy destruction or exergy loss. Additional loss in efficiency occurs due to geothermal fluid reinjection in the ground, which cause exergy loss. Referring to Figure 2.6, Table 2.3 shows the relations for evaluating exergy destruction or loss in each component of the cycle.

A maximum moisture content of 15% is kept as a constraint at the exit of the turbine in order to avoid problems occurring due to wetness inside the turbine. The simulation assumes condensation and separation in the intermediate stage if maximum moisture content limit occurs before the exit pressure limit. A wet cooling tower is used to cool the cooling water of the condenser. The cold water temperature is assumed to be $20\,^\circ\text{C}$.

2.3.3 Boiling point elevation of aqueous potassium carbonate solution

For thermodynamic analysis of a system using aqueous potassium carbonate as a scrubbing medium, boiling point elevation (superheat) of the aqueous potassium carbonate solution must be defined as a function of temperature. The superheat for a given concentration can be obtained using activity of the solvent in equilibrium with the vapor expressed as a function of the degree of superheat (ΔT) and heat of vaporization (ΔH_{vap}) as suggested by Bialik et al. [64]. The relation is expressed as:

$$\ln(a_{solvent}) = \frac{\Delta H_{vap}^0}{R}\left(\frac{1}{T^0 + \Delta T} - \frac{1}{T^0}\right) \tag{2.44}$$

where T^0 is the saturated temperature at a given pressure and R is the gas constant. The solvent activity coefficient, $a_{solvent}$, is calculated by the following equation:

$$\phi = \frac{-1000 \ln(a_{solvent})}{M_{water}(2m_K + m_{CO_3})} \tag{2.45}$$

where M_{water} is the molecular mass of water, m_i is the mass of species i and osmotic coefficient (ϕ) is given as:

$$\phi = 1 + \frac{2}{(m_K + m_{CO_3})}\left[\left(\frac{-A_\phi I^{3/2}}{1 + 1.2 I^{1/2}}\right) + m_K m_{CO_3}\left(B_{ca}^\phi + ZC_{ca}\right)\right] \tag{2.46}$$

where I is the ionic strength and A_ϕ is the Debye Huckel slope expressed as a function of temperature [98]. The parameter Z is expressed as:

$$Z = \sum m_i[z_i] \tag{2.47}$$

where z_i is the charge on ions.

Parameters defining the thermodynamic property of a single salt solution in equation (2.46) are given by the following equations:

$$B_{ca}^\phi = c_1 + c_2 \exp\left(-I^{1/2}\right) \tag{2.48}$$

$$C_{ca} = \frac{c_3}{2[z_K z_{co3}]^{1/2}} \tag{2.49}$$

where c_1, c_2 and c_3 are the Pitzers parameters are given by Kamps et al. [67] for aqueous potassium carbonate defined as a function of temperature (T):

$$c_1 = 0.38621 - \frac{82.67}{T} \tag{2.50}$$

$$c_2 = 21.975 - \frac{6974.6}{T} \tag{2.51}$$

$$c_3 = \frac{6}{\sqrt{2}}\left(-0.00872 + \frac{2.69}{T}\right) \tag{2.52}$$

The above relations obtained are derived empirically, and are valid up to a temperature limit of 473 K. Following the approach by Weres and Kendrick [64], superheat values above the saturation temperature of 473 K were obtained by extrapolation.

The solubility of the saturated solution can be obtained by curve fitting the experimental values obtained from Moore et al. [99]. The curve fit for the solubility of the saturated solution ($m_{solubility}$) as a function of temperature (T) is given as:

$$m_{solubility} = 4 \times 10^{-4}T^2 - 0.4119T - 86.943 \tag{2.53}$$

2.4 Computational modeling and experimental investigation of aqueous potassium carbonate droplets in superheated steam flow

A computational model for simulating aqueous potassium carbonate solution droplets in superheated steam flow is developed and implemented in OpenFOAM. The model simulation results are verified using experiments for salt solution injection in superheated steam.

2.4.1 Computational Modeling

Computational modeling of salt solution droplets in superheated steam involves equations for gas phase (superheated steam), dispersed liquid phase (aqueous salt solution droplets) and the interaction between the two phases. The dissertation work uses solver called *sprayFoam* in OpenFOAM which is modified for the current case study. The solver uses the Eulerian approach for the gas phase and the Lagrangian approach for the liquid phase. For the gas phase, governing equations are the conservation equations for continuity, momentum, and energy. The liquid phase is assumed to be in the form of discrete droplets which involves equation for motion, heat and mass transfer, concentration, breakup, dispersion, and evaporation. The solver considers two-way coupling by including source terms calculated by sub-models for the liquid phase, which are added in the gas phase equations to include the effect of liquid droplets on the gas phase. The modification in the existing solver includes the addition of concentration as an additional droplet parameter and a thermodynamic model for boiling point elevation to include the effect of salt concentration on boiling point. Liquid phase density and thermal conductivity, which change significantly based concentration, are taken into account.

2.4.1.1 Equations for the continuous phase

2.4.1.1.1 Continuity equation

The governing differential equation for mass continuity of steam is expressed as:

$$\frac{\partial \rho_s}{\partial t} + \nabla \cdot \rho_s V_s = S_M \tag{2.54}$$

where ρ_s is the density, V_s is the velocity of steam and S_M is the source term for mass addition to the steam from the droplets due to evaporation.

2.4.1.1.2 Momentum balance equation

The equation for the conservation of momentum for the steam phase is expressed as:

$$\frac{\partial \rho_s V_s}{\partial t} + \nabla \cdot (\rho_s V_s V_s) = \nabla \cdot \mu_{eff} \nabla V_s + \nabla \cdot \mu_{eff} \left[(\nabla V_s)^T - \frac{2}{3} tr((\nabla V_s)^T)I \right] + \rho_s g - \nabla p + S_V \tag{2.55}$$

where μ_{eff} is the effective dynamic viscosity, g is the acceleration due to gravity, p is the pressure, tr is the trace operator, I is the Identity matrix, T is the transpose operator, and S_V is the source term for the momentum added to the steam from the droplet motion.

2.4.1.1.3 Energy conservation equation

The equation for the energy conservation for the steam phase is expressed as:

$$\frac{\partial \rho_s H_s}{\partial t} + \nabla \cdot (\rho_s V_s H_s) = \nabla \cdot \lambda_{eff} \nabla H_s + \frac{Dp}{Dt} + S_H \tag{2.56}$$

where H_s is the specific enthalpy of the steam, λ_{eff} is the effective thermal diffusivity, and S_H is the source term for the heat energy.

2.4.1.2 Equations for the droplets in the dispersed phase

Liquid droplets represent the discrete phase modeled using the Lagrangian approach. To save computation cost, droplets with the same characteristics are represented by a single computational particle called parcel, tracked separately. Models for different phenomena such as breakup, heat transfer, and evaporation are introduced during computation.

2.4.1.2.1 Droplet motion

The major forces causing droplet motion are the drag force (F_D) and net force due to gravitation and buoyancy (F_g). The basic equation for the droplet motion is expressed as:

$$m_d \frac{d\vec{V}_d}{dt} = \vec{F}_D + \vec{F}_g \tag{2.57}$$

where m_d is the droplet mass, and V_d is the velocity of the droplet. The drag force (F_D) is expressed as:

$$\vec{F}_D = m_d \frac{18\mu}{\rho_d d_d^2} \frac{C_d Re}{24} (\vec{V}_s - \vec{V}_d) \tag{2.58}$$

Where μ is the fluid viscosity, ρ_d is the droplet density, d_d is the droplet diameter, Re is the Reynolds number and C_d is the drag coefficient for the spherical droplet. The drag coefficient (C_d) is related to the droplet Reynolds number [100] as:

$$C_d = \begin{cases} \frac{24}{Re}(1 + 0.15Re^{0.687}) & Re_d \leq 1000 \\ 0.44 & Re_d \geq 1000 \end{cases} \tag{2.59}$$

where Re_d is the droplet Reynold number.

2.4.1.2.2 Droplet heat, mass and concentration balance

The openFOAM solver *sprayFoam* uses an empirical model for evaporation which is applied for fuel injected in a low pressure environment to cause flash boiling. The current work uses a model proposed by Frydman et al. [77] for the case of water droplet injection in superheated steam. For pure water droplets in superheated steam, mass transfer due to evaporation by diffusion does not occur because no gradient of molecular density is available, as both gas and droplet consist of same matter, that is water. For water droplets with dissolved salt, condensation can occur until the droplet reaches its respective boiling point. However, the condensation is insignificant, considering the short time frame of temperature reaching boiling point as reported by Gardner [66] and is therefore not taken into account. The equation for heat transfer to the droplet from the steam is given as:

$$m_d \frac{dT}{dt} = hA_d(T_s - T_d) \tag{2.60}$$

where A_d is the droplet surface area, T_s and T_d are the steam and the droplet temperature, and h is the heat transfer coefficient obtained from Nusselt number (Nu), which is expressed as [95]:

$$Nu = 2 + 0.6Re^{\frac{1}{2}}Pr^{\frac{1}{3}} \tag{2.61}$$

where Pr is the Prandtl number.
Assuming dissolved salt as non-volatile, the evaporation caused by heat transfer is expressed as [77]:

$$\Delta H_v \frac{dm_d}{dt} = hA_d(T_s - T_d) \tag{2.62}$$

where ΔH_v is the latent heat of vaporization for water.

The equation for change in droplet concentration with time is given as:

$$m_{d_{t+1}} c_{d_{t+1}} = m_{d_t} c_{d_t} \tag{2.63}$$

where m_{d_t} and c_{d_t} are the respective droplet mass and concentration at time t respectively.

2.4.1.2.3 Droplet properties

For modelling droplet evaporation, boiling point elevation (superheat) of the aqueous potassium carbonate solution is required as a function of droplet temperature and salt concentration. The superheat for a given concentration is obtained using the model discussed in Section 2.3.3.

To take into account the effect of droplet concentration on thermal conductivity, the relation for concentration dependence of thermal conductivity ratio (k_d/k_w) of aqueous salt solution droplets as given by Chiquillo [101] is expressed as:

$$\frac{k_d}{k_w} = 1 + A_1 c + A_2 c^2 \tag{2.64}$$

where A_1 = -0.0194401, A_2 = -0.017091, and c is the concentration of aqueous potassium carbonate solution. The subscript w denotes pure water and d denotes the salt solution droplet.

For obtaining the effect of the droplet concentration on its density, relation for the concentration dependence of the relative density (ρ_d/ρ_w) of the aqueous salt solution droplet is obtained using the curve fit from values of densities at different temperature and salt concentration given by Liley et al. [72]. The values are given up to $100\,^{\circ}$C. Density of the salt solution at higher temperatures is obtained by extrapolation. The curve fit equation is given as:

$$\frac{\rho_d}{\rho_w} = 1.0031 + 0.1101c - 0.005c^2 \tag{2.65}$$

where the density of pure water (ρ_w) is a known function of temperature, available in the solver.

2.4.1.2.4   Simulation method

The geometry used for the simulation is of the same scale as that of the experimental setup. Figure 2.8 shows the 3D view of the geometry and the grid for the injection and separation system. The dimensions are given in Table 2.4. The injection system consists of a Pease-Anthony type venturi unit with a cone orifice of 1 mm diameter for salt solution injection. The separator used for droplet separation is a Bangma type [102] cyclone separator. In total 5 runs of simulation are carried out. All flow variables for the superheated steam are kept constant in the runs. The only parameter changed in each run is the concentration of the aqueous potassium carbonate injected which is 0.02, 1.1, 1.81, 3.41 and 5.27 in mol kg^{-1} respectively. The density and thermal conductivity of the injected salt solutions are fixed in accordance with salt solution concentration. The constant parameters and boundary conditions for the simulation are given in Table 2.5.

(a)   (b)
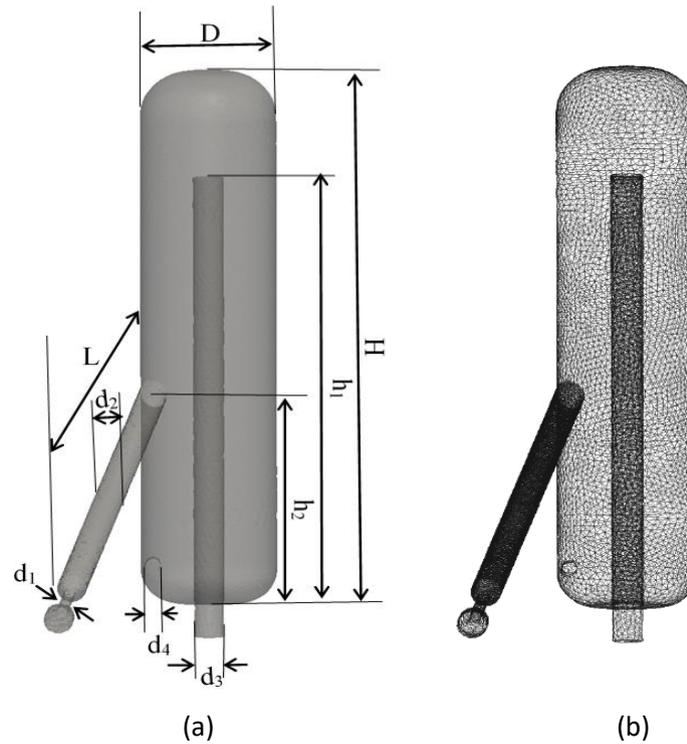
FIGURE 2.8: Schematic and grid representation of the injection and separation assembly considered: (a) 3D view of the geometry (b) 3D view of the CFD grids

Table 2.4: Geometry of the injection and separation system (D = 70 mm)

H/D	d_1/D	d_2/D	d_3/D	d_4/D	h_1/H	h_2/H	L/D
4.28	0.02	0.05	0.05	0.0266	0.4	0.8	5

Table 2.5: Parameters used in the work

Droplet phase		Gas phase	
Inlet salt temperature (℃)	98	Inlet velocity (ms^{-1})	15
Specific heat (J kg^{-1} K^{-1})	4205	Inlet temperature (℃)	148
Injection type	Cone	Inlet pressure (bar)	2.6
Size distribution	Rosin-Rammler	Turbulence model	k-ε
salt solution injection rate (ml min^{-1})	3.6	Wall boundary temperature	Zero gradient
Mean diameter (μm)	197	Wall boundary velocity	Zero
Size distribution parameter	3		
Parcel per second	4000		
Heat transfer model	Ranz and Marshall		
Breakup Model	Reitz and Diwakar		
Wall interaction	rebounding		

2.4.2. Model implementation in OpenFOAM

The solver for simulating the droplets in steam flow is based on the PIMPLE algorithm [89] for accomplishing pressure velocity coupling. Equations for continuity, momentum, and energy as given by Equation 2.53, 2.54 and 2.55 are solved within the loop. The source term in each equation is obtained using the *evolve* function in OpenFOAM, which initiates

calculation for each parcel. Additionally, a turbulence model is required in the solver. The dissertation work uses the *k-ε* model with *epsilonWallFunction* option specified as a part of the wall boundary conditions for transport variables. Details of chosen schemes for discretization, interpolation, and methods for solving equations are specified in Table 2.6.

Table 2.6: Numerical methods and finite volume schemes for fluid flow fields required for droplets in steam flow

Numerical method	P	U, k and ε	ρ	H_s	H_2O
Solver	GAMG	smoothSolver	PCG	PBiCG	PBiCG
smoother	GaussSeidal	symGaussSeidal			
Under relaxation factor	0.1	0.1	0.1	0	0
terms	Finite volume schemes				
divergence	Gauss upwind				
gradient	Gauss linear				
Laplacian	Gauss linear corrected				

2.4.3 Experimental setup and procedure

The experiment setup lay out for the study of salt solution injection in superheated steam is similar to that of experimental setup for silica particle deposition, while replacing the particle feeder assembly with that of salt solution injection assembly consisting of a peristaltic pump and a venturi unit.

The photos of the salt solution assembly and the venturi section are shown by Figure A.4 and Figure A.5 respectively in appendix A. The venturi unit is of Pease-Anthony type with a cone orifice at the throat section for solution injection. The injected solution droplets break and disperse due to momentum exchange with high velocity steam and turbulence. The aqueous salt solution droplets are then collected at the bottom of a cyclone separator (S_2). The separated steam is passed through the condenser (C_1) in order to measure the flow rate before disposal. The system is well insulated to minimize heat loss which can cause condensation.

For measurements, superheated steam was run through the system initially without salt solution injection. Pure water is then injected at a constant rate until a steady state was observed. Keeping the same pump feed rate, injection was done for different solution concentrations. Since it was not possible to measure the concentration and temperature of each droplet directly along the flow line, the temperature was measured at the separator bottom where the droplets are collected after obtaining thermal equilibrium with the steam. The separator bottom obtains a steady state temperature sometime after the onset of injection. The separated liquid was removed for the concentration measurement at the outlet after valve Cv_1. The method offers an easy way of measuring collected solution steady state average temperature and concentration for a given fixed inlet concentration injected into the superheated steam. Concentration measurement of the collected samples was done using inductively coupled plasma atomic emission spectroscopy (ICP-AES).

2.5 Silica scrubbing from geothermal steam using aqueous potassium carbonate solution: Experimental investigation

An experimental setup was designed in order to verify the effectiveness of the proposed method for scrubbing silica from the superheated steam. The setup consists of a combination

of particle feeding and injection assembly and fluid injection system used for experiments regarding silica deposition and salt solution droplets in superheated steam. Although a relatively low value of temperature and pressure is obtained due to design constraints as compared to that of IDDP-1, the degree of superheat is sufficiently in the range upto 40 ℃, enough to show the effect of the elevation of the boiling point while scrubbing with a salt solution. The details of the setup and procedure for measurements are explained below.

2.5.1 Experimental Setup

The experimental setup consists of an additional salt solution injection assembly to the design setup used for the study of silica deposition, shown in Figure 2.3. The modified experimental unit is shown in Figure 2.9. The salt solution injection and separation system consist of a variable speed peristaltic pump for feeding solution into a venturi scrubber, which consists of a converging section, throat, and a diffuser. The venturi scrubber used is Pease-Anthony type such that liquid is injected through an orifice in the throat section. The injected solution droplets break and disperse because of momentum exchange with the high velocity steam and turbulence; causing collision and attachment of solution droplets with the silica particles present in the steam. Droplets containing silica are removed in the cyclone separator (S_2). Here the injected solution mass flow is found to increase with increase in solution concentration, causing density to increase. Therefore, the injection rate was kept constant by volume during the experiment, as the scrubbing efficiency depends on the volume fraction of liquid in the gas. The constant injection rate at different salt concentration causes the volume of the salt solution droplets to vary with the amount of potassium carbonate injected keeping the volume of the solution constant.

The sampling unit consists of an annulus pipe with a linear contracting section. The contracting section has a stainless steel probe attachment was to collect the samples. The probe is 10 cm long and 3.65 mm in diameter and is sharpened at the entrance with the other end connected to a cone shaped flask made of cast iron. Due to high turbulence occurring in the ejector and a narrow cross-section in the venturi throat, particle agglomeration may occur. Size distribution of the actual particles entering the sampling unit are therefore, required to be measured. Filter paper for collecting particles was placed on a wired mesh present in the cone flask, as shown in Figure 2.9. A membrane filter with 0.45 μm pore size and 47 mm diameter was used for collection. The filter is stable in the steam up to 180 ℃. The flowing steam is passed through a valve (Cv_4) to control flow velocity through the probe for isokinetic sampling. Particle sampling on filter paper with solution injection was not possible due to the risk of getting wet. Also, chances of error exist due to the minimum size limit of the filter pore for particles to escape. Therefore, particle concentration in the flow is measured by passing sampled steam through the condenser (C_1) for collection and analysis. The steam from the test section is also collected after condensation in the condenser (C_2) to measure the total flow rate. The system is well insulated and heat is supplemented by means of heating tape.
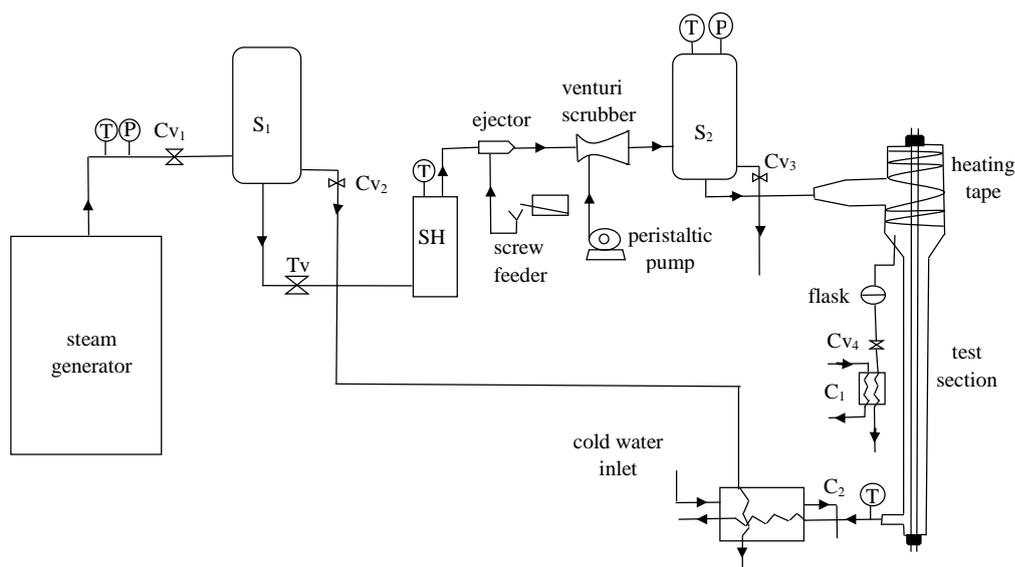
FIGURE 2. 9: Schematic diagram of the experimental setup

2.5.2 Measurement Procedure

The steam flow rate is limited by the boiler capacity of 150 l min^{-1} and the absolute pressure of 4.5 bar. A large pressure drop occurs in the ejector section after expansion in the nozzle. Superheated steam up to 145 $^{\circ}$C and 1.3 bar is obtained at the separator end. The steam flow has a superheat of 40 degree. Though the temperature and pressure of the steam flow during the experiment is low compared to that of the fluid from IDDP-1 well, the degree of superheat is comparable to the actual state of the fluid from the geothermal well even though the pressure and temperature conditions are much higher in the later case. It is more important to consider the degree of superheat since the amount of mass transfer from the liquid droplets in the superheated steam is mainly governed by the temperature difference between the droplet and the surrounding medium that is steam.

The particle selected was silica fume, described in Section 2.2.2. The system was run at the beginning without silica particle and solution injection until a steady state of flow rate and system temperature was obtained. Upon obtaining the steady state temperature as measured at the separator S_2, the particle feeder was started. A constant feed rate of 6 mg min^{-1} was kept at the micro screw feeder, corresponding to a silica concentration of nearly 40 ppm concentration in the steam flow. The sample for particle size distribution was then obtained using filter paper in the sampling unit. Then the filter arrangement was removed and the sampling probe was directly connected to the condenser C_1. Water injection began and was adjusted to obtain a saturated state temperature in the separator S_2, corresponding to the conventional method of wet scrubbing. A constant injection rate of 3.6 ml min^{-1} was used; as measured to obtain the saturated state conditions. The condensed steam from C_1 was then sampled. While keeping constant particle and pump feed rate, the salt solution was injected for different concentrations. Sampling was done with a standardized procedure with a time gap between different concentrations injected. A temperature rise occurs with the change in concentration due to the decrease in droplet evaporation rate. Sampling was started once a constant temperature was achieved in the separator S_2 for every change in concentration of the solution. The samples were analyzed using inductively coupled plasma atomic emission spectroscopy (ICP-AES) for silica and potassium ion concentration.

3 RESULTS

3.1 Computer simulation and experimental validation of silica particle deposition in superheated steam flow

For modelling silica particle deposition in superheated steam, an advection-diffusion model based on Euler-Euler approach was selected. The advection-diffusion was implemented and simulated using OpenFOAM. Figure 3.1 shows the simulation results as well as results from the experiments for the deposition velocity of the silica particles in superheated steam as a function of relaxation time. A comparison of the experimental results for silica in superheated steam can be made with experimental data from the literature for aerosol in air flow by normalizing the relaxation time, plotted in Figure 3.1. The figure shows three different regimes of deposition for two-phase flow with particles in a dispersed phase. For particles with the lowest relaxation time, there is the turbulent diffusion regime where deposition occurs mainly due to Brownian and turbulent diffusion, termed as the first regime. A decrease in deposition velocity occurs with increasing relaxation time due to the decrease in Brownian diffusion, which is the dominating mechanism for particle motion near to the wall. The decrease in Brownian motion occurs due to an increase in particle size. The second regime, which occurs at intermediate relaxation times, the diffusion-impaction regime, consisting of a steep increase in deposition velocity with relaxation time due to lift and turbophoretic forces. The third regime, at high relaxation times, is the inertia regime, where deposition velocity gradually slows down due to a decrease in time of interaction with eddies as particle inertia increases with increase in particle size. The relaxation time range is limited by fluid velocity and the range of particle sizes.

The current experiment is carried out for silica particles with sizes ranging from 1 μm to 20 μm and the superheated steam as a flow medium. The flow velocity is kept constant for the given design setup and electric boiler unit capacity. The relaxation time range is therefore obtained using the available particle size distribution. For the available particle size range, the setup is designed to obtain flow velocity such that the relaxation time range correspond to the impaction-diffusion regime (the second regime), where an increase in deposition is expected. The results for silica and superheated steam flow show a steep increase in deposition rate with increasing relaxation time in the diffusion-impaction regime. In geothermal systems with superheated steam, silica particles agglomerate after precipitation, which causes particle size to increase, and therefore increases the average relaxation time. For particles close to or within the intermediate range, agglomerated particles with larger relaxation time will have higher deposition velocity and therefore having higher deposition rate than the smaller particles. Thus for the same concentration, the scaling rate is found to be higher in steam flow with more agglomerated particles. Results for the non-dimensional deposition velocity obtained in the

current work are consistent with results from the literature involving aerosols in air flow for the same non-dimensional relaxation time range. An error is expected for low relaxation times because the likelihood of small particles sticking to the surface of the probe due to bends and the small cross-sectional area. A simulation was performed using the implemented model based on the experimental conditions and boundary constraints. Results from the simulation show agreement with the published literature experimental data of the diffusion-impaction regime (second regime). The deposition curve obtained from the simulation for all three regimes is consistent with the results from the literature, involving aerosols in air flow for the same non-dimensional relaxation time.
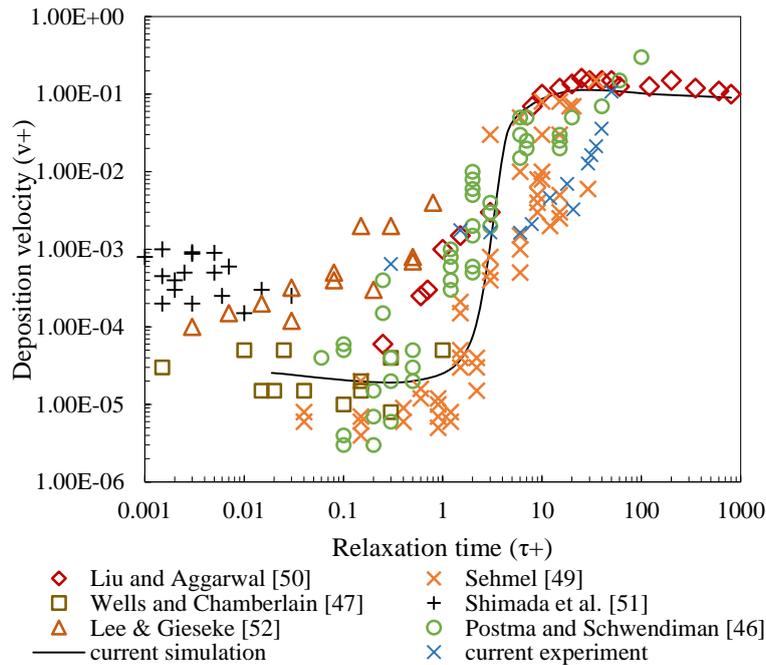

FIGURE 3.1: Variation of non-dimensional deposition velocity with non-dimensional particle relaxation time. Results from simulations and experiments for silica in superheated steam in this work are plotted along with values for particles in air from the literature.

A better understanding of the deposition process and different aspects of silica particle transport in superheated steam flow can be obtained from the simulation. The simulation assume complete absorption of particles at the wall. Figure 3.2 shows the variation of non-dimensional silica particle concentration, wall-normal velocity and forces per unit mass along wall normal distance for different dimensionless particle relaxation times. The particle acceleration due to each force is represented as force per unit mass, showing the magnitude of each force presented by terms on the right hand side of equation 2.12. Flow through a pipe is physically bounded by wall which creates a heterogeneity in the flow. Flow with heterogeneous nature are subject to turbophoretic forces which create a non-uniform distribution or preferential concentration of particles along the the direction of heterogeneity as shown by concentration profiles in Figure 3.2(a) and 3.2(b). The presence of turbulence near wall causes the formation of dense clusters of particles as explained by Eaton and Fessler [103]. The degree of preferential concentration describing the accumulation of particles within specific regions of the instantaneous turbulence field depends upon the ratio of particle to fluid inertia. The preferential concentration of silica particles in superheated steam is high due to

the high density ratio of silica and steam. Though the turbophoretic force helps in building up a convective flux of particles from the buffer region to the near wall, a continuous removal mechanism is required otherwise the particles will accumulate adjacent to the wall and a steady state will never be achieved. As the particles enter near wall region, particles with relatively large inertia, the flux towards the wall is mainly convective. Very small particles however rely on mechanism of Brownian and turbulent diffusion in the near wall region for their flux towards the wall. As the inertia increases with further increase in particle size, the particles become too sluggish to have a longer response during an eddy's lifetime, hence preferential concentration decreases (fig. (3.2c), fig. (3.2d)). Larger particles, however, on the other hand observe increase in lift force as shown by Figure 3.2(c) and 3.2(d). The particle flux towards the wall is therefore mainly convective occurring due to the lift force. In this range, particle motion is mainly governed by impaction. The negative value of velocity and forces in the graph represent direction towards the wall. The net particle acceleration can be obtained by subtracting the drag force from the sum of all forces acting towards the wall. Figure 3.3 shows the animation view of the concentration profiles and the particle clustering effect as obtained from the simulation.

The computational model successfully captures the concentration distribution. The model, however, predicts excessive particle concentration near the wall as the particle size increases because of the assumption of local equilibria. The so-called memory effect in which a particle retains the turbulent characteristics of an eddy previously passed through before is ignored. An improved model for the turbophoretic force is therefore required to avoid limitation. Despite limitations, the assumption of local equilibrium is effective in predicting the gross features correctly.


(a)

(b)
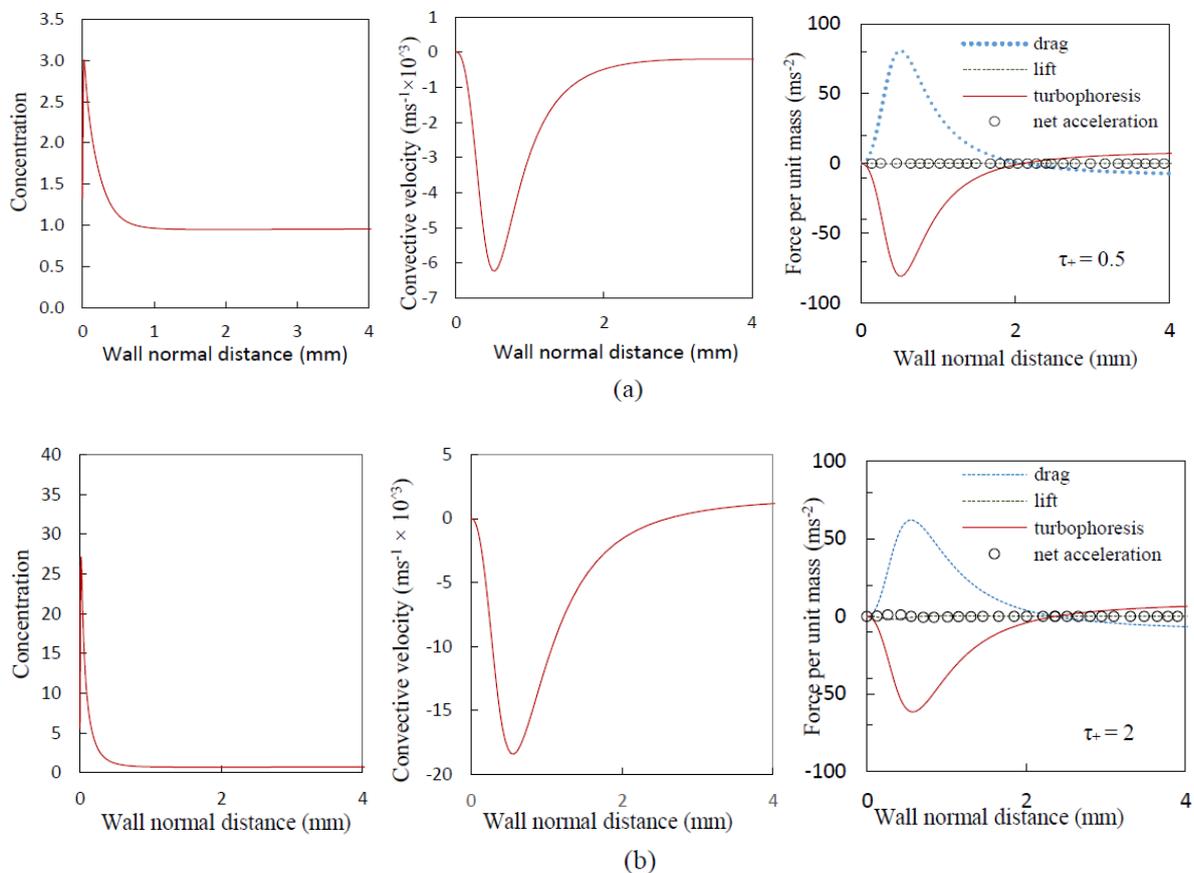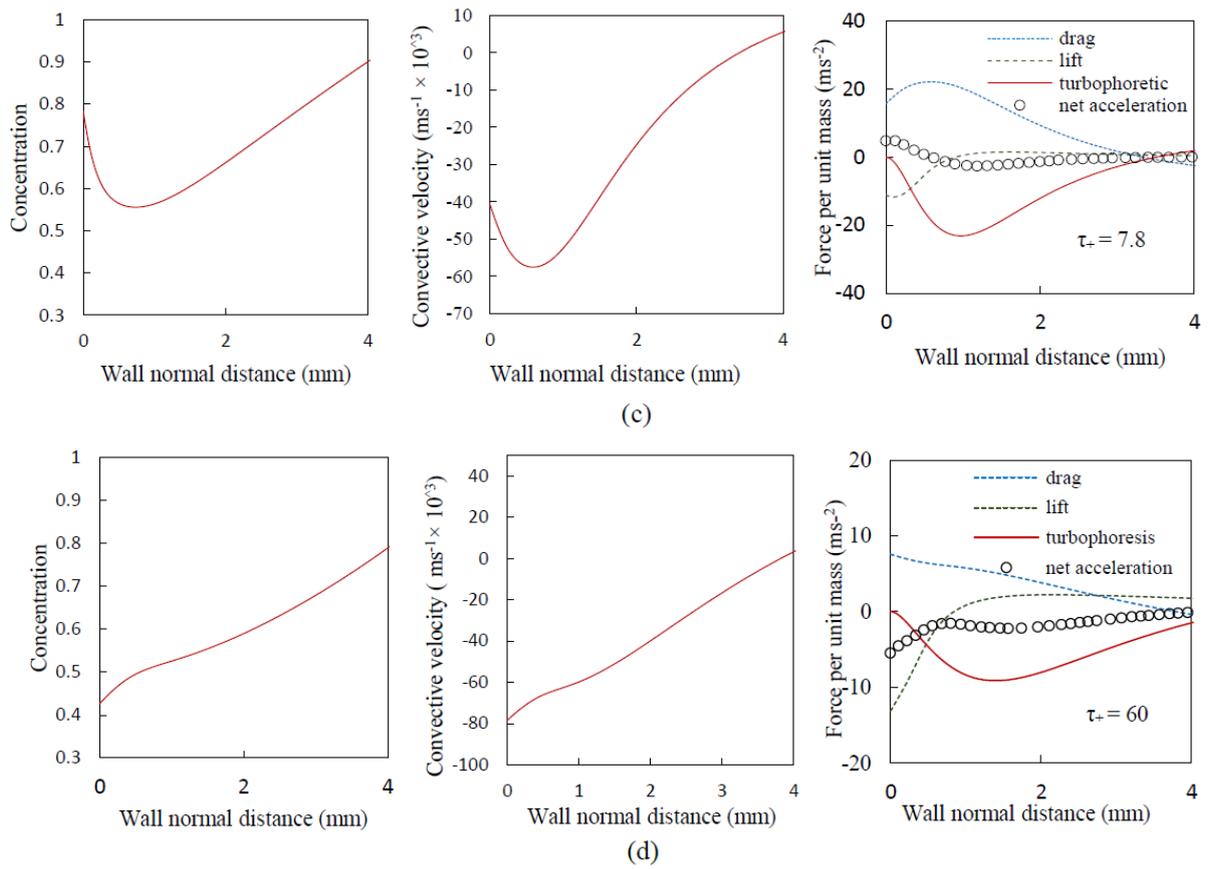
FIGURE 3.2: Particle concentration non-dimensionalized by bulk mean concentration (c_p), Wall normal velocity and Forces per unit mass (acceleration) for different dimensionless particle relaxation times (a) 0.5 (b) 2.0 (c) 7.8 (d) 60
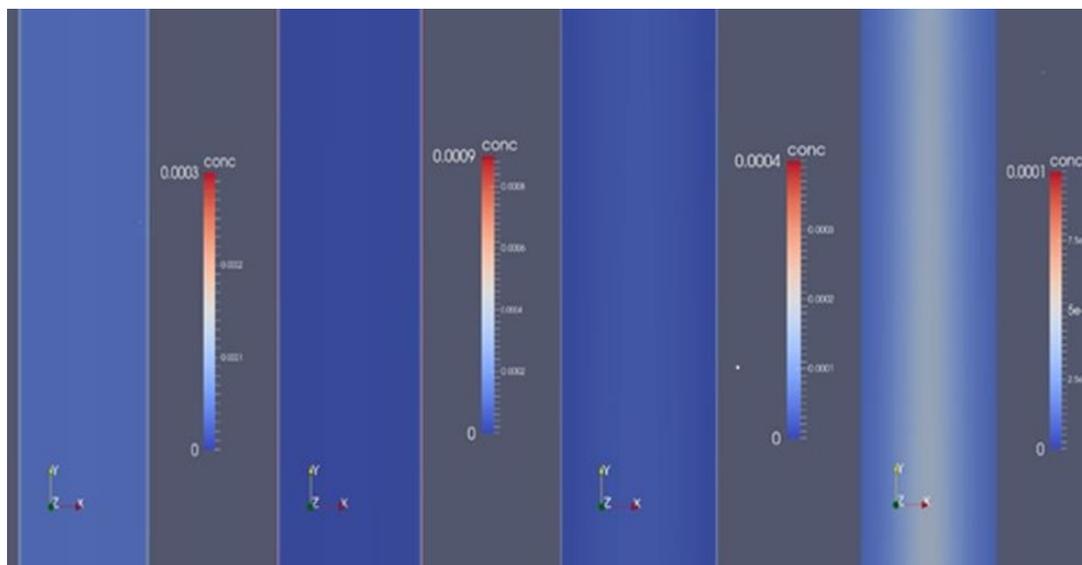
(a) $\tau_+ = 0.5$ (b) $\tau_+ = 2$ (c) $\tau_+ = 7.8$ (d) $\tau_+ = 60$

FIGURE 3.3: Particle concentration profiles at different relaxation times

3.2 Silica scrubbing using aqueous Potassium Carbonate solution: Thermodynamic analysis

The dissertation proposes silica scrubbing from superheated steam using aqueous potassium carbonate. The technique utilizes the boiling point elevation of the salt solution for scrubbing superheated steam while retaining the superheat. Thermodynamic performance analysis of the proposed scrubbing technique was done for IDDP-1. Figure 3.4 shows the simulation results from the thermodynamic model for the degree of steam superheat achieved corresponding to different temperatures by liquid aqueous potassium carbonate solution at a saturated concentration to that temperature. The values show a significant degree of superheat that can be attained without precipitation.
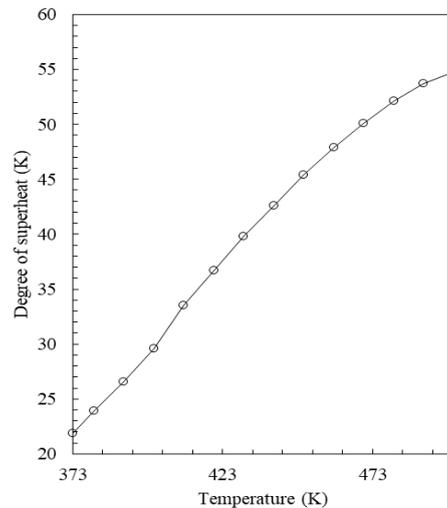

FIGURE 3.4: Attainable steam superheat as a function of temperature in equilibrium with a saturated aqueous solution of potassium carbonate

A comparative study of the thermodynamic performance for a power cycle using aqueous potassium carbonate scrubbing with that of traditional wet scrubbing was carried out. The cycle simulation was done up to a wellhead pressure limit of 7 MPa considering the validity of modeling equations for potassium carbonate superheat. Importantly, the analysis does not ignore the point of maximum output, obtained at much lower wellhead pressure as shown later. Figure 3.5 shows the variation of cycle utilization efficiency with wellhead pressure, based on flow test and enthalpy results for IDDP-1. The utilization efficiency first increases and then decreases with wellhead pressure. Variation of cycle efficiency with wellhead pressure is governed by the inlet state of working fluid to the turbine. For low inlet pressure, the exit state of the vapor in the turbine has a dryness fraction greater than the minimum assumed value for the fixed value of condenser pressure. Upon increasing the inlet pressure, the exit state approaches the minimum dryness fraction value, increasing specific enthalpy change of fluid along the turbine and hence increases the efficiency. The steam at the entrance of the turbine in the proposed cycle is superheated, offering greater efficiency in the turbine compared to that of the traditional wet scrubbing cycle. A decrease in utilization efficiency is observed with further increase in wellhead pressure, which decrease occurs due to limiting values of the minimum dryness fraction in the turbine, requiring a higher pressure at the exit.

Utilization efficiency up to 65% using aqueous potassium carbonate for scrubbing at 5 MPa wellhead pressure is obtained. The highest efficiency for using wet scrubbing is 58% obtained for the same wellhead pressure. The wellhead pressure of 5 MPa also represents the pressure for maximum work output. A gain of up to 7% points is observed in utilization efficiency by using potassium carbonate scrubbing at the wellhead pressure at which maximum work output occurs, equivalent to 12% increase in power output.
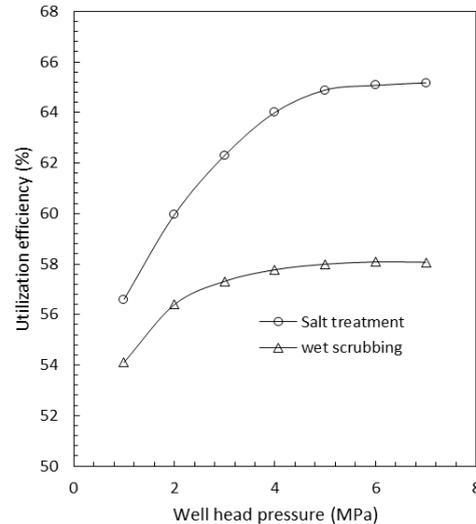

FIGURE 3.5: Variation of utilization efficiency with wellhead pressure

Figure 3.6 shows the variation of the net work output with wellhead pressure for the cycles utilizing conventional wet scrubbing and scrubbing using potassium carbonate solution based on the production curve of IDDP-1. The net work output first increases and then decreases with wellhead pressure. The net work output first increases with the increase in enthalpy change across the turbine as the turbine dryness fraction approaches the lower limit for the fixed value of condenser pressure. The increase in net work output is then countered by a decrease in mass flow rate (Figure 2.6) of geothermal fluid, which causes total work output to decrease at higher wellhead pressures. Greater turbine efficiency is obtained by having superheated steam at the turbine entrance in the proposed cycle, thus causing more work output than traditional wet scrubbing. An increase in work output up to 4.3 MW is observed at 5 MPa of wellhead pressure using treatment with aqueous potassium carbonate compared to wet scrubbing.

Figure 3.7 shows the exergy flow diagram for the case of the cycle utilizing scrubbing using potassium carbonate solution. The exergy loss due to reinjection is from separator 1 and 2, as well as from the exit of the condenser. The net work is calculated by deducing fan and pump power from the total turbine work output. The exergy input from added cold salt solution is almost negligible. The results show the condenser and turbine as major components in the proposed cycle that contribute to exergy destruction which applies to the cycle with a wet scrubbing unit as well. The heat recovery system added in the proposed cycle contributes least to exergy destruction. The analysis, however, needs to consider exergy destruction due to pressure loss.
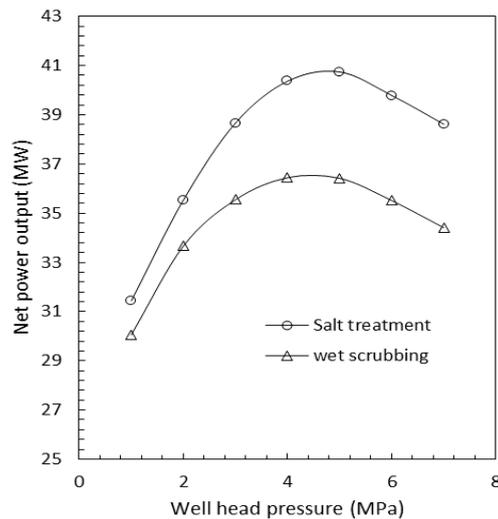
*FIGURE 3.6: Variation of net work output with wellhead pressure*
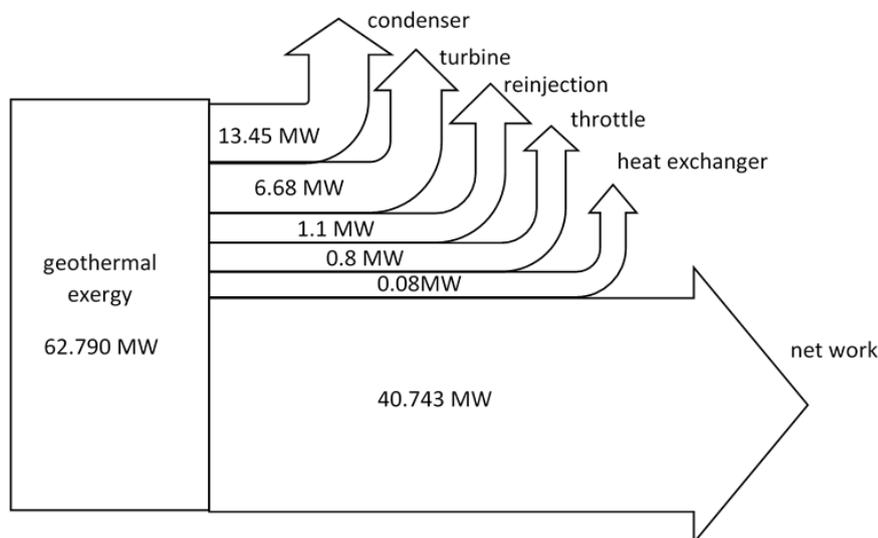
FIGURE 3.7: Exergy flow diagram at a wellhead pressure of maximum work output for cycle utilizing aqueous potassium carbonate for scrubbing

3.3 Computational modeling and experimental investigation of aqueous potassium carbonate droplets in superheated steam

3.3.1 Mesh independence

For any CFD problem, it is important to ensure that the solution is not affected by the grid size. For this grid independence verification is done before the model validation. For the problem involving aqueous potassium carbonate solution injection in superheated steam, temperature and concentration are the variables in the process. Simulations were run using the same initial parameters for three different mesh grids to investigate the effect of mesh

51

refinement on the steady state temperature of the steam at the separator bottom. Figure 3.8 shows the change in the bottom temperature of the separator after the start of injection for mesh sizes of 45082, 57698 and 70970. From the results shown in the figure, we conclude that the influence of refining mesh greater than 57698 is small. The mesh size was therefore kept 70970 for the model validation and further analysis.
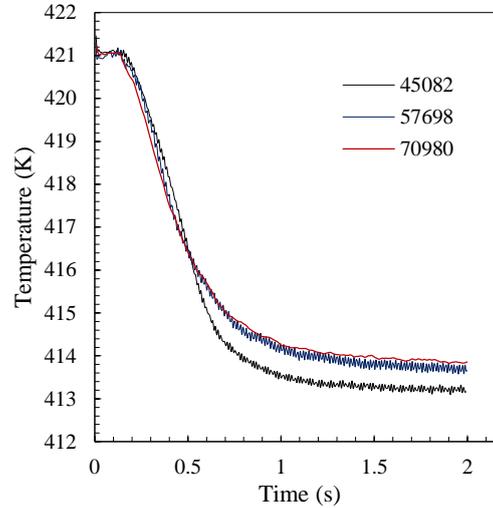

FIGURE 3.8: Grid independence verification

3.3.2 Model Validation

The model was validated by comparing the simulation results for the steady state temperature at the bottom of the separator with the measured value from the experiment. Capturing the transient process of the experiment is not possible because of the short residence time of the salt solution droplets in the flow. Therefore model validation is done using results from the experiment for the steady state after the injection, as proposed by Liu et al. [104]. The simulations and experiments were carried out for different injection salt concentration. Figure 3.9 (left) shows the simulation results for the temperature at the separator bottom after the start of injection for five different injected aqueous K_2CO_3 (aq) concentrations. Figure 3.9 (right) shows the comparison of the steady-state temperature from the simulation with the experimental values for different injection salt solution concentrations. Computation results show good agreement with the experimental measurements verifying the physical model
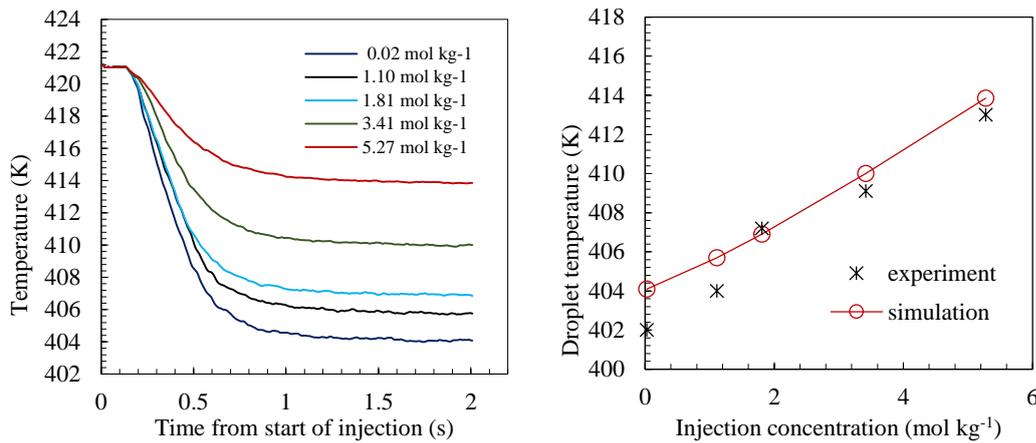
FIGURE 3.9: (Left) Simulations for temperature (K) at the separator bottom after the start of injection for different injected K2CO3 (aq) concentrations (mol kg-1). (Right) Simulation and experimental results for the steady state temperature

3.3.3 Temperature and concentration profiles

Figure 3.10 shows the steady state temperature fields in the separator for different injected K_2CO_3 concentrations. Separator bottom steady state temperature increases with increase in injected K_2CO_3 (aq) concentration. Also an increase in injected K_2CO_3 (aq) concentration led to an increase in boiling point elevation. The increase in boiling point elevation caused a decrease in droplet mass evaporated before obtaining thermal equilibrium with the surrounding steam. As a result of this, the drop in superheated steam temperature due to heat transfer between the two phases was reduced. The lowest temperature was found at the separator bottom due to K_2CO_3 (aq) separation and accumulation. The change in injected K_2CO_3 (aq) concentration had a relatively small effect on the separated superheated steam temperature because of the small scale of the experimental unit and low injection mass ratio due to the short residence time. Low injection mass ratio of K_2CO_3 (aq) was chosen since there is a significant change in droplet parameters to allow measurements with the laboratory scale experiment unit.

Figure 3.11 shows the salt concentration profile of the droplets along the flow for different injection concentrations. The K_2CO_3 (aq) concentration of the droplets increases along the flow line after the droplet evaporation starts which occurs due to mass loss caused by water evaporation. The K_2CO_3 stays in droplet form because of its non-volatile nature. The fraction of droplets carried upwards in the separator with the steam observes higher K_2CO_3 concentrations due to continuous heat gain from the incoming superheated steam at a higher temperature, which causes increased evaporation. For a scrubbing process using aqueous potassium carbonate as a scrubbing medium, the maximum salt concentration of the carry over droplets limits the degree of superheat the steam should have, in order to avoid precipitation.
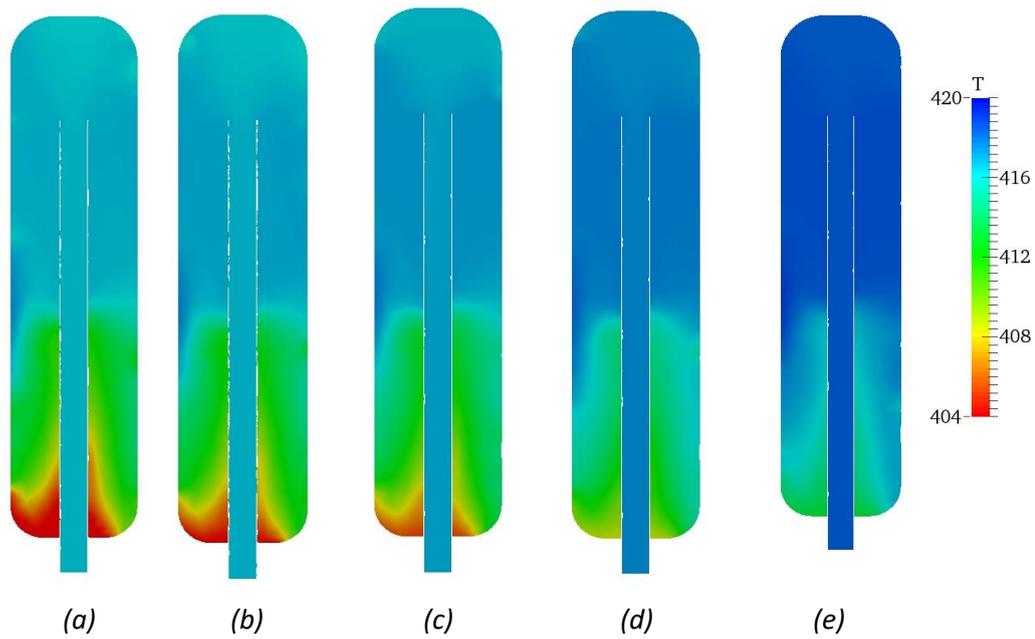
FIGURE 3.10: Steady state temperature fields in the separator for different injected K2CO3 concentrations: (a) 0.02 mol kg-1 (b) 1.1 mol kg-1 (c) 1.81 mol kg-1 (d) 3.41 mol kg-1 (e) 5.27 mol kg-1
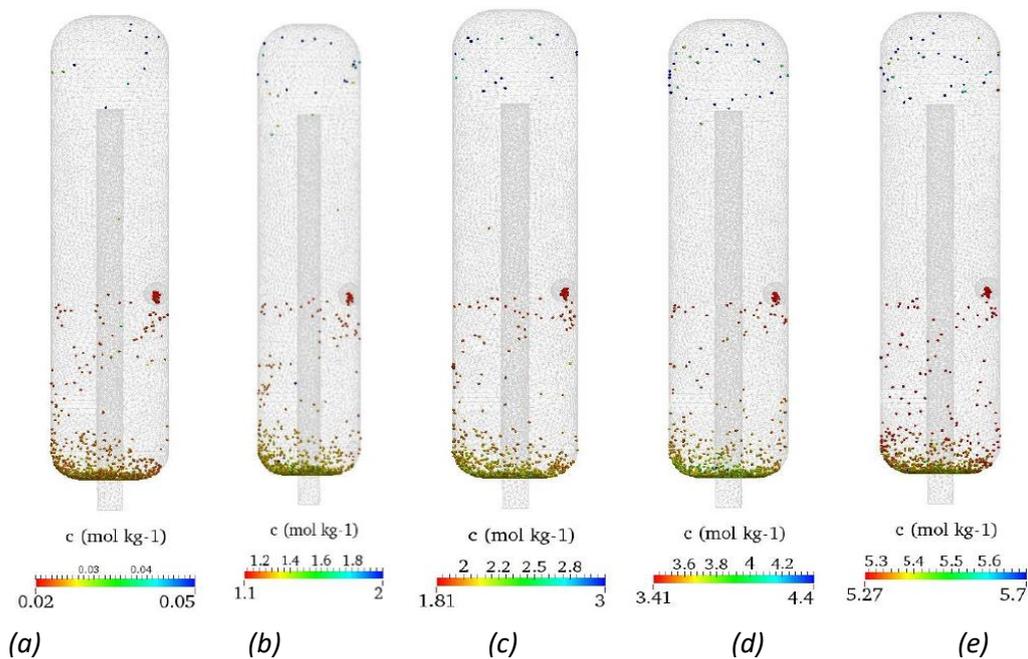
*FIGURE 3.11: Droplet salt concentration along the flow for different injection concentration: (a) 0.02 mol kg-1 (b) 1.1 mol kg-1 (c) 1.81 mol kg-1 (d) 3.41 mol kg-1 (e) 5.27 mol kg-1*

Data obtained from simulation for the concentration of salt solution droplets collected at the separator bottom was compared with that obtained from experimental measurements for

different injection salt concentrations. As seen from Figure 3.12, simulation results show an approximately 20% deviation in extracted liquid concentration from the experimental values, due to the rebounding boundary conditions assumed at the separator wall for the simulation. In reality, a fraction of K_2CO_3 (aq) droplets may attach to the separator wall before collecting at the bottom. Contact time of droplets with high temperature steam increases and cause an increase in K_2CO_3 concentration of the collected fluid. The high concentration droplets in the fluid and the droplets at the bottom were collected while flushing the condensate for sampling. The droplets that acquired a higher value of concentration near the top of the separator can also be observed from the simulation results.
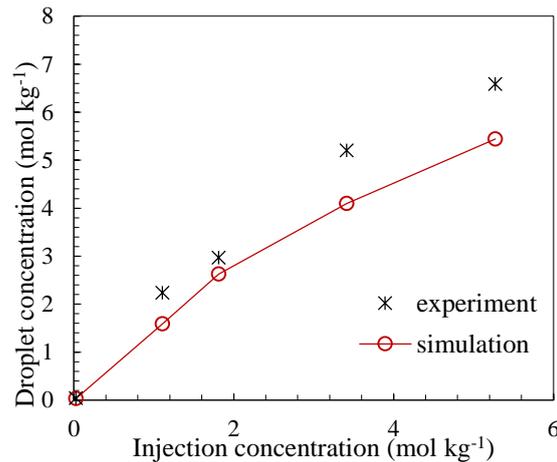

FIGURE 3.12: Concentration of K_2CO_3 in collected droplets with different injection concentration plotted along with results from computational simulations

3.4 Silica scrubbing using aqueous potassium carbonate solution: Experimental investigation

A laboratory experiment was done to estimate the performance of silica scrubbing from superheated steam using an aqueous potassium carbonate solution. The sample size distribution is obtained by processing the digital microscope images of the filter surface using ImageJ [91]. The particle diameter is calculated using the projected area method with a bandwidth of ±0.5 μm. Figure 3.13 shows the filter surface image (left) and the particle size distribution (right) obtained. The agglomerated particles lie within a limit of 20 μm diameter as was observed in IDDP-1 [20]. The minimum measurable size sampled by the filter is 0.45 μm which limits its application for concentration measurement. The steam sampling method and analysis using emission spectroscopy were therefore used to ensure concentration at the desired accuracy, since particles of all size ranges can be collected along with the sampled steam.

(a)   (b)
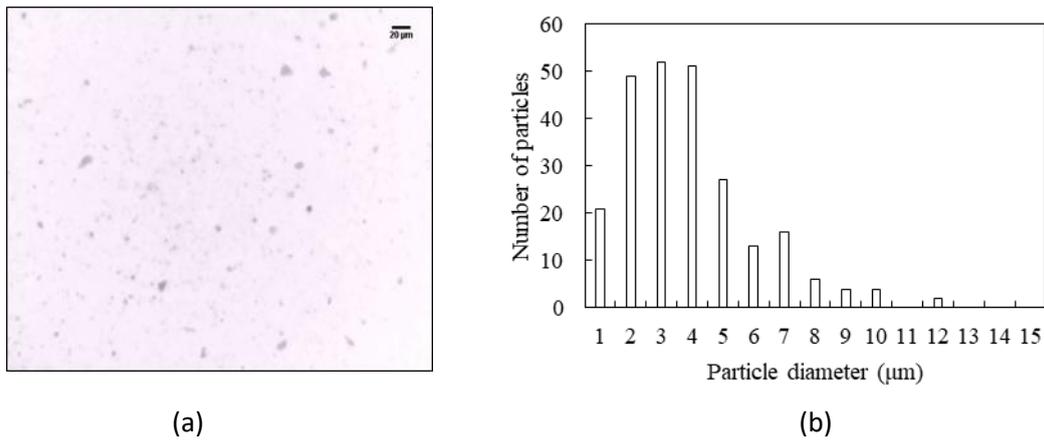
FIGURE 3.13: (Left) Image of filter surface. (Right) Size distribution

Figure 3.14 shows the variation of measured steam temperature and the corresponding superheat retained with injected solution concentration. The first point on the graph is for wet scrubbing using pure water. On injection of the concentrated solution, the separator temperature increases with increase in concentration. Since each droplet consists of a mass fraction of water less than one, condensation on the droplet can occur in the beginning due to diffusion, as observed by Gardner [58]. As the injected solution droplet temperature reaches the steam temperature, solvent evaporation due to heat transfer causes the droplet mass to decrease because of heat transfer between the droplet and superheated steam. With a decrease in the mass of droplet, the solute concentration increases. This occurs at a concentration lower than the saturation limit or if the available boiling point elevation is larger than the steam superheat. The steam flow temperature must be kept lower than the boiling point temperature of the droplet at the saturation value. Superheat up to 34 ℃ is achieved in the experiment at a maximum injection concentration of 50%. The injected solution concentration is also limited by its solubility at injection temperature to avoid precipitation in the pump and injection line.
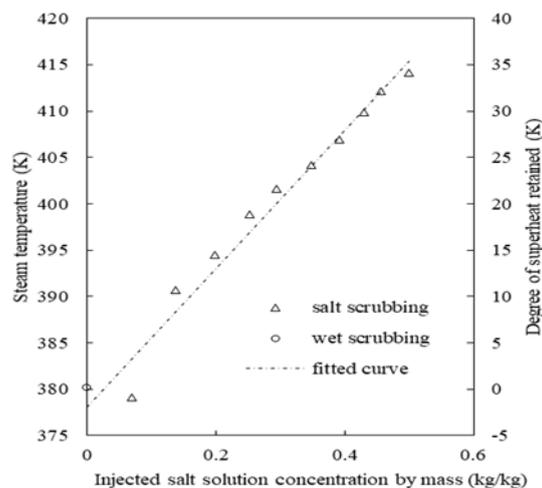

FIGURE 3.14: Variation of steam temperature with injected solution concentration

Figure 3.15 (left) shows the variation of silica concentration measured from the superheated steam collected after the separator S_2. The constant injection concentration of silica in

superheated steam is 40 ppm as measured. The setup consist of a venturi scrubber for removing silica particles from the superheated steam. The removal efficiency of a venturi scrubber is governed by various parameters such as droplet diameter, fluid velocity, volume flow rate and impaction. The dissertation work focuses on studying the effect of solution concentration on scrubbing efficiency, which causes a change in droplet thermophysical properties and its size distribution. All the other parameters are kept constant. Particle collection mechanism in a scrubbing process is mainly of three types: impaction, interception and diffusion. The mechanism for capturing the silica particles depends upon its size. The size of silica particles used in this study has a mean diameter of 3 μm as shown by Figure 3.13. The chances of particle to collide with the droplet depends upon the Stokes number as discussed by Kim et al [105]. With a mean particle diameter of 3 μm, the Strokes number of the particles is high enough to make particle follow the trajectory, implying collision with the droplet rather than flow around it. The particle removal therefore occurs by the process of impaction. The removal efficiency due to impaction is therefore mainly governed by velocity difference between the droplet and the silica particles along the flow.

An effective scrubbing efficiency is obtained by the unit for the set design parameters as shown by the point of zero injected solution concentration for the case of wet scrubbing using water. In addition, with an increase in solution concentration, silica particle scrubbing efficiency (fig. 3.15, right) increases, causing a decrease in silica concentration (fig. 3.15, left) in superheated steam collected after separation. This can be explained by the fact that as concentration increases, the droplet size decrease is low as less solvent evaporates due to an increase in boiling point elevation which helps in retaining volume fraction of liquid in superheated steam, and hence increases the chances of collision by impaction and attachment of particles. The scrubbing efficiency also depends on residence time of droplets in the superheated steam since the droplet concentration changes with time until thermal equilibrium is achieved with the surrounding steam. In addition, an increase in residence time increases chances of collision and attachment of the particles to the droplets. The residence time was kept the same during every sampling.
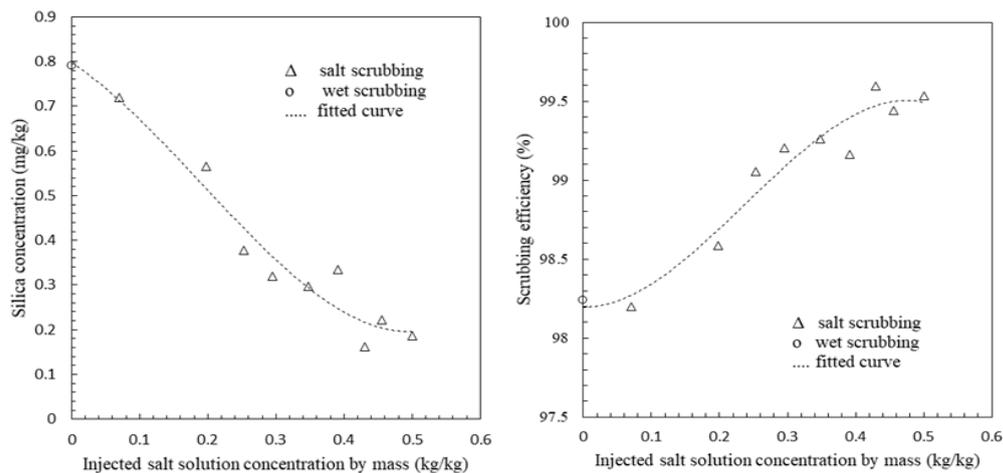

FIGURE 3.15: Variation of silica concentration (left) and scrubbing efficiency (right) obtained with injected solution concentration for a constant inlet silica concentration of 40ppm

Figure 3.16 shows the effect of injected solution concentration on potassium ion concentration in the superheated steam collected after separation. The results show efficient separation of injected salt solution droplets in the separator. A decrease in the concentration of potassium ion in collected samples is observed with increase in injection concentration, due to an increase in droplet density and a decrease in evaporation causing less reduction in droplet size of the injected salt solution. For fixed inlet flow conditions, cyclone separators have a minimum droplet size for separation [106]. Large droplet size and high density cause an increase in centrifugal force making a greater volume fraction of droplets likely to be separated in the cyclone separator. The unseparated droplet fraction in superheated steam is reduced and hence the salt concentration in the collected samples is reduced. The maximum value of droplet collection efficiency in the separator based on the salt concentration was found to be 99.74%. Study on application of gas-liquid cyclone separator for removing amine droplets in hydrogen gas flow was done by Ma et al [107]. Simulation and experimental study done shows removal efficiency upto 94.7% for a small scale unit. The designed gas-liquid cyclone separator was also tested in a high pressure environment upto 10 MPa for industrial application. The result shows removal efficiency upto 99.9%. The increase in droplet removal efficiency is justified by high value of mean droplet size having high centrifugal for separation. A similar increase in droplet removal efficiency is also expected for salt solution droplet removal from the superheated steam when applied on a larger scale unit.
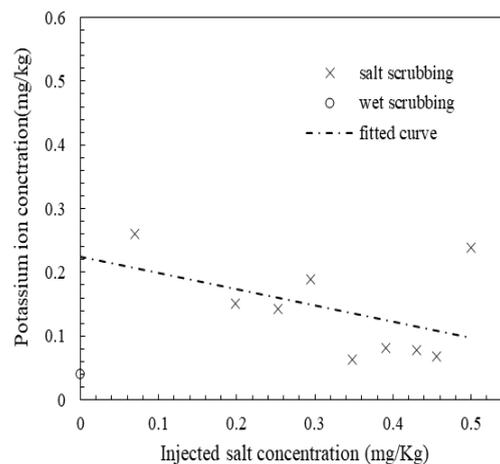

FIGURE 3.16: Variation of Potassium ion concentration in the collected steam after separation with injected solution concentration

4 Discussion

The dissertation work presents a study of utilization of the superheated geothermal steam containing acid gas and silica impurities as observed with the fluid from IDDP-1 well. To accomplish the task, simulation and experimental study on silica particle deposition in superheated steam flow was done. The study was done considering the scope of utilizing a heat recovery system which can be used to regain the superheat after scrubbing the steam. Advection-diffusion model was implemented in OpenFoam for simulating silica particle transport and deposition in superheated steam. Experiments were done for the validation of the model simulation. Superheat up to 48 degree was kept during the experiment in order to assure two-phase state consisting of dry steam with silica in dispersed phase. Results from the computational model and experiment shows the effect of particle relaxation time on deposition rate. The study shows a scope for controlling deposition rate by limiting the particle relaxation time.

To control silica deposition, study on developing a method for pre-treatment of the steam was done for the removal of silica before passing it through the heat recovery system. As observed from the study done on silica particle deposition, the deposition velocity is found to increase exponentially after a certain relaxation time. Therefore scrubbing particles with high relaxation time can reduce deposition in a component such as heat recovery system, which is to be placed after the scrubbing unit. However, it is required to retain the steam superheat during the scrubbing process in order to achieve the overall objective of maximizing the work output. To fulfill this, application of aqueous potassium carbonate solution, having the property of boiling point elevation, is proposed. Study was done to understand the behavior of salt solution droplets in the superheated steam in terms of degree of superheat retained and change in concentration. A computational model for simulating salt solution droplets in superheated steam was developed. Experiments were performed to validate the model simulating salt solution droplets in superheated steam. The experiments were done using an inlet steam flow with 40 degree of superheat in order to assure significant amount of mass transfer from the liquid droplets in the superheated steam which is mainly governed by the temperature difference between the droplet and the surrounding medium that is steam. Result from the simulation and experiment shows salt solution droplets to be stable in superheated steam up to significant degree without precipitation of the salt.

Since the overall efficiency of the method is to be governed by the amount of power output delivered, it is important to estimate the work output obtained using the selected method of scrubbing in combination with the heat recovery system. A power cycle was therefore proposed and a comparison study in terms of the thermodynamic output was done with that of the cycle utilizing wet scrubbing method. The thermodynamic evaluation of the proposed cycle helps to estimate the maximum amount of work that can be obtained utilizing the

proposed method without salt precipitation, considering the maximum salt solubity and the degree of superheat achieved at that concentration at different wellhead pressures. In addition, exergy analysis was done to calculate the contribution of each component in the cycle to the total exergy destruction. The comparison study for the IDDP-1 case shows improved output achieved utilizing the proposed method.

The proposed method requires verification in terms of scrubbing efficiency achieved and the degree of superheat retained while scrubbing. Experimental study of the proposed scrubbing technique was therefore done. Experiments were performed to study the effect of salt solution concentration of the injected droplets on the degree of superheat retained and the scrubbing efficiency obtained. Results show considerable degree of steam superheat retained and high scrubbing efficiency acheived utilizing the proposed scrubbing method.

4.1 Summary

Results from the dissertation work are summarized as follows:

- Silica particles in superheated steam flow represent a case of two-phase flow with silica particles as a dispersed phase in superheated steam as a gas medium.
- Simulation results for silica particle deposition from the advection-diffusion model in superheated steam flow show agreement with the experimental data for particles in superheated steam.
- Computational study and experimental investigation for silica particles in superheated steam show an increase in deposition velocity with particle relaxation time in the diffusion-impaction regime.
- Comparing the application of aqueous potassium carbonate for scrubbing versus traditional wet scrubbing shows improvement in utilization efficiency using the proposed technique of scrubbing using aqueous potassium carbonate solution.
- Computational study and experimental investigation of aqueous potassium carbonate solution droplets in superheated steam flow show an increase in boiling point elevation with an increase in injection salt concentration.
- Simulation results for the boiling point elevation of the salt solution droplets from the model show good agreement with the experimental data.
- The separated droplet concentration obtained from the simulation results shows deviation up to 20% from the experimental values due to rebounding conditions for droplets assumed at the separator wall.
- The experimental investigation on silica scrubbing using aqueous potassium carbonate solution for superheated steam cleaning shows superheat up to 34 $^\circ$C retained for a given set of experimental conditions.
- Scrubbing efficiency and degree of superheat retained increases with increase in the concentration of the injected salt solution.

4.2 Conclusion

Based on the results from the study, following conclusions can be drawn:

- The issue of removing silica particles from superheated steam must be addressed if that resource is to be utilized for power generation.

- For silica particles in steam, relaxation time increases with an increase in particle size due to agglomeration. Controlling agglomeration can, therefore, help control deposition.
- The developed experimental setup with sampling and image processing techniques offers a promising method for the study of silica deposition in superheated steam flow.
- The implemented computation model can be used to study silica particle transport and deposition in superheated steam for more complicated geometries. The implemented model in OpenFOAM offers an advantage of computational time and cost saving due to its Eulerian approach. The model can be applied to the design and analysis of geothermal systems involving silica and superheated steam flow.
- Thermodynamic analysis of the proposed cycle utilizing aqueous potassium carbonate for scrubbing shows improved performance for the case of the IDDP-1well. A significant increase of revenue for a geothermal power plant can be obtained, considering the number of similar wells to IDDP-1.
- The computation model for simulation of aqueous potassium carbonate solution droplets in superheated steam can help to estimate the amount of superheat retained by the steam without salt precipitation.
- The dissertation work presents model development for the study of aqueous potassium carbonate solution in superheated steam. The model is able to predict the effect of salt solution concentration on its droplet characterisitics. A similar approach can be adopted for modeling and studying different salt solutions and their behavior in superheated steam flow.
- Experimental investigation of the proposed technique for silica scrubbing shows the scope of utilization in the geothermal industry for cleaning solid silica impurities from superheated steam and obtaining improved thermal and scrubbing efficiency.

4.3 Recommendation and future work

Advection-diffusion model was implemented and verified experimentally for the study of silica particle transport and deposition in superheated steam flow. Recommendations include application of the implemented model for geothermal energy purposes involving design and study of systems with silica in superheated steam flow.

The dissertation work shows improved scrubbing and thermal efficiency utilizing aqueous potassium carbonate solution for scrubbing superheated steam. The thermodynamic cycle analysis and computational model developed is based on the model for boiling point elevation. The model is derived from empirical results from the literature and their extrapolation. However, future work should be focused on experimental studies regarding salt solution properties at higher temperature and pressure near to supercritical state. The author however, with no doubt recommends the proposed technique and the developed computational model for application to vapor dominated geothermal sources with medium level temperature and pressure states. Experimental investigation of the silica scrubbing process using aqueous potassium carbonate is presented in the work. Development of computational model for simulating the scrubbing process involving three phase flow is recommended.

The experimental work done in the dissertation study is limited by laboratory scale conditions involving steam at low temperature and pressure states. Validation of the

proposed method by onsite experiments involving geothermal steam in a superheated state at high temperature and pressure is additionally recommended. The dissertation presents early results related to this matter, which are non-the-less interesting and valuable and lay out the needs and methods for further research.

REFERENCES

[1] Renewables 2018, Global Status Report.

[2] P.E. Ellis, D. M. Anliker, "Geothermal power plant corrosion experience-A Global survey", Materials Performance, 21, pp. 9-16, 1982.

[3] J.C. Dunn, H.C. Hardee, "Superconvecting geothermal zones", Journal of Volcanology and Geothermal Research 11, pp. 189-201, 1981.

[4] T. Hashida, G. Bignall, N. Tsuchiya, T. Takahashi, K. Tanifuji, "Fracture generation and water rock interaction process in supercritical deep-seated geothermal reservoirs", Geothermal Research Council Transactions 25, pp. 225-229, 2001.

[5] A. Albertsson, J.O. Bjarnason, T. Gunnarsson, C. Ballzus, K. Ingason, "Part III: Fluid handling and evaluation. In: G.O. Fridleifsson., Iceland Deep Drilling Project, Feasibility Report", Orkustofnun Report OS2003-007. pp. 33, 2003.

[6] G.O. Fridleifsson, W.A. Elders, A. Albertsson, "The concept of the Iceland deep drilling project", Geothermics, 49, pp. 2-8, 2014.

[7] S. Hjartarson, G. Sævarsdottir, K. Ingason, B. Palsson, W.S. Harvey, H. Palsson, "Utilization of the chloride bearing, superheated steam from IDDP-1", Geothermics, 49, pp. 83–89, 2014.

[8] H. Armannsson, T. Fridriksson, G.H. Gudfinnsson, M. Olafsson, F. Oskarsson, D. Thorbjornsson, "IDDP-The chemistry of the IDDP-01 well fluids in relation to the geochemistry of the Krafla geothermal system", Geothermics, 49, pp. 66-75, 2014.

[9] G. Allegrini, G. Benvenuti, "Corrosion characteristics and geothermal power plant protection. U.N. Symposium on the Development and Utilization of Geothermal Resources", Geothermics, 2(1), pp. 865-881, 1970.

[10] P. Hirtz, J. Miller, E. Prabhu, "Operational results of a dry steam resource chloride corrosion mitigation system", Geothermal Resources Council Transactions, 14(2), pp. 1667–1675, 1990.

[11] P. Hirtz, C. Buck, R. Kunzman, "Current techniques in acid-chloride corrosion control and monitoring at the geysers", 16th Work-shop on Geothermal Reservoir Engineering, Stanford University, Stanford, CA, pp. 83-95, 1991.

[12] A. Paglianti, E.V. Vivianvi, E, Brunazzi, F. Sabatelli, "A simple method to compute hydrogen chloride abatement in geothermal power plant", Geothermics, 25(1), pp. 37-62, 1996.

[13] A. Bahadori, H.B. Vuthaluru, "Prediction of silica carry-over and solubility in steam of boilers using simple correlation", Applied Thermal Engineering, 30, pp. 250-253, 2010.

[14] S.H. Markusson, T. Hauksson, "Utilization of the hottest well in the world, IDDP-1 in Krafla", World Geothermal Congress, Melbourne, Australia, 2015.

[15] S.J. Zarrouk, B.C. Woodhurst, C. Morris, "Silica scaling in geothermal heat exchangers and its impact on pressure drop and performance: Wairakei binary plant, New Zealand", Geothermics, 51, pp. 445-459, 2014.

[16] M.G. Dunn, A.J. Baran, J. Miatech, "Operation of gas turbine engines in volcanic ash clouds", ASME, 94-GT-170, 1994.

[17] A. Einarsson, IDDP 1 Flow test 2010-2012, Landsvirkjun, 2013.

[18] N. Moller, J.P. Greenberg, J.H.Weare, "Computer Modeling for geothermal systems: Predicting carbonate and silica scale formation, CO_2 breakout and H_2S exchange", Transfer in Porous Media, 33, pp. 173-204, 1998.

[19] M. Nazami, Sutopo, "Mathematical modelling of silica scaling deposition in geothermal wells", Earth and Environmental Science, 42, 2016.

[20] T. Hauksson, M. Sigurdur, K. Einarsson, S.N. Karlsdottir, A. Einarsson, A. Moller, t. Sigmarsson, "Pilot testing of handling the fluids from the IDDP-1 exploratory geothermal well, Krafla, N.E. Iceland", Geothermics, 49, pp. 76-82, 2014.

[21] K. Brown, M. Dunstall, "Silica scaling under controlled hydrodynamic conditions", World Geothermal Congress, Kyushu-Tohoku, Japan, 2010.

[22] S. Elghobashi, "On predicting particle laden turbulent flows", Applied Scientific Research, 52, pp. 309-329, 1994.

[23] P. Karasek, L. Stavikova, J. Planeta, B. Hohnova, M. Roth, "Solubility of fused silica in sub and supercritical water: Estimation from a thermodynamic model", The Journal of Supercritical Fluids, 83, pp. 72-77, 2013.

[24] A. Guha, "Transport and deposition of particles in turbulent and laminar flow", Annual Review of Fluid Mechanics. 40, pp. 311-341, 2008.

[25] G.A. Kallio, M.W. Reeks, "A numerical simulation of particle deposition in turbulent boundary layers", International Journal of Multiphase Flow, 15(3), pp. 433-446, 1989.

[26] H. Ounis, G. Ahmadi, J.B. McLaughlin, "Brownian particle deposition in a directly simulated turbulent channel flow", Physics of Fluids A, 5, pp. 1427-1432, 1993.

[27] F. Greifzu, C. Kratzsch, T. Forgber, F. Lindner, R. Schwarze, "Assessment of particle-tracking models for dispersed particle-laden flows implemented in OpenFOAM and ANSYS FLUENT", Engineering Applications of Computational Fluid Mechanics, 10(1), pp. 30-43, 2015.

[28] J.R. Fessler, J. Eaton, "Turbulence modification by particles in a backward-facing step flow", Journal of Fluid Mechanics. 394, pp. 97–117, 1999.

[29] J. Boree, T. Ishima, I. Flour, "The effect of mass loading and interphase collisions on the development of the polydispersed two-phase flow downstream of a confined bluff body", Journal of Fluid Mechanics. 443, pp. 129–165, 2001.

[30] S.K. Friedlander, H.F. Johnstone, "Deposition of Suspended Particles from Turbulent Gas Streams", Ind. Eng. Chem. 49 (7), pp. 1151–1156, 1957.

[31] C.N. Davies, "Aerosol Science", London: Academic Press, 1986.

[32] S.K. Beal, "Deposition of Particles in Turbulent Flow on Channel or Pipe Walls" Nuclear Science and Engineering, 40(1), 1-11, 1970.

[33] M.W. Reeks, "On model equations for particle dispersion in inhomogeneous turbulence", International Journal of Multiphase Flow, 31(1), pp. 93–114, 2005.

[34] C.M. Venier, S.M. Damian, N.M. Nigro, "Numerical aspects of Eulerian gas-particle flow formulations", Computers and Fluids. 133, pp. 151-169, 2016.

[35] L.I. Zaichik, V.A. Pershukov, M.V. Kozelev, A.A. Vinberg, "Modeling of dynamics, heat transfer, and combustion in two-phase turbulent flows: 1. Isothermal flows", Experimental   Thermal and Fluid Science, 15(4), pp. 291-310, 1997.

[36] L.I. Zaichik, V.A. Pershukov, M.V. Kozelev, A.A. Vinberg, "Modeling of dynamics, heat transfer, and combustion in two-phase turbulent flows: 2. Flows with heat transfer and combustion", Experimental Thermal and Fluid Science, 15(4), pp. 311-322, 1997.

[37] L.I. Zaichik, N.I. Drobyshevsky, A.S. Filippov, R.V. Mukin, V.F. Strizhov, "A diffusion-inertia model for predicting dispersion and deposition of low-inertia particles in turbulent flows", International Journal of Heat and Mass Transfer, 53 pp. 154–162, 2010.

[38] S.T. Johansen, "The deposition of particles on vertical walls", International Journal of Multiphase Flow, 17(3), pp. 355-376, 1991.

[39] J.B. Young, A. Leeming, "Particle deposition in turbulent pipe flow", Journal of Fluid Mechanics. 340, pp. 129–159, 1997.

[40] A. Guha, "A unified Eulerian theory of turbulent deposition to smooth and rough surfaces", Journal of Aerosol Science, 28(8), pp. 1517–1537, 1997.

[41] D. Eskin, J. Ratulowski, K. Akbarzadeh, "Modeling of particle deposition in a vertical turbulent pipe flow at a reduced probability of particle sticking to the wall", Chemical Engineering Science. 66(20), pp. 4561-4572, 2011.

[42] S.A. Slater, J.B. Young, "The calculation of inertial particle transport in dilute gas-particle flows", International Journal of Multiphase Flow, 27(1), pp. 61–87, 2001.

[43] S.A. Slater, A.D. Leeming, J.B. Young, " Particle deposition from two-dimensional turbulent gas flows", International Journal of Multiphase Flow, 29(5), pp. 5721-750, 2003.

[44] OpenFOAM, "Userguide, 2nd edition", OpenCFD Ltd, 2014.

[45] N. Stavropoulos, "Deposition of particles from turbulent gas streams", M.Sc Thesis, Columbia University, New York, 1954.

[46] A.K. Postma, L.C. Schwendiman, L.C., "Studies in micrometrics: I. Particle deposition in conduits as a source of error in aerosol sampling", Report HW-65308. Richland, Washington: Handford Laboratory, 1960.

[47] A.C. Wells, A.C. Chamberlain, "Transport of small particles to vertical surfaces", British Journal of Applied Physics, 18, pp. 1793-1799, 1967.

[48] M.S. El-Shobokshy, "Experimental measurements of aerosol deposition to smooth and rough surfaces", Atmospheric Environment, 17, pp. 639-644, 1983.

[49] G.A. Sehmel, "Aerosol deposition from turbulent airstreams in vertical conduits", Report BNWL-578, Richland, Washington: Pacific Northwest Laboratory, 1968.

[50] B.Y. Liu, J.K. Agarwal, "Experimental observation of aerosol deposition in turbulent flow", Journal of Aerosol Science, 5(2), pp. 145-155, 1974.

[51] M. Shimada, K. Okuyama, M. Asai, "Deposition of submicron aerosol particles in turbulent and transitional flow", AIChE Journal, 39, pp. 17-26, 1993.

[52] K.W. Lee, J.A. Gieseke, "Deposition of particles in turbulent pipe flows", Journal of Aerosol Science, 25, pp. 699-709, 1994.

[53] L.G. Alexander, C.L. Coldren, "Droplet transfer from suspending air to duct walls", Industrial and Engineering Chemistry, 43, pp. 1325-1331, 1951.

[54] S. Namie, T. Ueda, "Droplet transfer in two-phase mist flow. Part I: experiment of droplet transfer rate and distribution of droplet concentration and velocity", Bull, JSME, 15, pp. 1568-1580, 1972.

[55] D.D. McCoy, T.J. Hanratty, "Rate of deposition of droplets in annular two-phase flow", International Journal of Multiphase flow. 3, pp. 319-331, 1977.

[56] W. Kvasnak, G. Ahmadi, R. Bayer, M. Gaynes, "Experimental investigation of dust particle deposition in a turbulent channel flow", Journal of Aerosol Science. 24, pp. 795-815, 1993.

[57] R.S. Frank, E.W. Nancy, "Environmental Engineers Mathematics Handbook" CRC Press, New York, USA.

[58] S.V. Manyele "Toxic acid gas absorber design considerations for air pollution control in process industries", Educational Research and Review, 3, pp. 137-147, 2008.

[59] T.W. Chien, H. Chu, "Removal of SO_2 and NO from flue gas by wet scrubbing using an aqueous $NaClO_2$ solution", Journal of Hazardous Materials, 80, pp. 43-57, 2000.

[60] B. Han, H.J. Kim, Y.J. Kim, K.S. Han "Removal characteristics of gaseous contaminents by a wet scrubber with different packing materials", Journal of Korean Society for Atmospheric Environment. 23(6), pp. 744-751, 2007.

[61] S. Kurella, M. Balla, P.K. Bhukya, B.C. Meikap "Scrubbing of HCl gas from synthesis gas in a multistage dual-flow sieve plate wet scrubber by alkaline solution", Journal of Chemical Engineering and Process Technology, 6(5), pp. 1-7, 2015.

[62] D.W. Fisher, D.B. Jung, "Alternatives to traditional water washing used to remove impurities in superheated geothermal steam", Geothermal Resources Council Transactions,   20, pp. 737-741, 1996.

[63] P.N. Hirtz, M.L. Broaddus, D.L. Gallup, "Dry steam scrubbing for impurity removal from superheated geothermal steam", Geothermal Resources Council Transactions, 26, pp. 751-754, 2002.

[64] O. Weres, C. Kendrick, "Corrosion by HCl in Dry Steam Wells Controlled using Potassium Carbonate without Destroying Superheat", Geothermal Resources Council Transactions, 34, pp. 1097-1103, 2010.

[65] X. Ge, X. Wang, "Estimation of freezing point depression, boiling point elevation and vaporization enthalpies of electrolyte solutions", Industrial and Engineering Chemistry Research, 48(4), pp. 2229-2235, 2009.

[66] G.C. Gardner, "Evaporation of small water drops containing salt in a high pressure steam environment", Journal of Fluids Engineering, 103(1), pp. 112-118, 1981.

[67] A.P. Kamps, E. Meyer, B. Rumpf, G., Maurer, "Solubility of CO_2 in aqueous solutions of KCl and in aqueous solutions of K_2CO_3", Journal of Chemical and Engineering Data, 52, pp. 817-832,   2007.

[68] G.G. Aseyev, "Electrolytes Equilibria in solutions and phase equilibria. Calculation of multicomponent systems and experimental data on the activities of water, vapour pressures and osmotic coefficients", Begell House, Inc., New York, pp. 254-283,   1998.

[69] L.V. Puchkov, V.V. Kurochkina, "Vapor pressure of aqueous potassium carbonate solutions" Zh. Prikl. Khim. 43, pp. 181-183, 1970.

 [70] M. Sarbar, A.K. Covington, R.L. Nuttall, R.N. Goldberg, "Activity and osmotic coefficients of aqueous potassium carbonate", Journal of Chemical Thermodynamics, 11, pp. 695-702, 1982.

[71] S.I. Pak, K.S.   Chang, "Performance estimation of a Venturi scrubber using a computational model for capturing dust particles with liquid spray", Journal of Hazardous Materials, 138(B), pp. 560-573, 2006.

[72] P.E. Liley, G.H. Thomson, D.G. Friend, T.E. Daubert, E. Buck, "Section-2: Physical and Chemical Data In: Perry´s chemical engineers handbook", 7th ed. New York, NY: McGraw-Hill, 1999.

[73] G.S. Srikantiah, S.S. Wang,   "Numerical modeling of phase separation in steam separators by a three-dimensional two-fluid model", 4th International Topical Meeting on Nuclear Reactor Thermal-hydraulics, Karlsruhe, F.R.G., 1, pp. 1031-1036, 1989.

[74] T. Nakao, H. Sooma, T. Kawasaki, I. Sumida, "Analysis of droplet behavior in a dryer with wave-type vanes", Journal of Nuclear Science and Technology, 30(12), pp. 1303-1305, 1993.

[75] T. Nakao, Y. Saito, H. Souma, T. Kawasaki, G. Aoyama, "Droplet behavior analysis in the BWR dryer and separator", Journal of Nuclear Science and Technology,   35(4), pp. 286-293, 1998.

[76] L. Jia, H. Suyi, W. Xiaomo, "Numerical study of steam-water separators with wave-type vanes", Chinese Journal of Chemical Engineering, 15(4), pp. 492-498, 2007.

[77] A. Frydman, J. Vasseur, F. Ducept, M. Sionneau, J. Moureh, "Simulation of spray drying in superheated steam using computational fluid dynamics", Drying Technology: An International Journal, 17, pp. 1313-1326, 1999.

[78] F. Ducept, M. Sionneau, J. Vasseur, "Superheated steam dryer: simulation and experiments on product drying", Chemical Engineering Journal, 86, pp. 75-83, 2002.

[79] M. Bialik, P. Sedin, H. Theliander, "Boiling point rise calculations in sodium salt solutions", Industrial and Engineering Chemistry Research. 47(4), pp. 1283-1287, 2008.

[80] C.W. Tsang, M.F. Trujillo, C.J. Rutland, "Large-eddy simulation of shear flows and high speed vaporizing liquid fuel sprays", Computer and Fluids, pp. 262-279, 2014.

[81] M. Yousefifard, P. Ghadimi, H. Nowruzi, "Three-dimensional LES modeling of induced gas motion under the influence of injection pressure and ambient density in an ultrahigh-pressure diesel injector", Journal of Brazilian Society of Mechanical Sciences and Engineering, 37(4), pp. 1235-1243, 2015.

[82] M.M. Khan, J. Helie, M. Gorokhovski, N.A. Sheikh, "Experimental and numerical study of flash boiling in gasoline direct injection sprays", Applied Thermal Engineering, 123, pp. 377-389, 2017.

[83] Z.F. Zhou, G.Y. Lu, B. Chen, "Numerical study on the spray and thermal characteristics of R404A flashing spray using OpenFOAM", International Journal of Heat and Mass Transfer, 117, pp. 1312-1321, 2018.

[84] F. Menter, "Two equation eddy viscosity turbulence models for engineering applications", AIAA, 32(8), pp. 1598-1605, 1994.

[85] P.J. O´Rourke, "Collective drop effects on vaporizing liquid sprays", Los Alamos National Lab, NM, USA, 1981.

[86] P.G. Saffman,"The lift on a small sphere in a slow shear flow", Journal of Fluid Mechanics, 22, pp. 385-400, 1965.

[87] M. Caporaloni, F. Tampieri, F. Trombetti, O. Vittori, "Transfer of particles in nonisotropic air turbulence", Journal of the Atmospheric Science, 32, pp. 565-568, 1975.

[88] M.W. Reeks, "On a kinetic equation for the transport of particles in turbulent flows", Physics of Fluids A, 3, pp. 446-456, 1991.

[89] S.V. Patankar, D.B. Spalding,. "A calculation procedure for heat, mass and momentum transfer in three dimensional parabolic flows", International Journal of Heat Mass Transfer. 15, pp. 1787-1806, 1972.

[90] M.S. Abd-Elhady, C.C.M. Rindt, J.G. Wijers, A.A. van Steenhoven, E.A. Bramer, Th.H. van der Meer," Minimum gas speed in heat exchangers to avoid particulate fouling", International Journal of Heat and Mass Transfer, 47, pp. 3943-3955, 2004.

[91] C.A. Schneider, W.S. Rasband, K.W. Eliceiri,"NIH Image to ImageJ: 25 years of image analysis", Nature Methods, 9(7), pp. 671-675, 2012.

[92] G. Culivicchi, A. Lenzi, R. Parri, M.C. Volpe, G. Rispoli, "Characteristics and performances of chlorine scrubbing systems in the Larderello area", Proceedings World Geothermal Congress, Antalya, Turkey, 2005.

[93] A.M. Ali, C. Yan, Z. Sun, H. Gu, K. Mehboob, "Dust particle removal efficiency of a venturi scrubber", Annals of Nuclear energy, 54, pp. 178-183, 2013.

[94] G.M. Brunner, W.V. Hauck, A. Adams, C.N. Mex, "Method for the purification of potassium carbonate", United States patent Office, 3079227, 1963.

[95] Y.E. Yuksel, M. Ozturk, "Thermodynamic and thermoeconomic analyses of a geothermal energy based integrated system for hydrogen production", International Journal of Hydrogen Energy, pp. 1-17, 2016.

[96] R. DiPippo, "Geothermal Power Plants: Principles, Applications, Case Studies and Environmental Impact", Second ed. Butterwort-Butterworth-Heinemann, 2008.

[97] A. Franco, M. Villani, "Optimal design of binary cycle power plants for water-dominated, medium temperature geothermal fields", Geothermics, 38, pp. 379- 391, 2009.

[98] N. Moller, "The prediction of mineral solubilities in natural waters: a chemical equilibrium model for the $Na-Ca-Cl-SO_4-H_2O$ system, to high temperature and concentration", Geochim. Cosmochim. Acta, 52(4), pp. 821-837, 1988.

[99] R.C. Moore, R.E. Mesmer, J.M. Simonson, "Solubility of potassium carbonate in water between 384 and 529 K measured using the synthetic method", Journal of Chemical and Engineering Data, 42, pp. 1078-1081, 1997.

[100] W.E. Ranz, W.R. Marshall, "Evaporation from drops", Chem. Eng. Prog. 48, , pp. 141-146, 1952.

[101] A. Chiquillo, "Measurements of the relative thermal conductivity of aqueous salt solutions with a transient hot-wire method", Juris Druck and Verlag, Zurich, 1967.

[102] P. Bangma, "The development and performance of steam-water separator for use on geothermal bores", Proc. UN Conference. New Sources Energy Rome 3/G/13), pp. 60-77, 1961.

[103] J. Eaton, J. Fessler, "Preferential concentration and settling of heavy particles by turbulence", International Journal of Multiphase flow. 20, pp. 169-209, 1994

[104] Liu, H., Zhang, W., Jia, M., Yan, Y., He, Y., (2018). " An improved method for coupling the in-nozzle cavitation with Multi-fluid-quasi-VOF model for diesel spray." Computer and Fluids, 177, 20-32.

[105] K.S. Kim, S.H. Lee, H.S. Park, "Prediction for particle removal efficiency of a reverse jet scrubber", Journal of Aerosol Science, 37, pp. 1826-1839, 2006.

[106] S.J. Zarrouk, M.H. Purnanto, "Geothermal steam-water separators: Design overview", Geothermics, 53, pp. 236-254, 2015.

[107] L. Ma, J. Wu, Y. Zhang, Q. Shen, J. Li, H. Wang, "Study and application of a cyclone for removing amine droplets from recycled hydrogen in a hydrogenation unit", Aerosol and Air Quality Research, 14, pp. 1675-1684, 2014.

Appendix A

Experimental Setup

The laboratory scale experimental unit was designed and constructed keeping the following three goals into consideration:

1. Study of the silica particle deposition in superheated steam flow.

2. Study of aqueous potassium carbonate solution droplets in superheated steam flow.

3. Experimental investigation of silica scrubbing using aqueous potassium carbonate.

A single experiment unit was designed and built for the measurements. Figure A.1- A.5 shows the photos of the experimental setup and the major component assemblies. The setup is modified based on the requirement of the experiment to be performed. For experiment on study of potassium carbonate solution droplets in superheated steam flow, particle feeding and injection assembly is removed. For experiments on silica deposition in superheated steam flow, the peristaltic pump assembly is removed. The final experiment on silica scrubbing in superheated steam includes complete assembly shown by figure A.1.
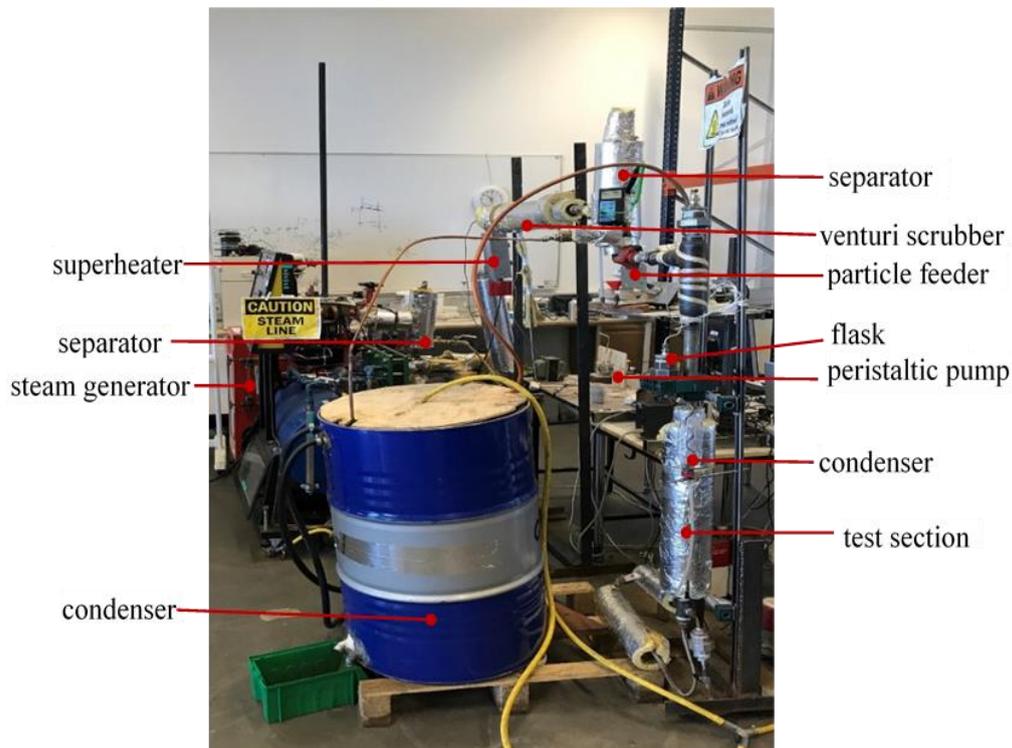

FIGURE A.1: Picture of the experimental setup

FIGURE A.2: Particle feeding (left) and ejector assembly (right)

FIGURE A.3: Sampling flask: top view (left) and front view (right)

oscilloscope

salt solution

weighting scale

peristaltic pump

non-return valve
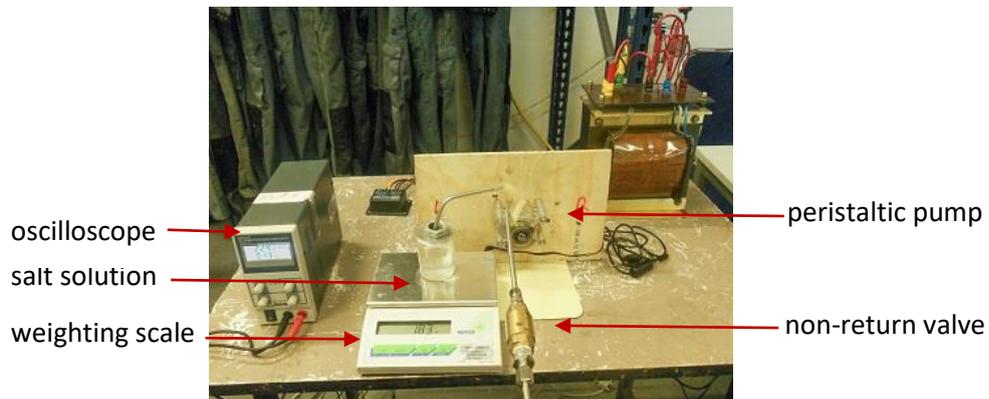
FIGURE A.4: Solution injection assembly
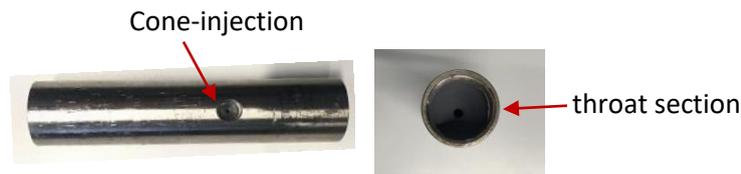
FIGURE A.5: Venturi section

The specification of each component used are as follows:

1. Boiler: Chromalox CHPES-48A high pressure electric steam boiler with 18kW heating capacity.

2. Superheater: Chromalox GCHCIS with 500W heating capacity.

3. Salt solution injection pump: Cole Palmer MasterFlex 7014-20 Peristaltic pump

4. Separator: Bangma type cyclone separator with an outer diameter of 70 mm and 300 mm height. The steam inlet and outlet has 15mm diameter.

5. Venturi unit: Pease Anthony type with a size reduction from 15mm pipe to 6mm diameter and a cone orifice of 1mm diameter.

6. Particle feeding system: Screw feeder with 12V DC motor and feed rate up to 40 mg min^{-1}.

7. Particle collection unit: Stainless steel probe with diameter of 3.65 mm and 10 cm length. A cone shaped flask made of cast iron with a wired mesh serving as a seat for the filter paper to collect particles. Membrane filter paper from MF-Millipore with 0.45 μm pore size and 47mm diameter, stable upto temperature of 180℃.

8. Test section assembly: Two 1.5 m long concentric steel pipes with a hydraulic diameter of 5 mm. The outer pipe consists of a conical section such that the annulus area decreases by a ratio of 1:10 at the entrance.

9. Heating tape: Omega SST051-040 ultra-high temperature heating tape, 470W.

   Figure A.6 shows the process of induction heating of the test pipe for boiling the lubricant. Figure A.7 shows the process of capturing images of the particles present on the test pipe surface.

Induction
heater

Pipe
section
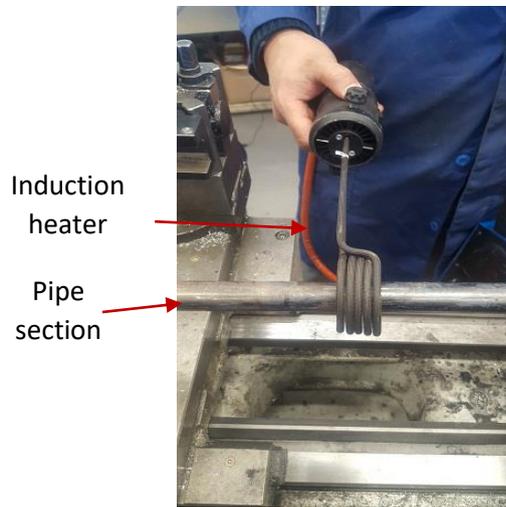
FIGURE A.6: Induction heating

Digital
microscope

Pipe
section
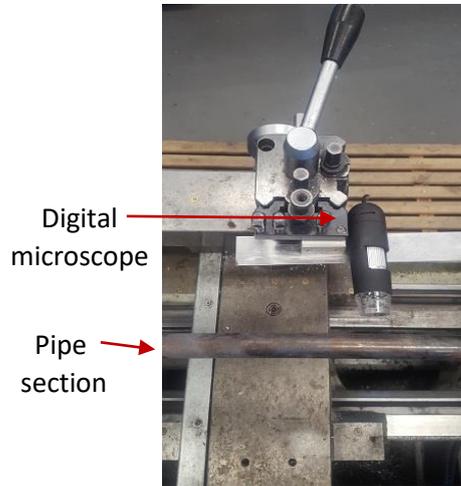
*FIGURE A.7: Capturing images using
digital microscope*